DEFECT CLUSTERING IN LiF TLD-700

By

XIAO-LIN YUAN

Bachelor of Science

Zhengzhou University

Zhengzhou, Henan, China

1983

Submitted to the Faculty of the
Graduate College of the
Oklahoma State University
in partial fulfillment of
the requirements for
the Degree of
MASTER OF SCIENCE
December, 1987

DEFECT CLUSTERING IN LiF TLD-700

Thesis Approved:

Thesis Advisor

Dean of the Graduate College

ACKNOWLEDGEMENTS

My thanks to my thesis advisor, Dr. S. W. S. McKeever, for his extremely kind hand-to-hand teachings and instruction in the full course of this research. He has given an unbelievable amount of care, patience and encouragement to me during the accomplishment of this thesis. In my view, he is not only a gifted expert in the thermally stimulated luminescence field, but also an excellent teacher and good friend. Without him this work would have been impossible. Thanks also to Dr. George Dixon and Dr. Jim Wicksted for their many discussions with me and for serving as members of my committee. Their care and suggestions also made the completion of this thesis possible. I wish to express my gratitude to Dr. Joel Martin and Mr. Charles Hunt for their friendly guidance in the use of the facilities in the crystal growth lab.

Julie Isch has done a wonderful job of typing this thesis. I appreciate her great effort and hard work which have brought this thesis into reality.

Financial support, provided in the form of Research Assistantship by the State of Oklahoma, is deeply appreciated.

My heartfelt thanks go to my family for their years of love and encouragement, and psychological support.

TABLE OF CONTENTS

LIST OF FIGURES

CHAPTER I

INTRODUCTION

Whenever a material has been previously exposed to irradiation (e.g., x-rays, β-rays, etc.), part of the irradiation energy is transferred from the irradiating source to the material through interaction between the incident source beam and atoms of the exposed material. After the exposure, the energy received may stay in the material for a long time. However, this energy can be released by providing a suitable amount of heat. When the discharge happens luminescence phenomena follow. In other words, the energy can be released in the form of visible light. This release of visible light by thermal stimulation following irradiation is known as Thermoluminescence (TL). The TL intensity versus read-out temperature is called a "glow curve".

Based on the above outline, any material which possesses a high sensitivity to irradiation (by sensitivity, I mean that when a material gives a strong TL signal when subjected to a radiation exposure) can be utilized to make a radiation dosimeter. Often, the intensity of TL from the material is proportional to the radiation received. By comparing the signal indicated on

such a dosimeter with a well-established irradiation-dose relation, we can tell precisely the level of dose received by the material of interest. Therefore, TL dosimetry has found wide application in the medical service, and in the nuclear power industry; indeed, anywhere where there is a suspicion that a radiation field may exist.

To be useful as a radiation dosimeter, a material of a wide energy band gap with stable chemistry will be favored [1]. From the Periodic Table, it is readily seen that the alkali halides meet such a demand. Especially, LiF has a relatively bigger band gap (~14 ev) than other compounds from the alkali halides. In addition, its high sensitivity, its human tissue-equivalence, as well as the fact that it is durable, resistent to corrosion and wear, and hardly soluble in water make LiF one of the most widely used dosimeter materials.

However, there are some problems with LiF which affect its role as a dosimeter. Fading is one of them. Julias and de Planque [2] found that at low storage temperature ($<50^{o}$ C.), the decrease in TL signal obtained on samples stored for varying periods before irradiation was similar to the signal loss obtained from those samples stored for the same periods but after irradiation. The fading of TL signal after irradiation may be partially due to the same processes that occur during fading before irradiation. The similarity between the two cases strongly indicates that it is the defects distribution itself which is changing

during the storage time. Specifically, the concentration variation with time of the defects responsible for TL signal in LiF:Mg is the main subject of this thesis.

To accomplish this work, optical absorption (OA), Thermally Stimulated Depolarization Currents (TSDC) and Photoluminescence (PL) will be used to establish correlations with the TL measurements. It is results of these measurements that form the main framework of the thesis.

CHAPTER II

THEORETICAL BACKGROUND

Crystal Structure of LiF

LiF is an ionic crystal with an f.c.c. structure. Its unit cell (Figure 1) consists of two interpenetrating f.c.c. lattices; one for F^-, the other for Li^+. The atomic structure is $1s^2 2s^1$ for the Li atom, $1s^2 2s2p^5$ for the F atom. So the F atom has a tendency obtaining an extra electron, with Li atom losing its valence electron. When this process gets finished actually, an electron is exchanged between the two atoms. As a result, both atoms are ionized to form a LiF molecule. The energy which is required to remove the electron is called "ionization energy", whereas, the energy to receive an electron is commonly termed "electron affinity".

The energy necessary to form this LiF molecule is called "formation energy", which is the difference between the ionization energy of the Li atom and the electron affinity of the F atom. The coulombic potential energy between the two ions is about 14.4 ev. The formation energy of the LiF molecule is about 1.8 ev. Since 14.4 ev >> 1.8 ev, the LiF molecule is consequently very stable under normal conditions.

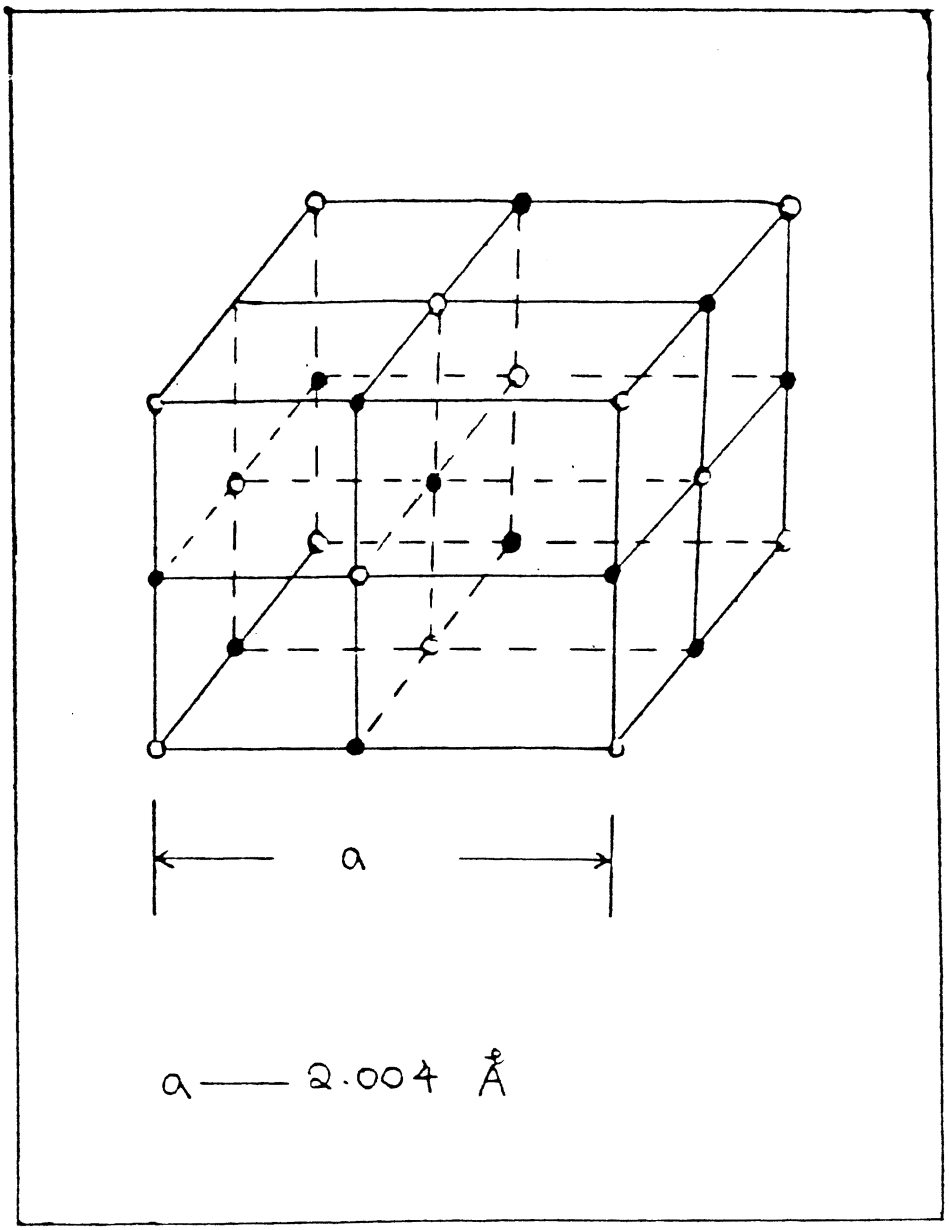

Figure 1. f.c.c. Structure of LiF

$^{+}$ $^{-}$

• Li ; • F

Defects in LiF:Mg.Ti

The most common impurities are divalent metal ions. In TL dosimetry, Mg^{2+} ions are most often used as an intentional dopant. Mg^{2+} enters the LiF crystal by substitutionally replacing Li^{+}. For the sake of electrical charge neutrality, as one Mg^{2+} is introduced, one extra cation vacancy has to be present (Figure 2). The vacancy will behave electrically as an effective negative charge. Due to the presence of the Mg^{2+} ion and the vacancy, various forms of defects are formed in the crystal. The situation for each of these defects will be described as follows.

Dipoles

Substitutional Mg^{2+} ion which interacts with the charge compensating cation vacancies give rise to the impurity-vacancy (I-V) dipoles (Figure 3). Thermodynamic equilibrium exist among free vacancies, Mg^{2+} ions and the dipoles. The dipole is a mobile defect. The motion of the dipole in the lattice take place through two ways. They are:

1) Reorientation of the dipole. In this case, the activation energy for the vacancy jump around the impurity is about 0.6 ev.

2) Exchange between the impurity Mg^{2+} and the cation vacancy. In this case, the movement of the dipole is done with activation energies which are usually higher than that in case 1).

Surrounding the Mg^{2+} ion, the vacancy can be either in

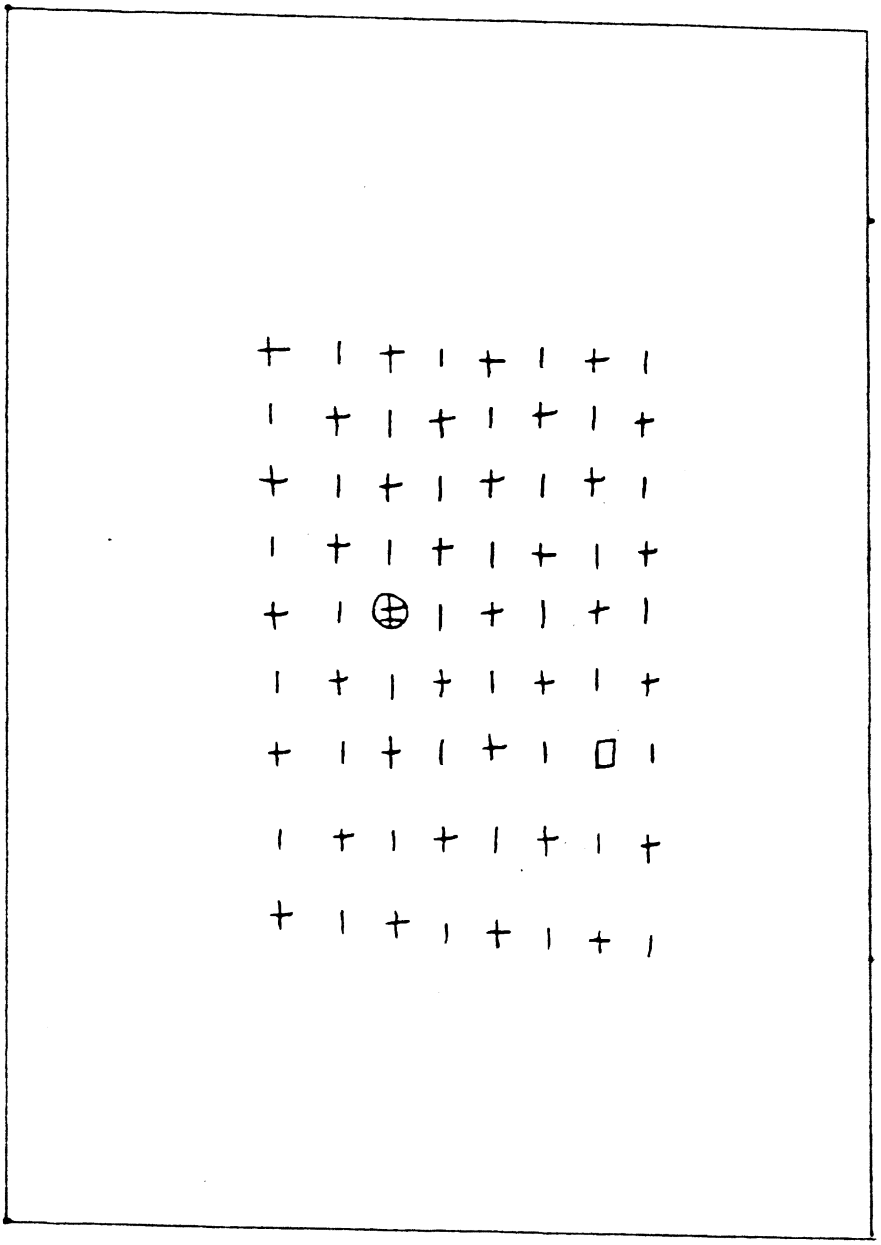

Figure 2. Production of a Cation Vacancy Due to Doping with a Mg^{2+} Ion. ⊕ = Mg^{2+} Ion; □ = Cation Vacancy.

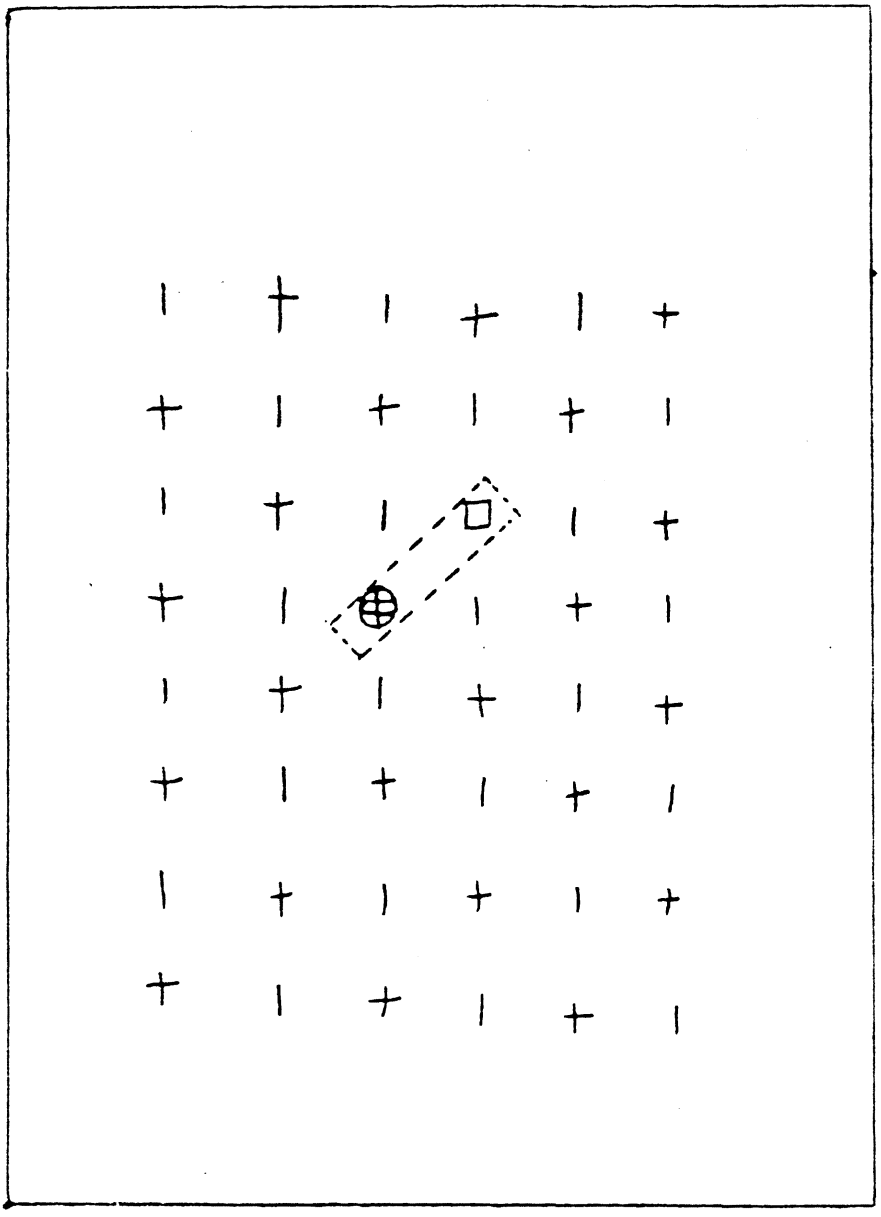

Figure 3. Representation of a Dipole ⊕ : Mg^{2+} ; □ ; Cation Vacancy

n.n. or n.n.n. positions. The former is dominant for impurity ions larger than the host cation [3] and [4]. In the case of n.n., there will be 12 such positions for vacancies. In the case of n.n.n., there will be 6 positions. In LiF:Mg, both n.n. and n.n.n. are present. The formation energies of the two are nearly equal [1]. The configurations of the two situations are shown in Figure 4 and Figure 5, respectively.

However, the vacancy which is part of the dipole can be somewhere else instead of n.n. or n.n.n. [1]. Since the interaction within the dipole is coulumbic, the potential energy changes significantly as the separation between the Mg^{2+} ion and the vacancy varies, expecially when the vacancy stands farther away from the Mg^{2+} ion. The potential drops as r^{-1}. Therefore, a distant vacancy can be hardly considered to still have an appreciable interaction with the Mg^{2+} ion particularly at low temperature. Consequently, models of dipoles consisting of either n.n. or n.n.n. will be used throughout this thesis, unless otherwise stated.

Dimers

The association of two dipoles can form a "dimer". The dimerization process happen basically due to the fact that a free dipole is a rather mobile defect and it can diffuse through the crystal. Additionally, when two free dipoles approach each other during the diffusion, they join together to form a single body, or a dimer, due to the couloumbic

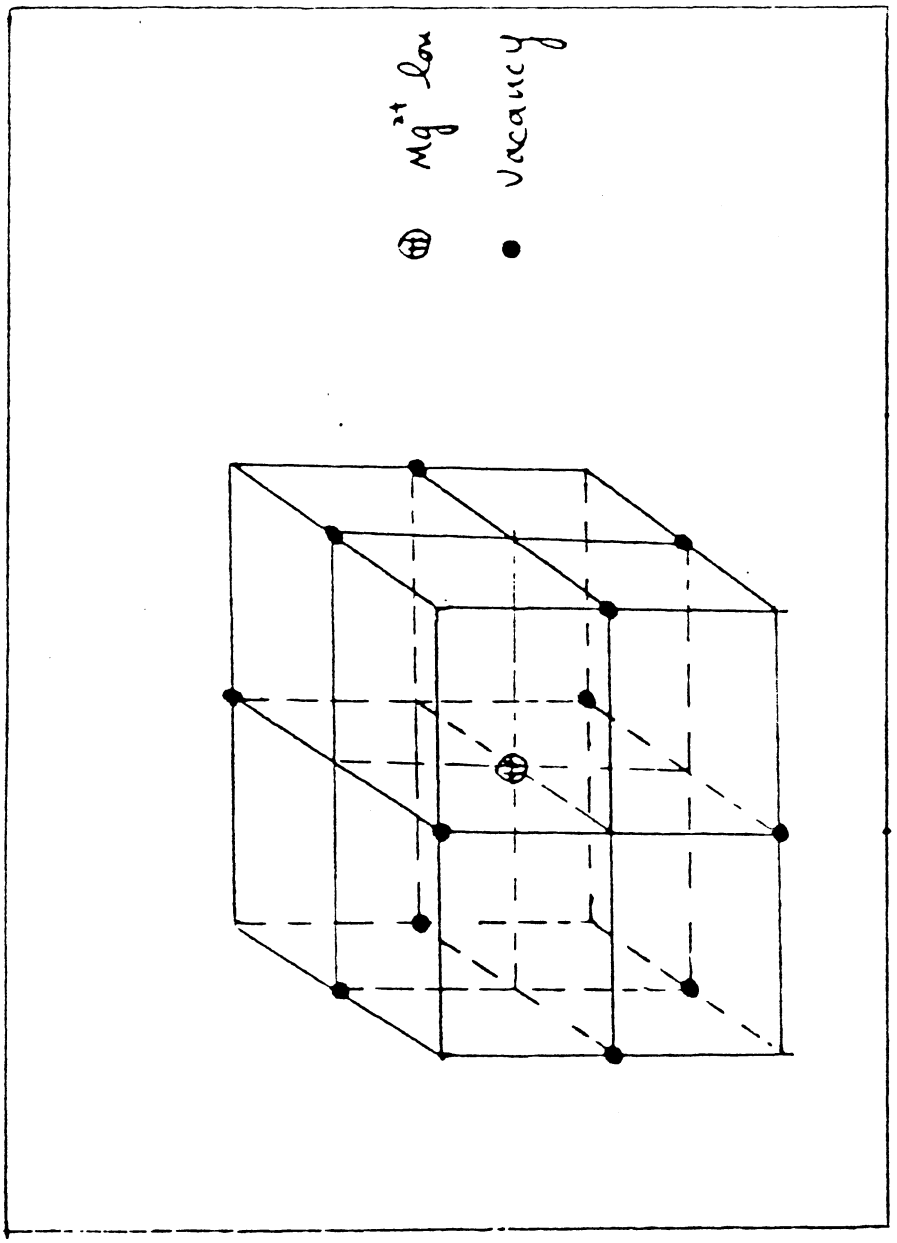

Figure 4. n.n. Configurations for a Dipole

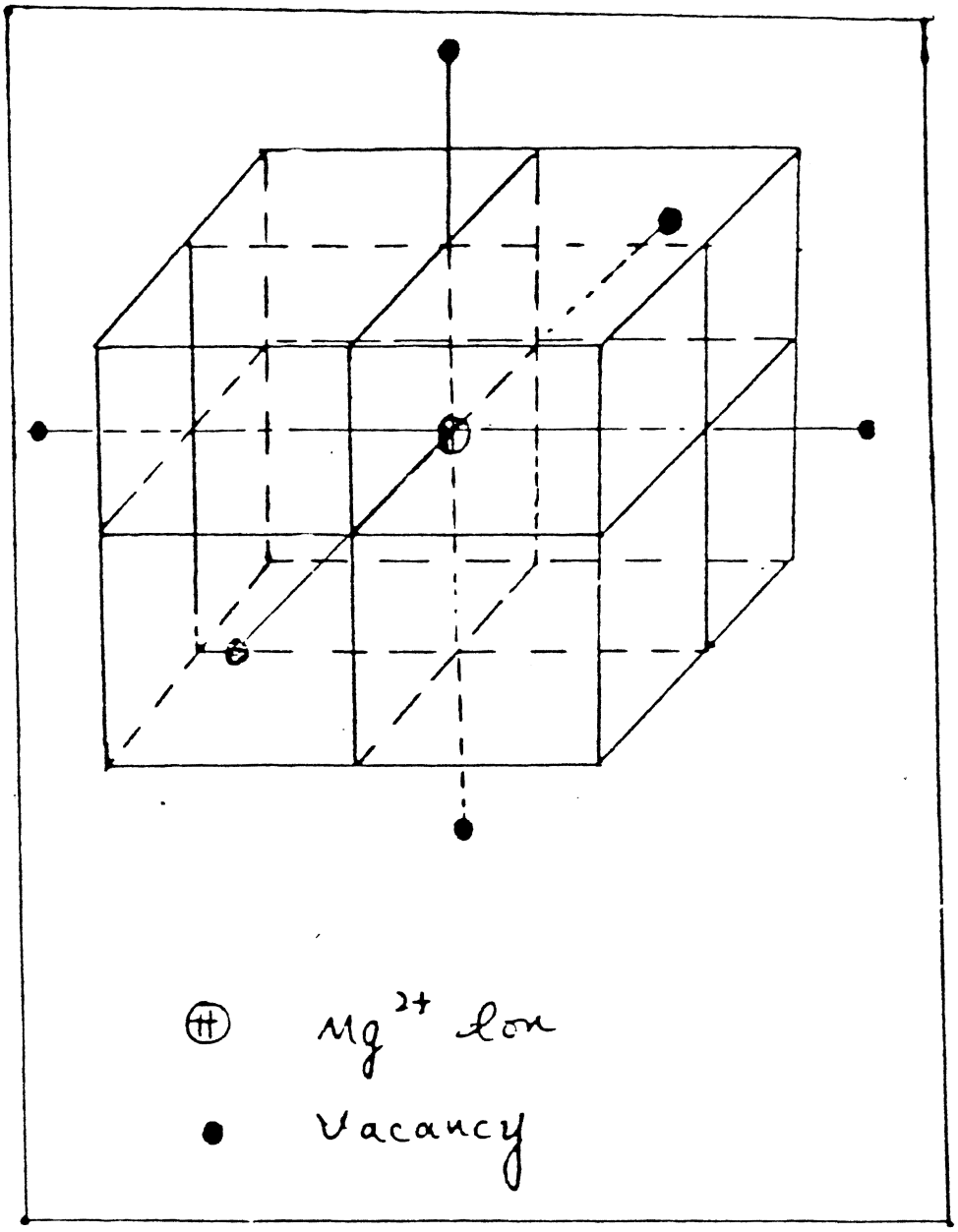

Figure 5. n.n.n. Configurations for a Dipole

potential. The experimental evidence for the existence of the dimer was reported by Unger and Perlman [5]. However, a dimer is unstable as the binding enthalpy of the dimer was found to be very small in a number of materials. For $NaCl:Pb^{2+}$, it is ≤ 0.13 ev and for $NaCl:Ca^{2+}$ $\leq$ 0.02 ev [6] and [7]. Several possible configurations for a dimer are shown in Figure 6 [8].

Trimer

Simultaneous encounter of three dipoles can form a "trimer". The binding energy of the trimer for $LiF.MgF_2$ is about 0.95 ev [9]. Again, coulombic interaction causes these dipoles to cluster together to form a single body. The concentration of the trimers depends upon the thermal history of the material. Experimentally, it is possible to obtain a particular content of trimers by the application of some special annealing treatments which will be described later. In analogue to the dimer, there are several proposed configurations for the structure of a trimer and they are shown in Figure 7 [8].

Precipitate

The aggregation of six dipoles forms a "precipitate". The structure of the precipitate, shown in Figure 8, was originally determined, using x-ray diffraction techniques, by Suzuki [10] for 6 $NaCl.CaCl_2$. Lilley and Newkirk [11] found that the precipitation of the phase 6 $LiF.MgF_2$

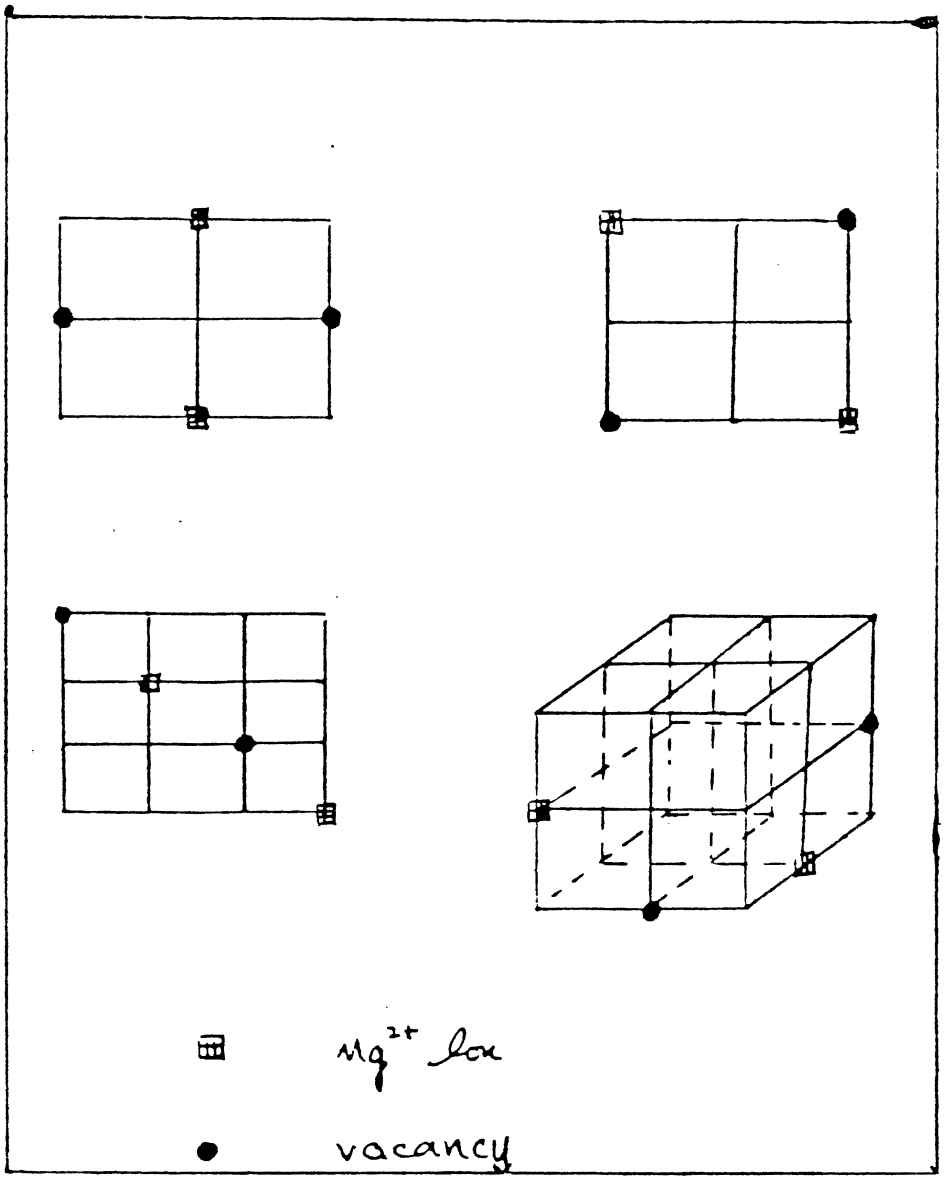

Figure 6. Several Possible Configurations for a Dimer

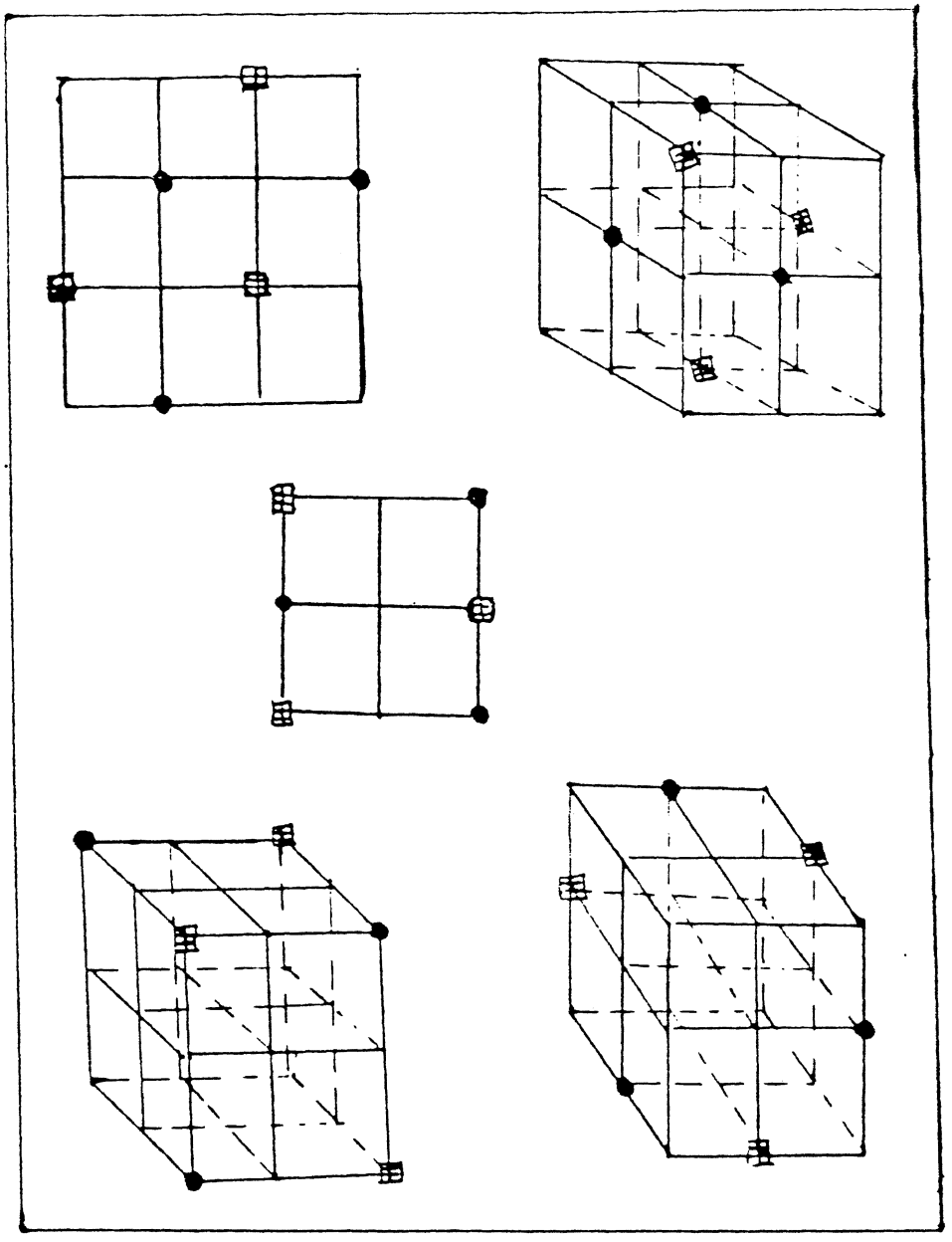

Figure 7. Possible Configurations of a Trimer

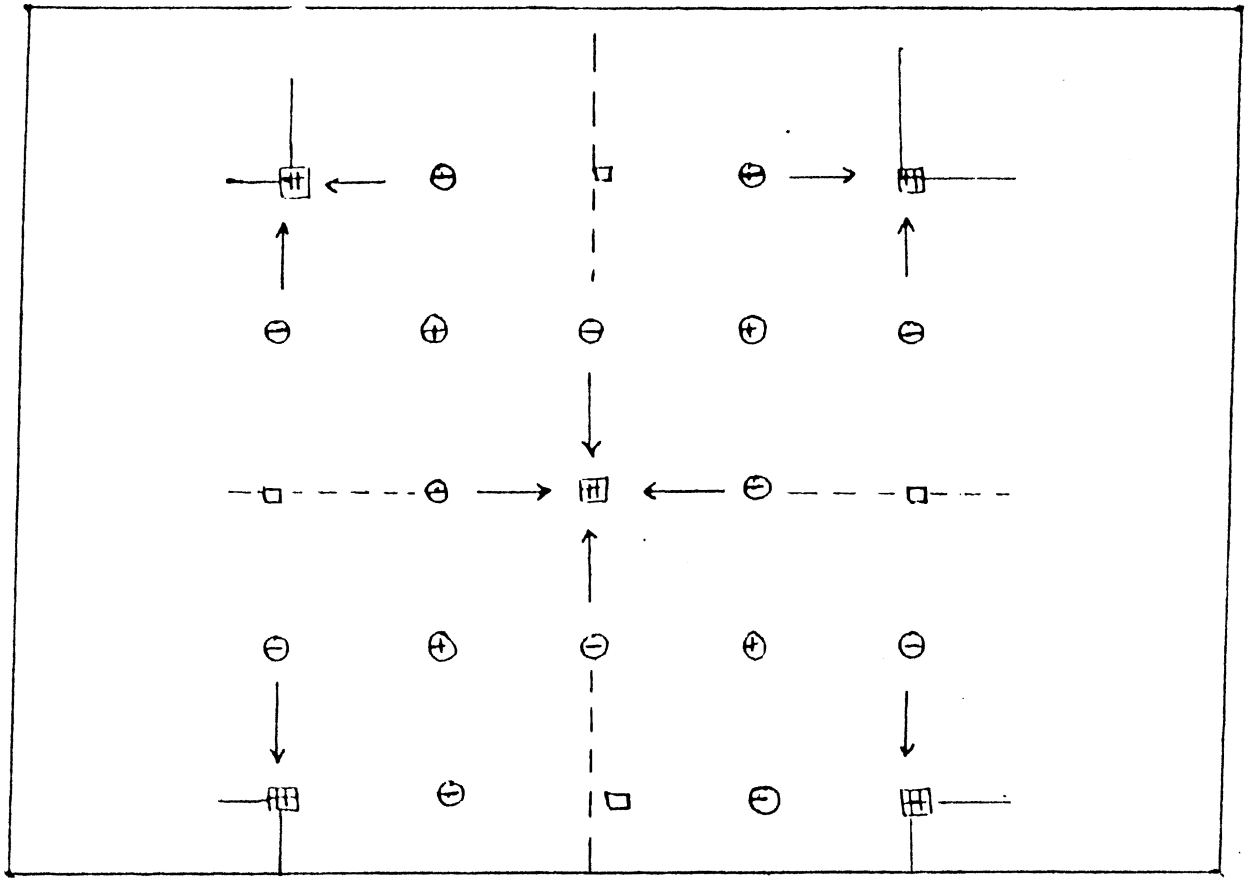

Figure 8. Arrangement of Ions in the (100) Plane of the Proposed Unit Cell of GNaCl.CdCl (10),

Cl^- Ion Displacement : Cd^{2+} ;

$\oplus = Na^+$, $\ominus = Cl^-$; ▦ = Cation Vacancy

occurred in LiF/MgF_2 system in crystals which contain about 450 mole ppm Mg^{2+} dopant. One of their conclusions is that the effect of the precipitation on the TL response can be significant. Finally, the configuration of 6 $LiF.MgF_2$ is shown in Figure 9.

Ti-related Defects (Ti^*)

Ti^{4+} is an essential component of LiF:Mg.Ti in TL dosimetry. Due to the charge neutrality requirement, Ti^{4+} can be bound to three cation vacancies at near-neighbor positions, or to three OH^{-1} or three O^{-1} ions, or to a combination of cation vacancies, O_2^{-1} and OH^{-1} ions [12]. In TLD-100, it is assumed that such defects are well dispersed during crystal growth and the mobility of the defect is low compared with that of the Mg^{2} -related defects. Traditionally, an optical absorption band at 200 nm is believed to be caused by Ti-OH [12].

In summary, I-V dipoles, dimers, trimers and precipitates are major defects associated with Mg^{2+} impurity. Due to the presence of these defects, the fading of TL may take place. Because these defects probably act as "traps" in TL, then, as the relative concentrations of these defects are altered, changes in TL are expected.

One way to study the defect structure is by ionic conductivity. The measurements made with this technique can highlight the temperature regimes within which one particular defect predominates over another. In Figure 10, ionic

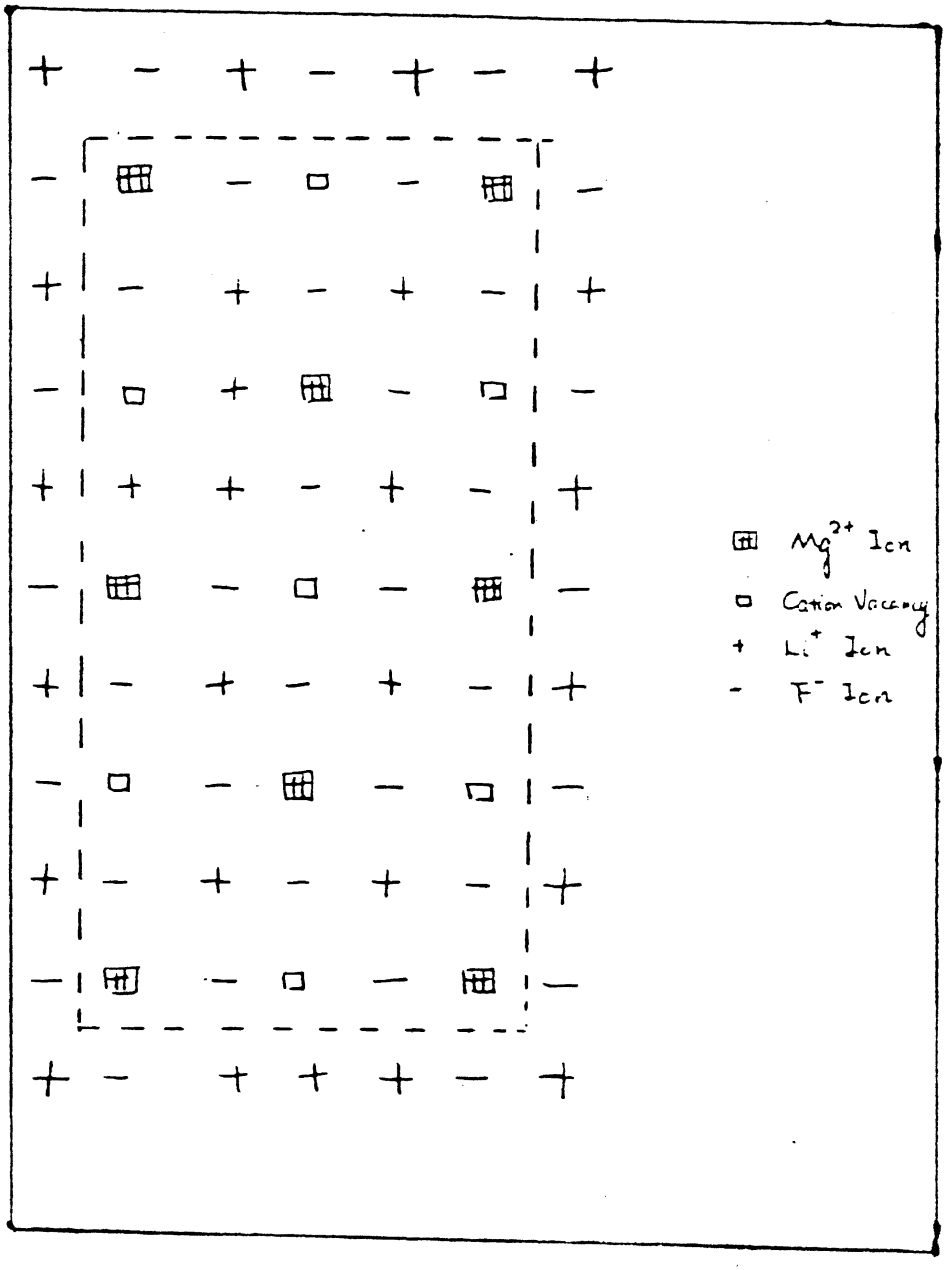

Figure 9. Suzuki Phase of $6LiF.MgF_2$

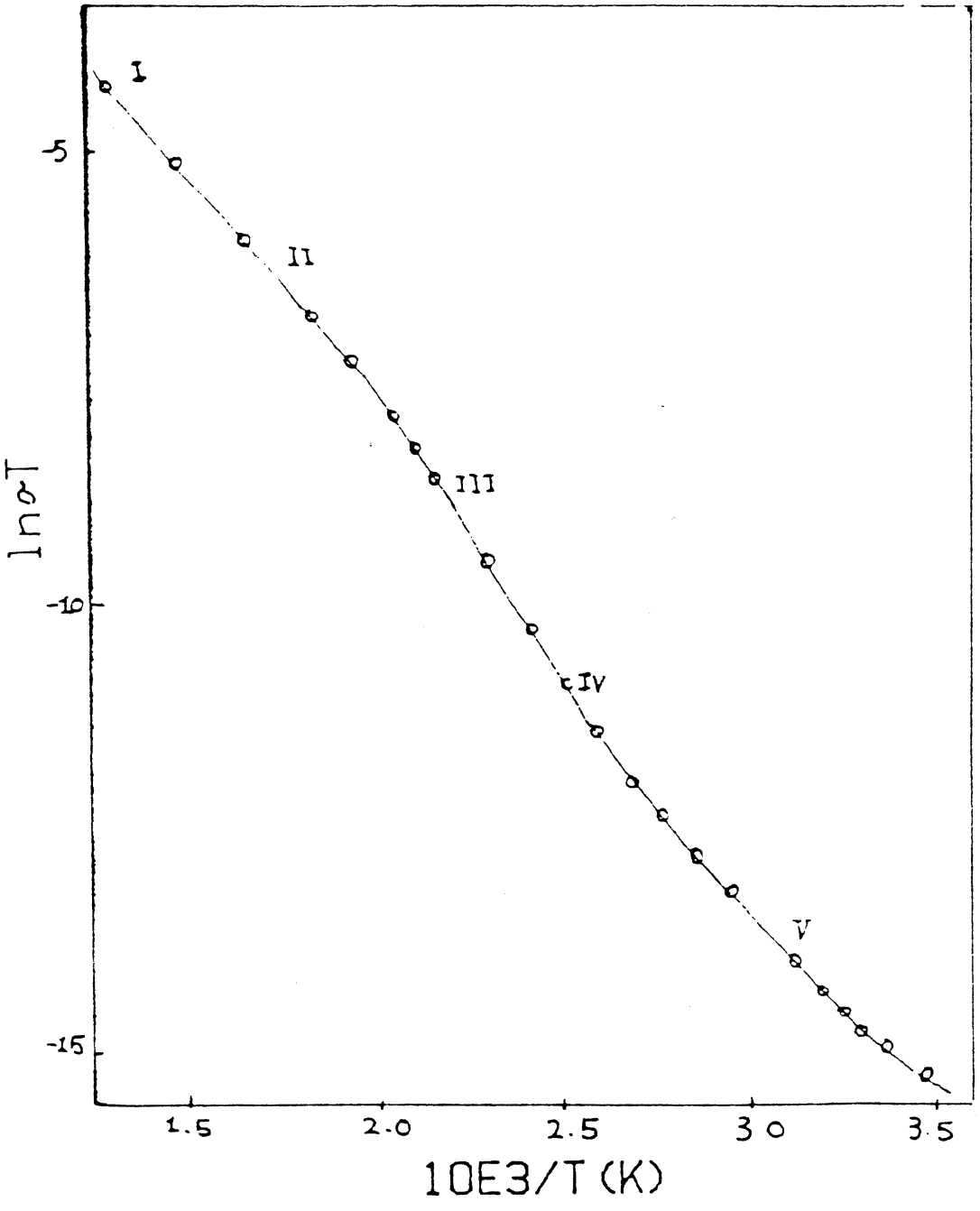

Figure 10. Ionic Conductivity Plot for $NaCl{=}Mg^{2+}$;10 ppm [1]

conductivity versus temperature is illustrated for Nacl:Mg. As seen from the figure, these are generally five regions. They are:

1) Region I: intrinsic conductivity found at high temperatures. Thermally generated free vacancies dominate.

2) Region II: extrinsic conductivity, where association between divalent cation impurities and vacancies is negligible. Impurity related free vacancies dominate.

3) Region III: association region in which vacancies and divalent ions form predominantly n.n. or n.n.n. I-V dipoles.

4) Region IV: aggregation and precipitation will occur. At first, as the temperature is lowered, more vacancies will associate with impurity ions. As a result, an increase in activation energy follows. Further decrease in temperature will cause the concentration of impurities in the crystal to exceed the solubility limit and precipitation is produced.

5) Region V: low temperature association was also reported [1]. This region can extend to room temperature.

Figure 11 is also provided here for further illustration.

Clustering Relations and Rate Equations

Several chemical reactions can take place due to the presence of the defects described above. The reactions may affect TL, expecially the fading of TL. Taylor and Lilley

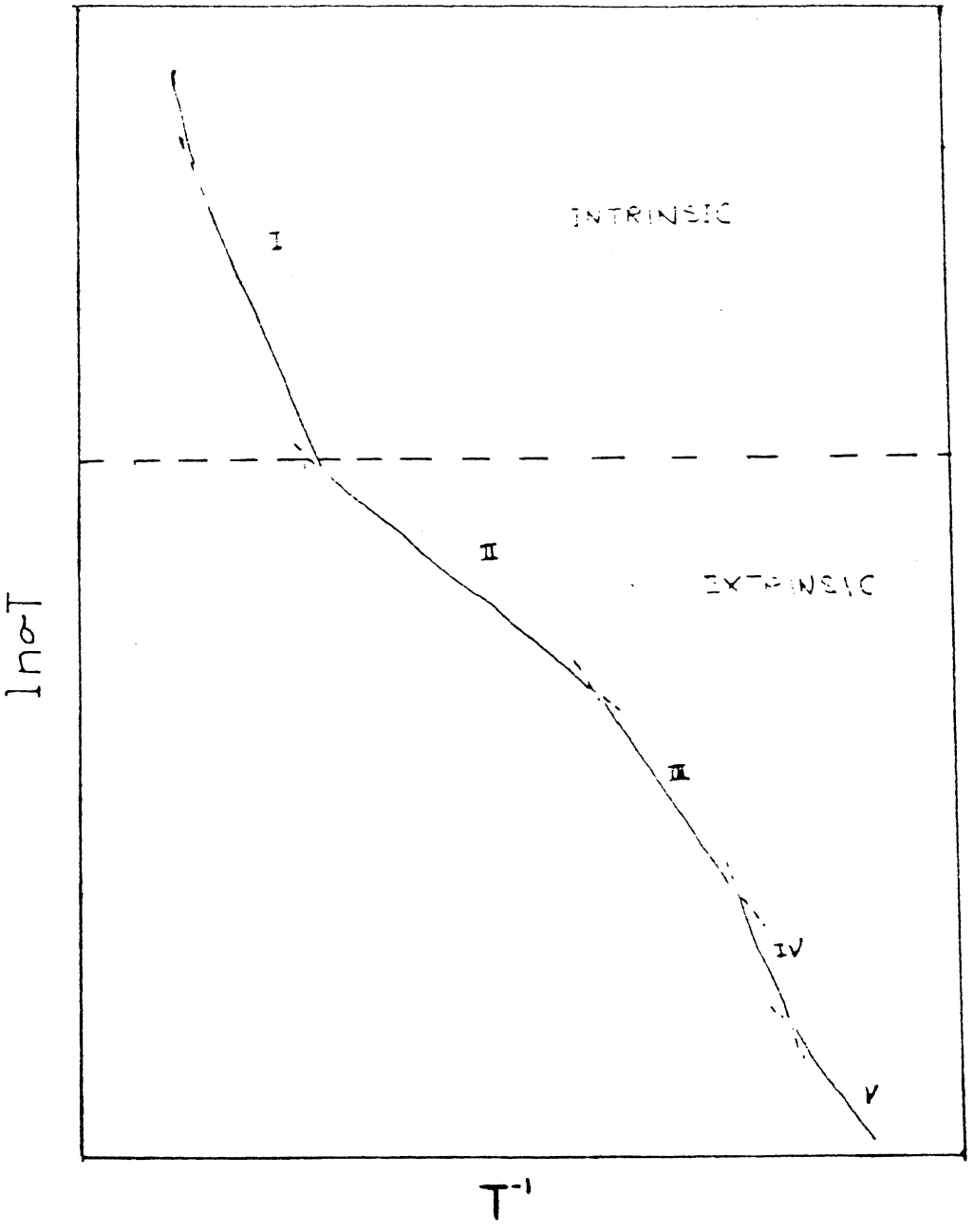

Figure 11. Schematic Plot of Ionic Conductivity Versus T^{-1} Showing Different Regions

[13] for the first time pointed out that this fading is due to the clustering of Mg-defects. Since then, a great deal of effort has been made to understand the mechanism of the clustering process. The long-existing controversy concerns whether or not the clustering process is a pure second-order dimer formation or a pure third-order trimer formation reaction. The problem originated from the observed decay of I-V dipoles with time, as shown in Figure 12, in which the decay proceeds at different rate in three regions. They are:

1) An initial decay;

2) A "plateau", or nearly constant region;

3) A further decay.

In the case of 2), a possible explanation is that the following reaction occurs in which dipoles are directly converted into trimers:

$$3[Mg^{2+}V^{-}] \rightleftharpoons [Mg^{2+}V^{-}]_3, \qquad (2.1)$$

where

$[Mg^{2+}V^{-}]$ = a Dipole,

$[Mg^{2+}V^{-}]_3$ = a Trimer.

In the case of 3), the region consists of further aggregation into high-order complexes and is found to follow a third-order law:

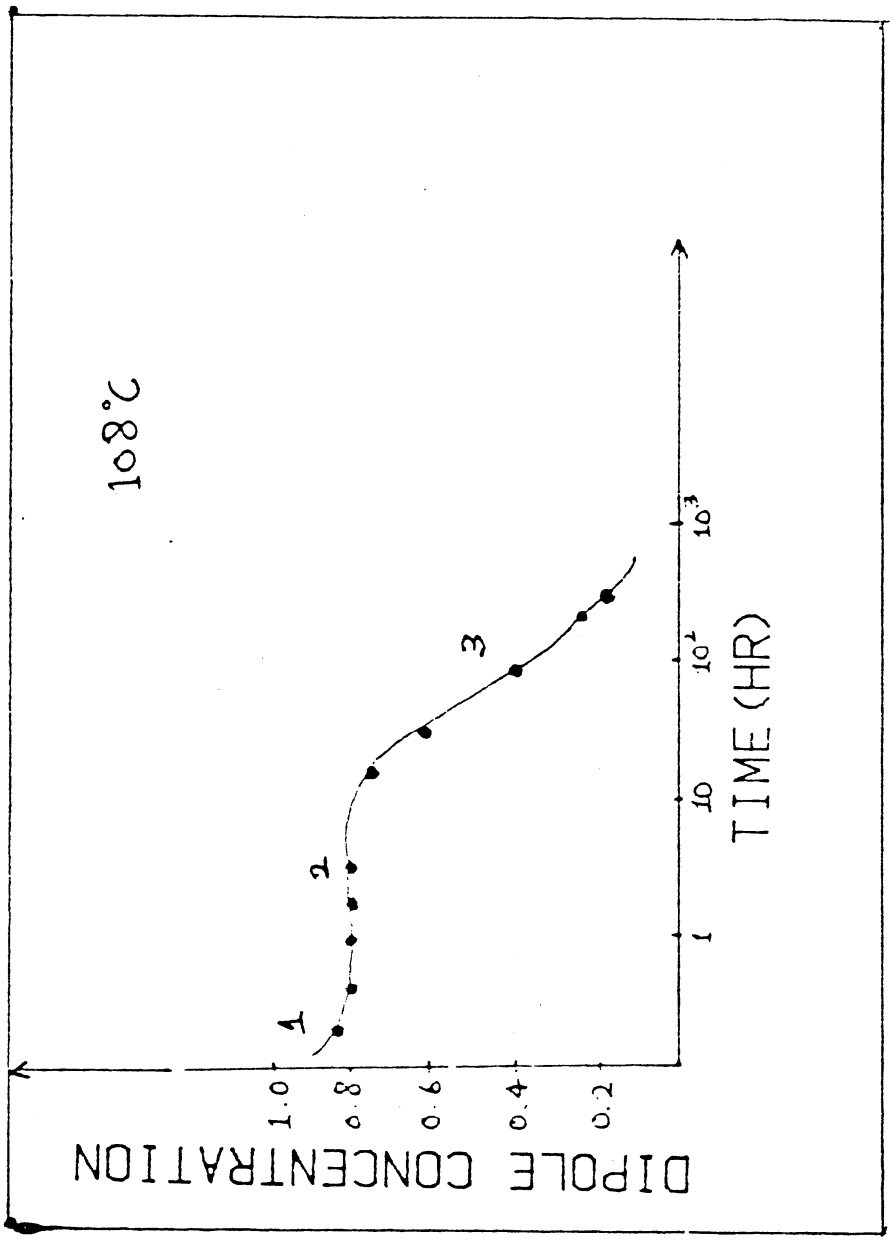

Figure 12. Decay in Dipole Concentration in a Sample of KCl:S 2+ . 140 ppm [1]

$$[Mg^{2+} - V^{3}] + n[Mg^{2+} - V^{-}] \rightleftharpoons \text{higher complex} \qquad (2.2)$$

However, main controversies still exist about the explanations of the first and the second stage. During the first stage, dipole decay is fast. Dryden, Cook and Harvey [14] and [15] were the first to analyze the kinetics of dipole aggretation of several divalent impurities in NaCl and KCl using the dielectric absorption technique. They concluded that the initial stage of the aggregation process was governed by a third-order kinetics law. This finding is equivalent to considering that the first aggregation product is a trimer formed directly from three dipoles. This result is rare since even in the gas phase the probability of three-body encounter is low compared with that of two-body encounter. Later, Crawford [16] proposed an alternative which finally leads to third-order kinetics through an intermediate stage. The two-stage reaction is:

a) Two dipoles form a loosely bound dimer.

b) Subsequently, the dimer captures a third dipole to form a trimer.

McKeever and Lilley [16] agreed with Dryden about the second stage kinetics and both thought the plateau is the equilibrium between dipoles and trimers. Furthermore, they obtained additional evidence that if the dimerization process indeed occurred, it did so at the very beginning of the first stage.

Unger and Perlman [17] and [18] analyzed the original data of Dryden's as well as their own. The conclusion was

that a pure second-order reaction governed the first and the second stages of the aggregation provided that the back reaction of the following reaction was considered.

$$2[Mg^{2+}V^{-}] \rightleftharpoons [Mg^{2+}V^{-}]_2 \qquad (2.3)$$

where

$[Mg^{2+}V^{-}]_2$ = a Dimer

Unger and Perlman also pointed out that a mistake Dryden had made was in the neglect of the back reaction of the reaction (2.1). According to their opinion, the back reaction is always important and has to be taken into account when experimantal data are analyzed.

A third group headed by Hartmanova, Thurzo and Besedicova [19] performed some similar experiments. The results obtained made them propose that the dimer are the initial product in the aggregation process. The detailed study and excellent analysis made their conclusions quite convincing. However, the exact kinetics of the initial stage is still contradictory.

In general, a clustering process in which n dipoles combine to form an n-mer can be expressed by the following reaction:

$$n[Mg^{2+}V^{-}] \underset{K_2}{\overset{K_1}{\rightleftharpoons}} [Mg^{2+}V^{-}]_n , \qquad (2.4)$$

where n is number of free dipoles; K_1 is forward reaction rate constant; and K_2 is back reaction rate constant.

K_1 and K_2 affect the concentration of dipoles at this stage [20]. The rate equation governing this process is:

$$\frac{dx}{dt} = K_1 X^n + K_2 X_n \qquad (2.5)$$

where X_n is concentration of n-mers; X is concentration of free dipoles. With the condition $X + NX_n = X_o$ where X_o is initial concentration of dipoles.

These are two special cases. They are described separately.

Dimer Formation (n=2)

The Equation (2.5) reduces to:

$$\frac{dx}{dt} = - C_3 X^2 + C_4 X_2 \qquad (2.6)$$

where C_3 is forward reaction rate constant; C_4 is back reaction rate constant; X is concentration of free dipoles; X_2 is concentration of dimers.

Equation (2.6) is good under the following assumptions:

1) The formation and disassociation of trimers is negligible.

2) The concentration of trimers is neglected.

3) The plateau region in the dipole-decay curve is obtained for $X/X_o >> 1/3$.

Under these conditions, the solution to equation (2.6)

will be:

$$\ln[(n-b)/(n-a)] = (a-b)C_1 t + \ln[(n_o-b)/(n_o-a)], \quad (2.7)$$

where

$a = X_s$ the equilibrium concentration of free dipoles;

and

$b = -X_o X_s /(X_o - X_s)$.

So, if the kinetics are second-order, a plot of $\ln[(n-b)/(n-a)]$ versus t will yield a straight line.

Trimer Formation (n=3)

In this case, Equation (2.6) reduces to:

$$\frac{dx}{dt} = -C_5 X_3^3 + C_6 X_3, \quad (2.8)$$

where X_3 is concentration of trimers; C_5 is forward reaction rate constant; C_6 is back reaction rate contant.

With the conditions

1) $X + 3X_3 = X_o$; 2) X_2 is negligible; 3) $X(t=o) = X_o$; 4) At the plateau the equilibrium condition is:

$$C_5 X_s^3 = C_6 (X_o - X_s)/3,$$

under these conditions, the solution to Equation (2.8) is:

$$\ln(X-a) = C_5 t X_s^2 (3X_o-2a)/(X_o-a) + \ln(X_o-a)$$

So if the kinetics of clustering are third-order, a plot of ln(X-a) versus the annealing time t will give a straight line.

An important factor affecting the concentration of dipoles is the rate constant, as can be seen from Equation (2.5). The detail of such an excellent analysis was given by Riveros and co-workers [20]. They also established criteria according to which the neglect of one of the two terms in right side of Equation (2.5) can be made. They came to the convincing conclusion that dimers are indeed formed during the earlier stage of aggregation from their experimental data.

In summary, it seems that all evidence indicates the formation of dimer is in the very initial stage and soon the formation of trimer follows up to the plateau where equilibrium state between trimers and dipoles is reached.

A final word about dipoles, trimers, and dimers is that the binding energy of them will determine their stabilities. Since in general each of these defects is in a metastable state, the greater the formation energy, the more stable the defect is. Trimers have a formation energy about 1.00 ev [21]; dimers have a 0.02~0.13 ev [22] and dipoles have ~0.37 ev [23]. Therefore, generally speaking, a trimer is more stable than a dipole, and dipoles than dimers.

TL Glow Curve

Historical Background and Defects Relevant to TL

In the temperature range 25 °C. to 400 °C., there are at least 5 TL peaks as illustrated in Figure 13. Room-temperature-irradicated TLD-100 has TL peaks at ~100 °C. (peak 2), ~148 °C. (peak 3), ~184 °C. (peak 4), and ~210 °C. (peak 5), at heating rate of 1 °/S [24].

The TL peaks have been related to Mg^{2+}-type defects such as dipoles, trimers, etc. for decades. Initially, Jackson and Harris [25] found an apparent correlation between the decay of peaks 2 and 3 and the OA band at 380 nm (Figure 14), and between peaks 4 and 5 and the band at 310 nm. In an earlier time Grant and Cameron [26] investigated the pre-irradiation isothermal (67 °C.) decay of $[Mg^{2+} V^{-}]$ dipoles (using dielectric loss) and of TL and found a correlation between TL peak 2 and I-V dipoles. The correlation is shown in Figure 15. However, Taylor and Lilley [27] repeated the experiments performed by Grant and Cameron. The conclusion they reached was that Ti^{*}, which is Ti^{4+} associated with O_2^{-1}, OH^{-1} ions and/or vacancies, is responsible for TL peak 2, instead of IV dipoles. Comparison of Grant and Camerons's procedure with that of Taylor and Lilley's revealed that the annealing temperatures were taken differently. In the former case, 67 °C., 81 °C., and 95 °C. were used separately as annealing temperatures. In the

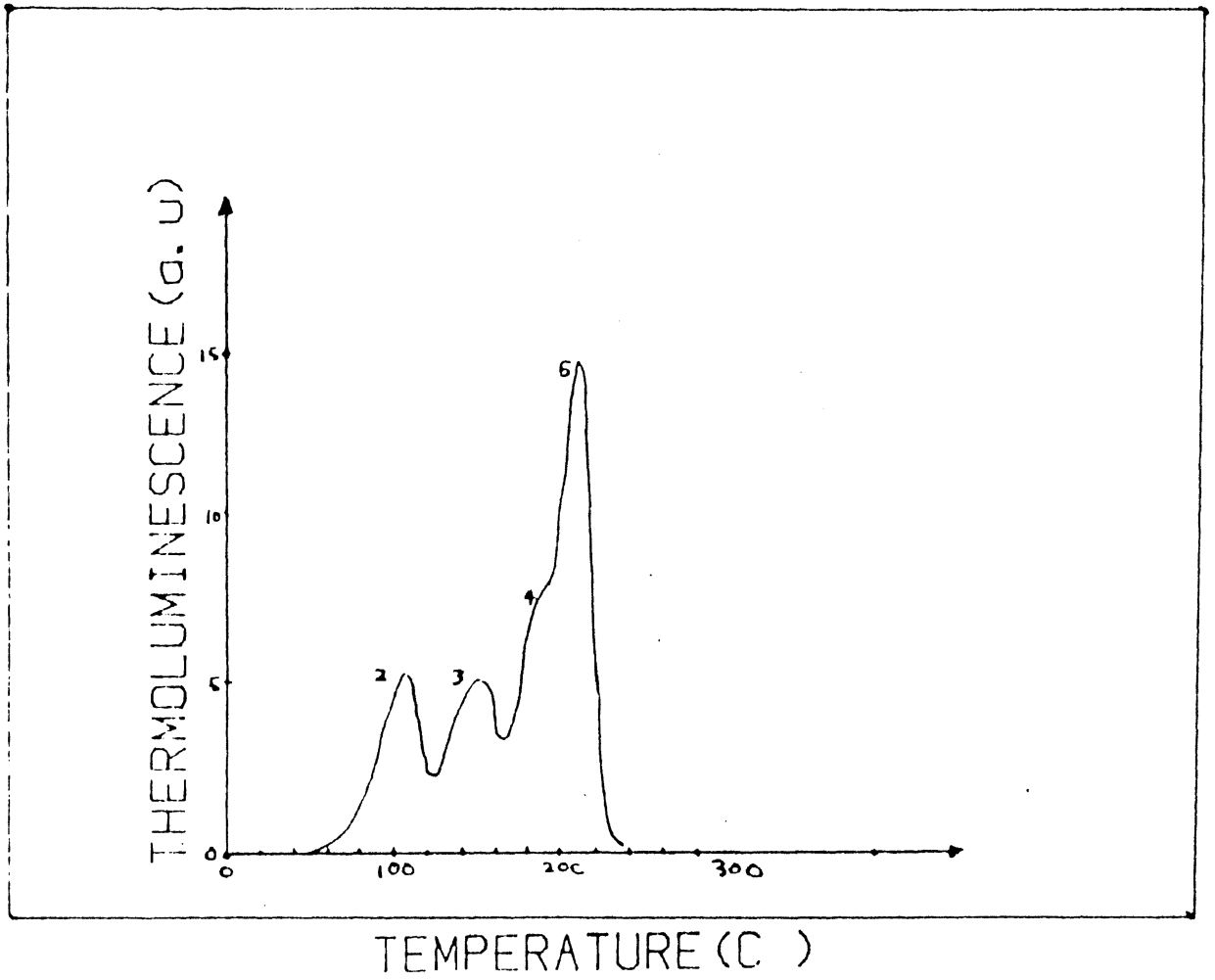

Figure 13. Typical Glow Curve from TLD-100. The Peaks Referred to in the Text are Labled. [23]

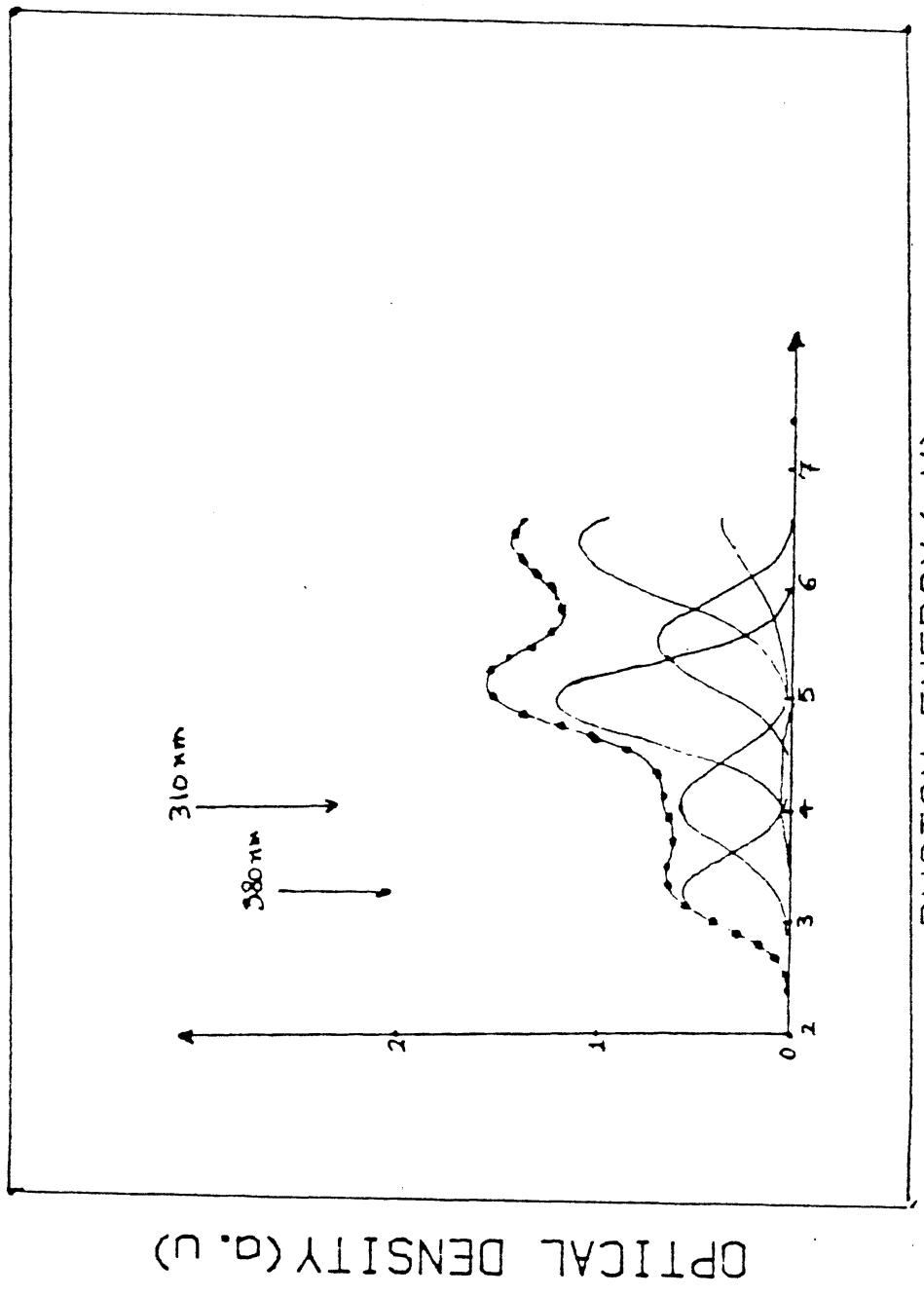

Figure 14. OA and Resolved Gaussian Bands [28]

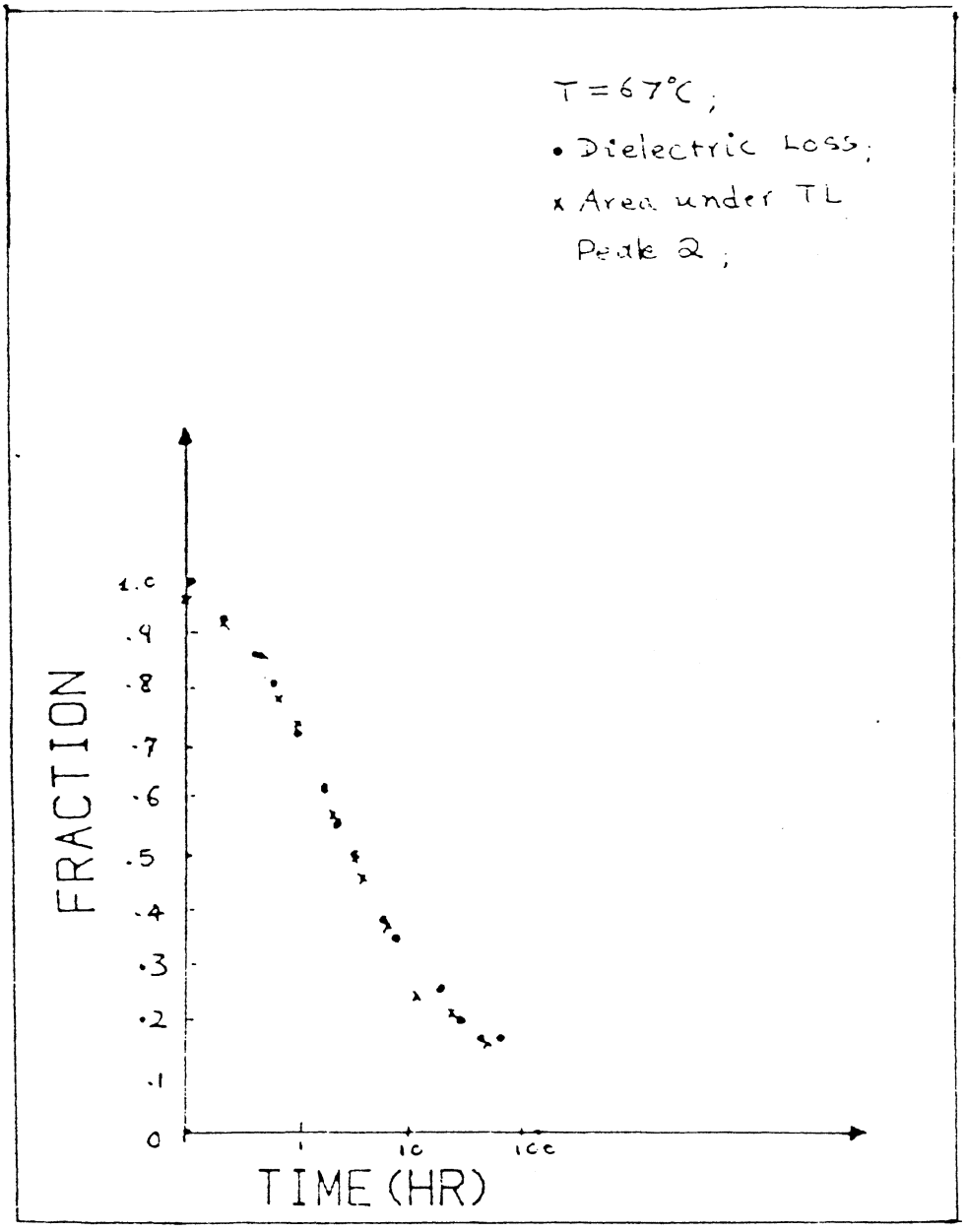

Figure 15. Correlation of the Fraction of the ^{o} 105 C. Glow Peak Remaining after Pulse Annealing for t Hours Prior to Irradiation with the Dielectric Loss Due to Dipoles after Pulse-Annealing for the Same Time t [26]

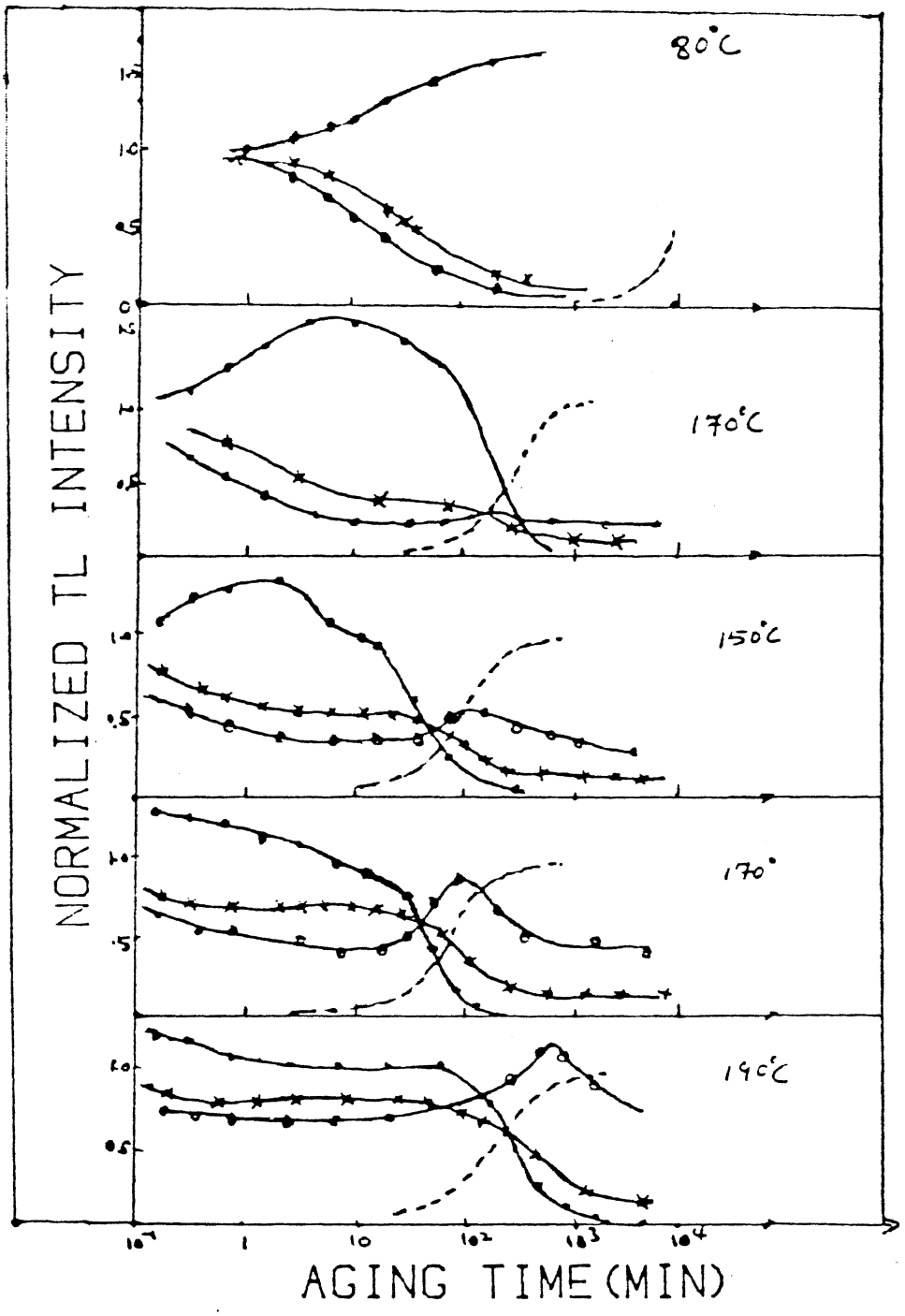

Figure 16. Normalized Dipole Concentration (+), Peak 2 Intensity; (o); Peak 5 Intensity; (.); and Fraction Precipitation (---) versus Aging Time[27]

latter case, 80°C., 170°C., 150°C., 170°C. and 190°C. were used. The results of Taylor and Lilley are shown in Figure 16. Unfortunately, the correlation of the annealing at 81°C. was not presented by Grant and Cameron. But, that makes no difference, because both the decay of dipoles and of TL peak 2 were measured at the same annealing temperature. In other words, if the dipoles are really directly related to TL peak 2, then the rate of decay of TL peak 2 should be nearly equal to the rate of decay of dipoles, whatever annealing temperature is chosen. Therefore, the questions arise, "what actually causes TL peak 2 -- I-V dipoles or Ti^{*} ?"

Similarly, what causes TL peak 5, trimers or something else? Careful study reveals that Taylor and Lilley did not include the responsibility of any Mg^{2+} -type defects for TL peaks 2 and 5. This can not be absolutely true for the properties of TL peak 2 in TLD-100 and the Ti-only doped LiF (peak position, annealing behavior, emission spectrum) are entirely different [28]. Consequently, Mg^{2+} must be involved in the production of the TL peak 2. The question now is, whether or not I-V dipoles are directly responsible for it? Similarly, are trimers responsible for peak 5?

The answers to these questions are the main topics of this study. The previous annealing procedure used by Lilley and Taylor was adopted. There are two main differences. First, after the 400°C./1/2 hr. isothermal anneal, the quench was carried out by dropping the crystal quickly into

liquid nitrogen, instead of dropping it onto a metal plate. The former can ensure a greater concentration of dipoles than can the latter [29]. Second, instead of annealing the sample at a constant temperature following the quench, the crystal was heated up linearly to a given temperature and then rapidly cooled back to room temperature. This method is known as "pulse annealing". The concentration of dipoles was then monitored by the TSDC method.

Furthermore, the annealing procedures used in TSDC experiment were identically repeated for TL and OA measurements. After these measurements, we obtain a relation between the dipole concentration and the pulse annealing temperature (PAT). Similar relationships will be obtained for TL and OA, as a function of PAT. Through these relationships, whether or not there is a correlation between TL peak 2 and the dipole will be clarified.

Attention was also paid to PL measurements. Townsend et al [30] and Fairchild et al [31] analyzed the spectra of the light emitted from TLD-100 during TL production and found the presence of several closely-spaced emission bands and that the wavelength of the overall emission band depended upon which TL peak was being activated [28]. It has been believed that Ti is involved in the luminescence emission process in this material. Townsend et al suggested that Mg perturbs the emission which is caused by charge recombination at Ti sites [30]. In the measurements of the emission spectra from LiF during TL, they monitored

that the main TL peaks in TLD-100 (e.g., peaks 2, 3 and 5) emit at different wavelengths. The higher the peak temperature, the lower the emission wavelength. They found these peaks to have emission maxima at ~460 nm (peak 2, 115 °C.); ~435 nm (peak 3, 150 °C.) and ~425 nm (peak 3, 0 °C.). Why does this happen? Suppose the suggestion of Townsend and colleagues is true, then the Mg perturbing the emission at ~460 nm (peak 2, 115 °C.) may be different from that at ~425 nm (peak 5, 200 °C.). Indeed, the possible correlation [26] between I-V dipoles and TL peak 2 and trimers and TL peak 5 reminds us that probably the dipole is disturbing the emission producing peak 2, and the trimer is doing the same for peak 5. Due to the different forms of the Mg, the perturbations are different accordingly. The variation in the perturbation finally results in the shift of the emission maxima during TL. Therefore, the correlation established by Grant and Cameron [26] is consistent with the observations from the Townsend group. This consistency encouraged us to suggest that the same correlation may possibly be obtained if the annealing processes used in TL were repeated in PL. Since Ti-OH is believed to cause the OA band at 200 nm [28], emission spectra can be obtained if we excite the crystal at about 200 nm. Furthermore, if dipoles and trimers do disturb the luminescence centers associated with Ti-OH, we can expect the emission spectra to be different after the sample is subjected to different annealing treatments. In addition,

Delgado [32] believed that TL peak 5 is related to the OA band at 200 nm after he studied the effect of thermal treatments (quenching and annealing) on the OA and PL spectra of the Ti-related 200 nm absorption band. These studies and ideas lead us to perform PL measurements to establish possible correlations between PL and TL.

The description and discussion of the experiments form the basis of this thesis.

CHAPTER III

EXPERIMENTAL DETAILS

Thermally Stimulated Depolarization Current

In 1964, Bucci and Fieschi [33] introduced the Thermally Stimulated Depolarization Current technique which is a powerfull tool for studying electric-dipole relaxations in ionic crystal. Due to ionic motion, various types of polarizations can be formed in the crystal [1]. Particularly in alkali halides impurity-vacancy, (I-V) dipole polarization has been the center of much attention, because it was correlated to the TL peak 2 [26]. The TSDC method mainly consists of the following:

1) The sample is first polarized in a static field E, for a time t, at a temperature Tp. The temperature should be high enough such that the probability of the orientation of I-V dipoles is high and not too high, in order to avoid heavy space-charge polarizations. In alkali halides, the suggested polarization temperature is around 0^{o} C. [34].

2) The solid is cooled down to a temperature To<<Tp, where any ionic motion is completely prevented, then the field is taken off.

3) The solid is subsequently warmed up at a constant heating rate , and the discharge current is registered as

a function of temperature.

When the release of the electric static energy is due to the relaxation of the electric dipole, the peak of the function i(T) corresponds to the presence of a particular type of dipolar imperfection in the crystal, and can give information as to the relaxation parameters and the numbers of dipoles involved in the process.

Theory of Thermally Stimulate Depolarization Current Method

The relaxation time of an ionic dipole is $\tau = \tau_o \exp(-Ej/k_B T)$. Ej is the activation energy for dipole reorientation, i.e., the energy barrier which divides two equivalent dipole orientations, A and B (Figure 17).

At temperature Tp (polarization temperature), at which τ (Tp) is rather short, a static electric field Ep (polarization field) is applied to the sample for a time interval tp (polarization time) much longer than τ (Tp). In this way, dipoles are oriented to equilibrium (Figure 17). The sample, with the field always on, is cooled to T_f (the "frozen in" temperature), at which τ is very long (since Tf<<Tp). The field is turned off (c) (Figure 18), the dipoles, previously oriented remain in their preferred orientations, since τ (T_f) is extremely long; i.e., the polarization is frozen in. Then the sample is connected to the electrometer and heated at a constant rate, i.e.,

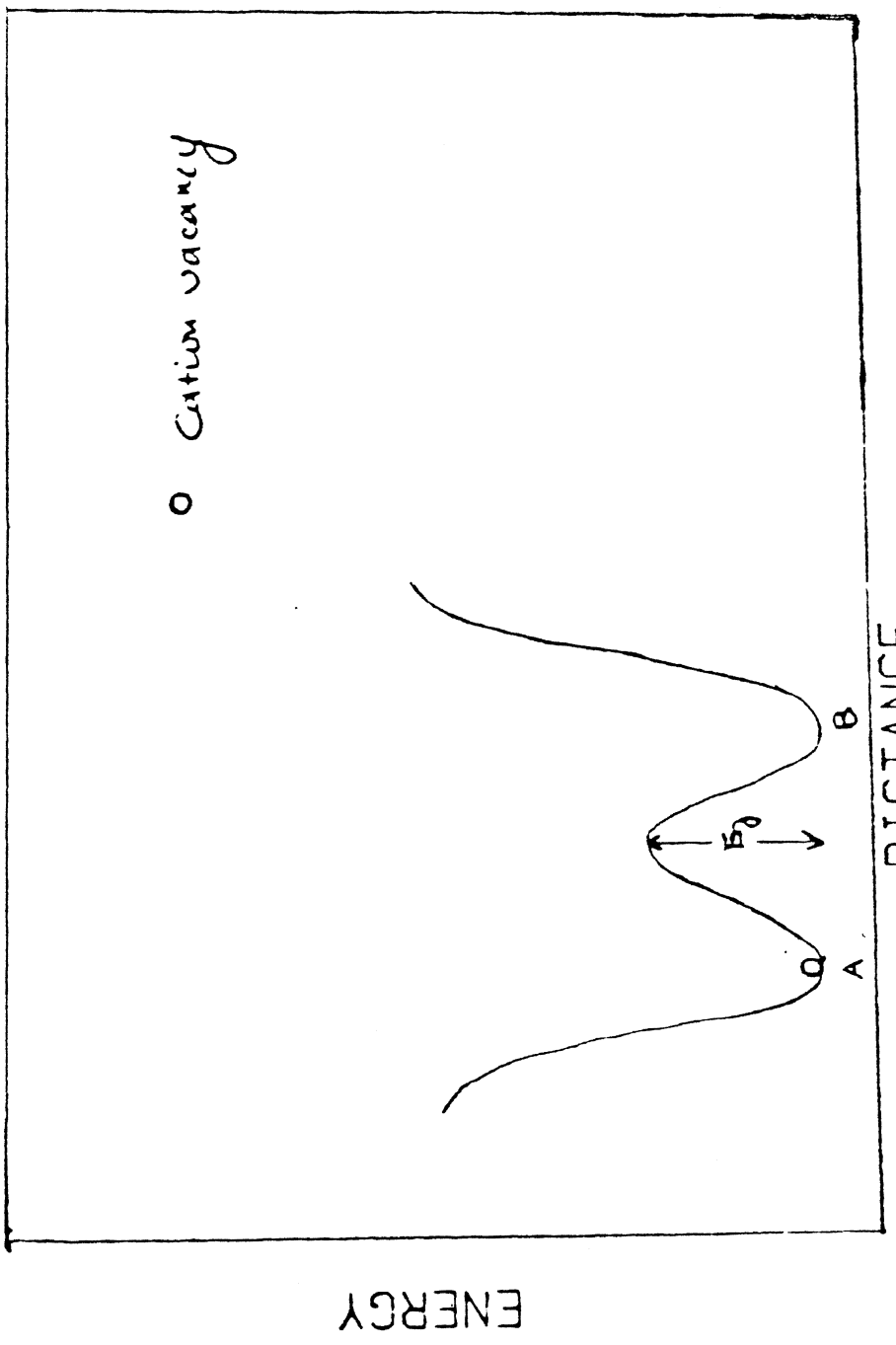

Figure 17. Two Equivalent Cation Vacancies Form Two Equivalent Dipole Orientations

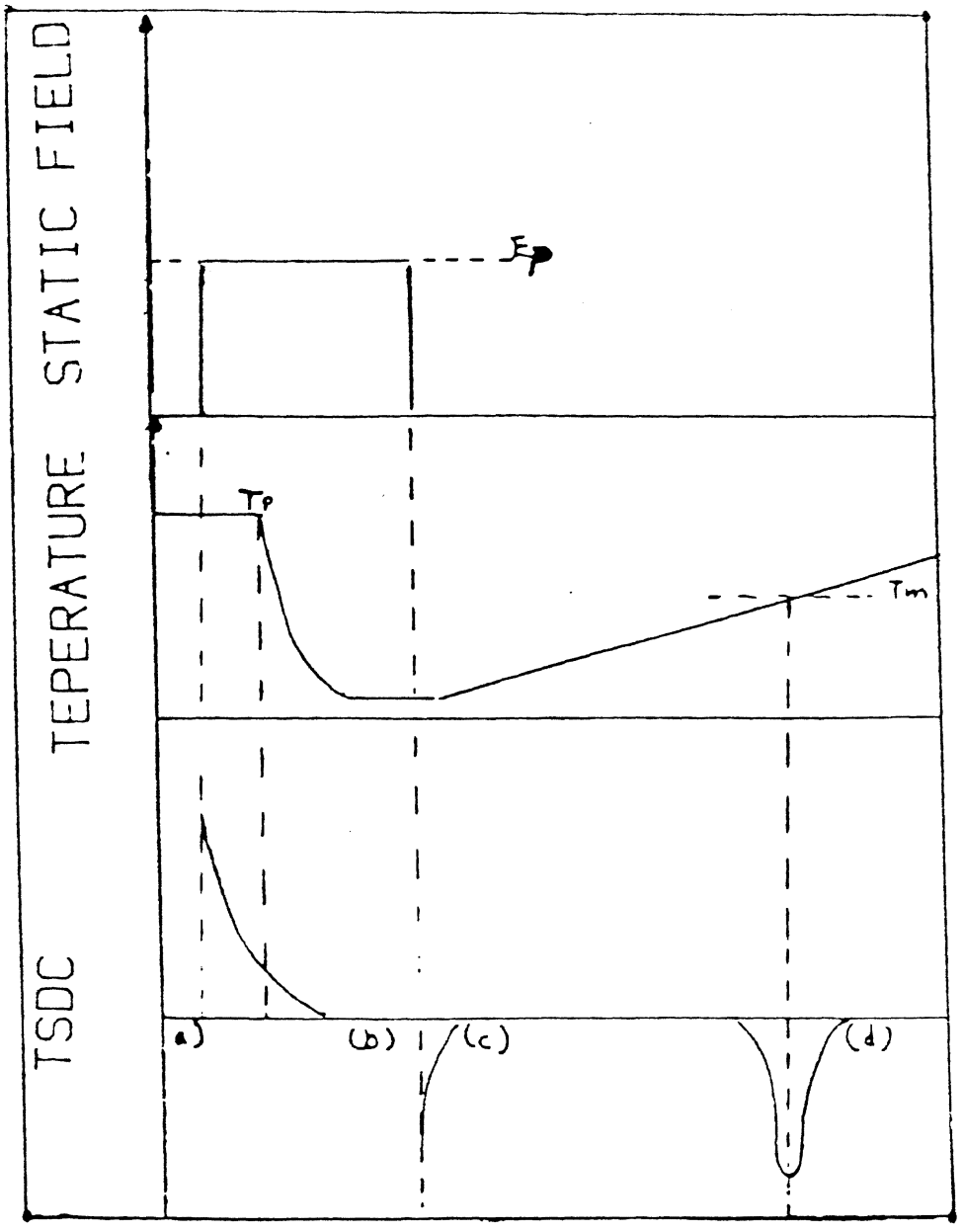

Figure 18(a). Layout of TSDC Technique

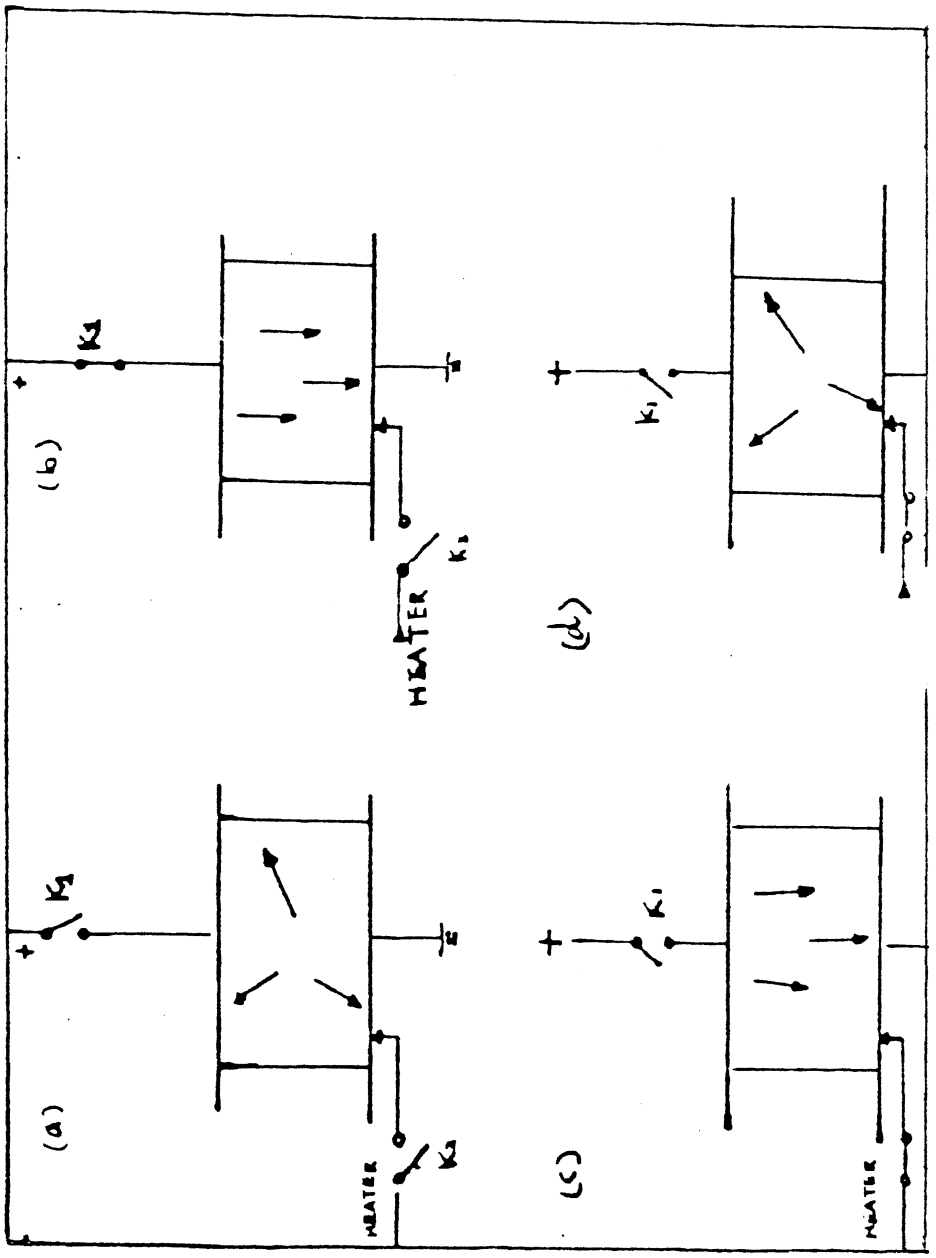

Figure 18(b). Basic Four Steps of TSDC Process
(a) Ep = 0, T = Tp >> Tf
(b) Ep = Ep, T = Tp >> Tf
(c) Ep = 0, T = Tf << Tp
(d) Ep = 0, T = Tp >> Tf

$\frac{dT}{dt} = \beta$. The dipoles experience relaxation times which become shorter and shorter as they gain mobility and hence they attain random orientations. This means that the sample polarization is changing with time, i.e., according to Maxwell's equation, a displacement depolarization current j(T) is monitored (d) (Figure 18). The current increases by increasing the temperature until the frozen-in polarization is exhausted, hence j(T) drops to zero. The j versus T plot thus gives the TSDC peak.

Basic TSDC Equations for Non-interacting Dipoles with a Single E.

In this case, the reorientation of free dipoles in the low-concentration limit is assumed to take place without interacting with the other dipoles which are present in the crystal. Under these conditions, the time dependence of the polarization P(t) can be described with first-order monoenergetic equations:

$$\frac{dP(t)}{dt} = -\frac{P(t)}{\tau} \qquad (3.1)$$

$$\text{with } \tau = \tau_o \exp(-E/K_B T) \qquad (3.2)$$

where τ_o is reciprocal frequency factor, and E the activation energy of dipoles for reorientation.

The decay of polarization due to the disorientation of dipoles following the removal of the static electric field

at t = 0 and temperature T, which is the solution to Equation (3.2), is given by:

$$P(t) = P(0) \exp\left(\frac{-t}{\tau(T)}\right) \tag{3.3}$$

where P(0) is the "frozen in" polarization at t = 0 and τ (T) relaxation time defined in Equation (3.2). Assuming a linearly increasing temperature from T_f, at a rate β (where $T = T_f + \beta t$), the non-isothermal equation for the depolarization is:

$$P(t) = P(0) \exp\left(-\int_0^t \frac{dt}{(t)}\right) \tag{3.4}$$

and thus the current density corresponding to this depolarization is:

$$j_D(T) = [P(0)/\tau_o] \exp\left(\frac{-E}{K_B T}\right) \exp\left(-\frac{1}{\beta \tau_o}\int_{T_f}^{T} \exp\left(-\frac{E}{K_B T'}\right) dT'\right) \tag{3.5}$$

where all parameters remain as defined previously.

In the TSDC experiment the initial polarization is performed at a high temperature Tp and the sample is cooled down to T_f. During the cooling, the polarization increases from its value at Tp to a high value of T_f. The increase can be considerable and depends upon the rate of cooling and upon E and τ_o [35]. Normally, T_{eff} which is called the "effective" polarization temperature is defined as:

$$P(0) = \frac{\alpha N \mu^2 F}{K_B T_{eff}} = \int_{T_f}^{T_z} j_D(T)\, dT \qquad (3.6)$$

where α is a geometrical factor which takes into account the possibile dipole orientations (α = 1/3 for free dipoles and for I-V dipoles in alkali halides); N is the number of dipoles present; μ is the dipole moment; F is the electric field; finally Tz is the temperature at which TSDC drops to zero after the TSDC peak.

Equation (3.6) can be derived from the Langevin function [34] by the approximation of weak-field.

Dipole-Dipole Interaction

The TSDC curve is completely described by the activation parameters E, τ_o and the number of dipoles N. Nevertheless, TSDC peaks deviating from the shape predicted by Equation (3.5) have been reported in some recent works in rare-earth-doped alkaline-earth halides [35].

These deviations involve mainly a broading of the TSDC peak, and the parameters E and τ_o, evaluated from Equation (3.2), show a systematic dependence with the impurity concentration. Den Hartog [35] has attributed these effects to dipole-dipole interactions and his group found that the agreement can be improved between the experimental and calculated curves, by assuming an activation energy

distribution. Both a Gaussian distribution and a Lorentzian distribution have been proposed.

The TSDC curve is now described with a four-parameter formula:

$$j_D^* = j'_D(T) \cdot F(Eo, \bar{\tau}o, p, T) \qquad (3.7)$$

with

$$F = \frac{1}{p\sqrt{\pi}} \int_o^{\infty} dE \left[- \frac{(E-Eo)}{K_B T} - \frac{(E-Eo)^2}{p^2} - \int_o^T \frac{1}{\bar{\tau}o} \right.$$

$$\left. \left(e^{-E/K_B T'} - e^{-E_o/K_B T'} \right) dT' \right]$$

where $j_D(T)$ remains as defined previously. F represents the correction factor when the dipole-dipole interactions are included.

The p parameter is a measure of the dipole-dipole interaction strength and it depends upon concentration N. If only electrostatic interactions are considered, p will depend upon N linerarly [35]. Eo is the mean of the activation energy distribution and is supposed to be concentration-independent. It should therefore correspond to the activation energy for low dipole concentration.

So far, no improvements have been reported regarding the application of activation energy distribution to dipoles in alkali halides. There are basically three

things which are expected if one uses the modified equation [36]. First is better agreement between experimental peaks and theoretical fits. Then constant values for the average activation energy Eo and frequency factor τ_o^{-1}, independent of the impurity concentration, are expected. At last, a correlation between p and the dipolar concentration N exists.

Calculation of Dipole Concentration by TSDC in Monoenergetic Model

The "effective" polarization temperature can be also obtained by setting $(T_{eff}) = 1$ [33] in Equation (3.2). The T_{eff} is:

$$T_{eff} = -E/K_B \ln \tau_o \qquad (3.8)$$

where all parameters remained as defined previously. Values of E and τ_o can be gotten from fitting experimental TSDC date - i.e., $j_D(T)$ to Equation (3.5). Once these two parameters are known, the concentration of dipoles can be calculated from Equation (3.6).

From Equation (3.6),

$$P(0) = \int_T^{T_z} j_D(T)\, dT.$$

From TSDC, the area A under $j_D(T)$ can be approximately calculated as follows (Figure 19): with reference to Figure 19, I have

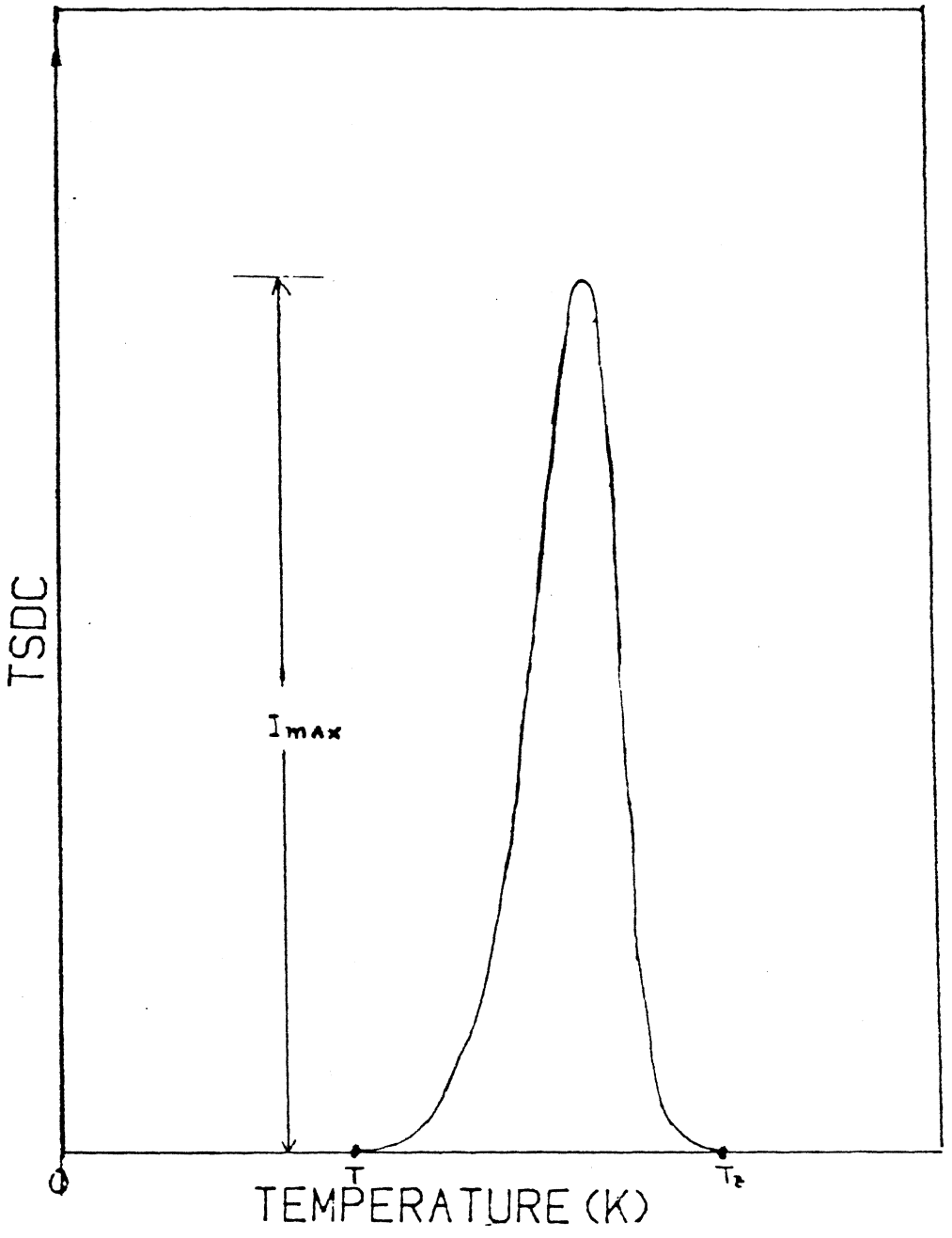

Figure 19. Approximate Calculation of the Area Under a Typical TSDC Peak

$$P(0) = A = \int_{T}^{T} j_{D}^{z}(T)dT = \int_{T}^{T} \frac{I}{z} \frac{D}{t_s} dT = \frac{I_{max}}{t_s} AT$$

or

$$P(0) = A = \frac{I_{max}}{t_s} T \qquad (3.9)$$

where I_{max} is the height of TSDC peak; its surface area of the sample; $\Delta T = T_z - T$ the breadth of the TSDC peak; A the area under the $j_D^z(T)$ curve. The dipole moment is then estimated by using either a n.n. model or a n.n.n. model. Finally, from Equation (3.6), the dipole number can be found, thus

$$N = \frac{I_{max} K B T_{eff}}{\alpha t_s \mu^2 F} \qquad (3.10)$$

The_Peak_Cleaning_Technique

The TSDC technique allows us to resolve overlapping peaks by following a special procedure. Suppose a situation in Figure 20 is encountered, i.e., three peaks are overlapping, and only peak 2 is wanted. Then the following simple steps can accomplish this provided the peaks are not overlapping too much. At first, start heating the crystal from liquid nitrogen temperature and proceed linearly. Halt the heating at T_2 and stabilize the

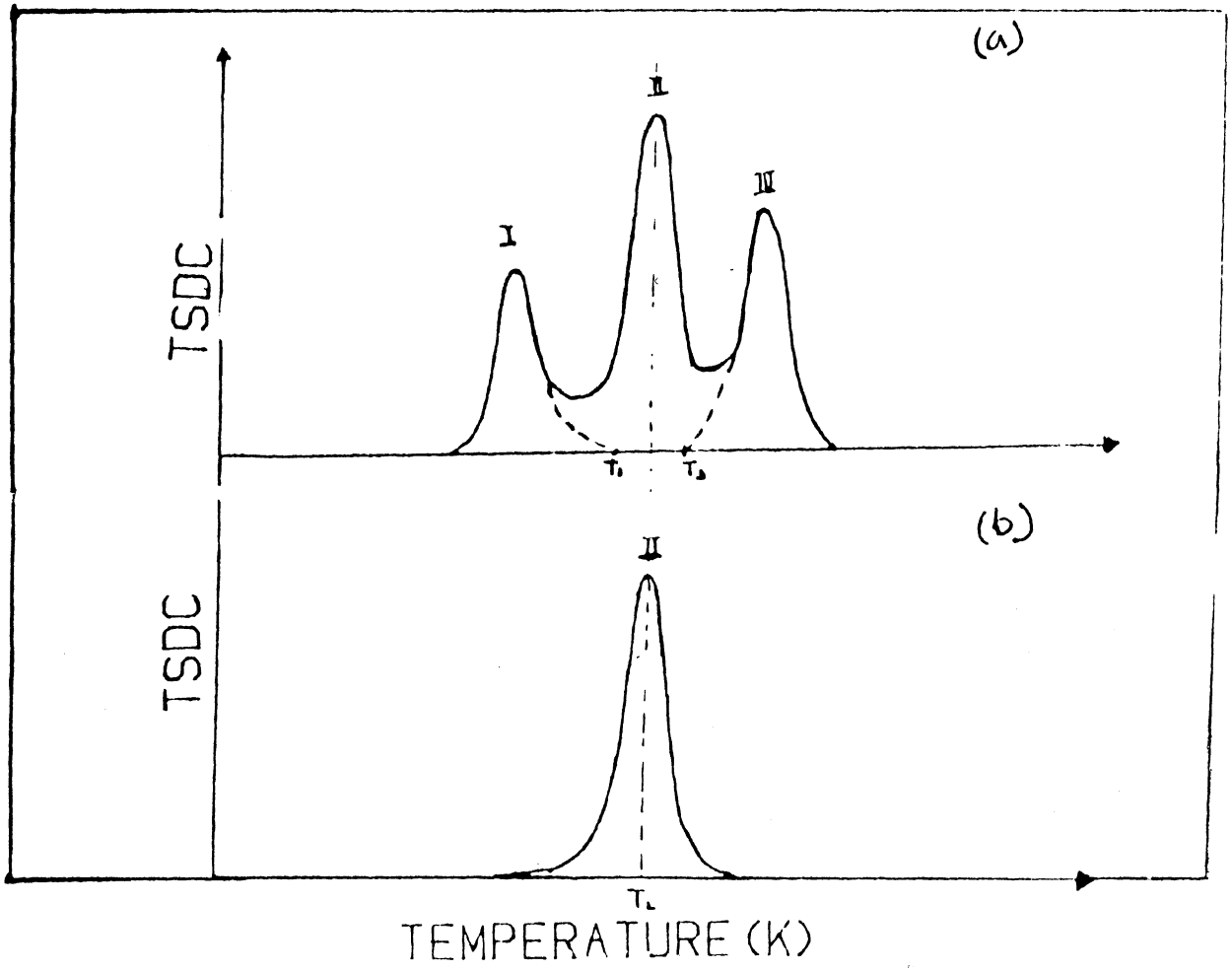

Figure 20. Demonstration of Peak Cleaning (a) Before Cleaning, (b) After Cleaning

temperature of the sample. Then, turn on the voltage. The consequence of this is that those dipoles producing peak 1 and peak 2 are polarized. But dipoles for peak 3 will remain in the state of random orientation, or no polarization. Therefore, no TSDC will occur during heating from T_2 to room temperature. Cool back from T_2 to liquid nitrogen temperature again. Now dipoles for peak 1 and peak 2 which are previously polarized will be "frozen in". Start heating again and proceed linearly. Halt heating when T_1 is reached. Then cool back to liquid nitrogen temperature (this liberates dipoles for peak 1 and they will remain randomized after this). Finally, monitor TSDC versus temperature from liquid nitrogen to room temperature. The result is that a clear peak 2 is produced.

The function of the cleaning technique is to obtain an accurate set of parameters such as E, τ_o and N. This is because the experimental curves are assumed to be a single peak in the fitting program.

Figure 21 shows the apparatus used to read TSDC data. The liquid nitrogen cryostat (Figure 22) can house the sample and is also connected to a vacuum system. The operational pressure is usually maintained at 4×10^{-6} mbar. A temperature controller is used to keep a constant heating rate ($\sim 0.12^{o}$ C./S). A high voltage power supply is used to polarize the sample (usually $V_p = 10^3$ V.). A digital multimeter is used to read the temperature of the

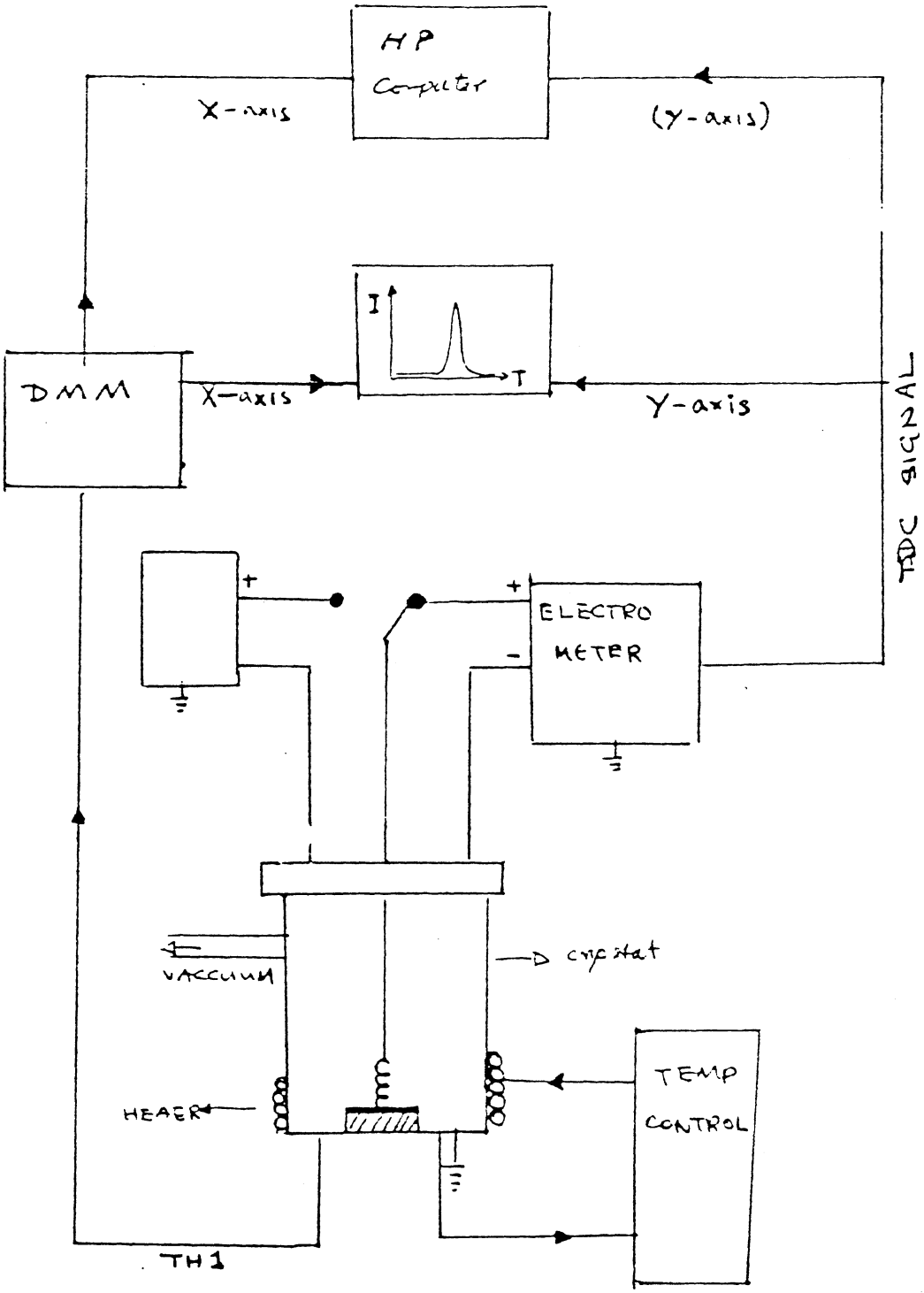

Figure 21. TSDC Apparatus

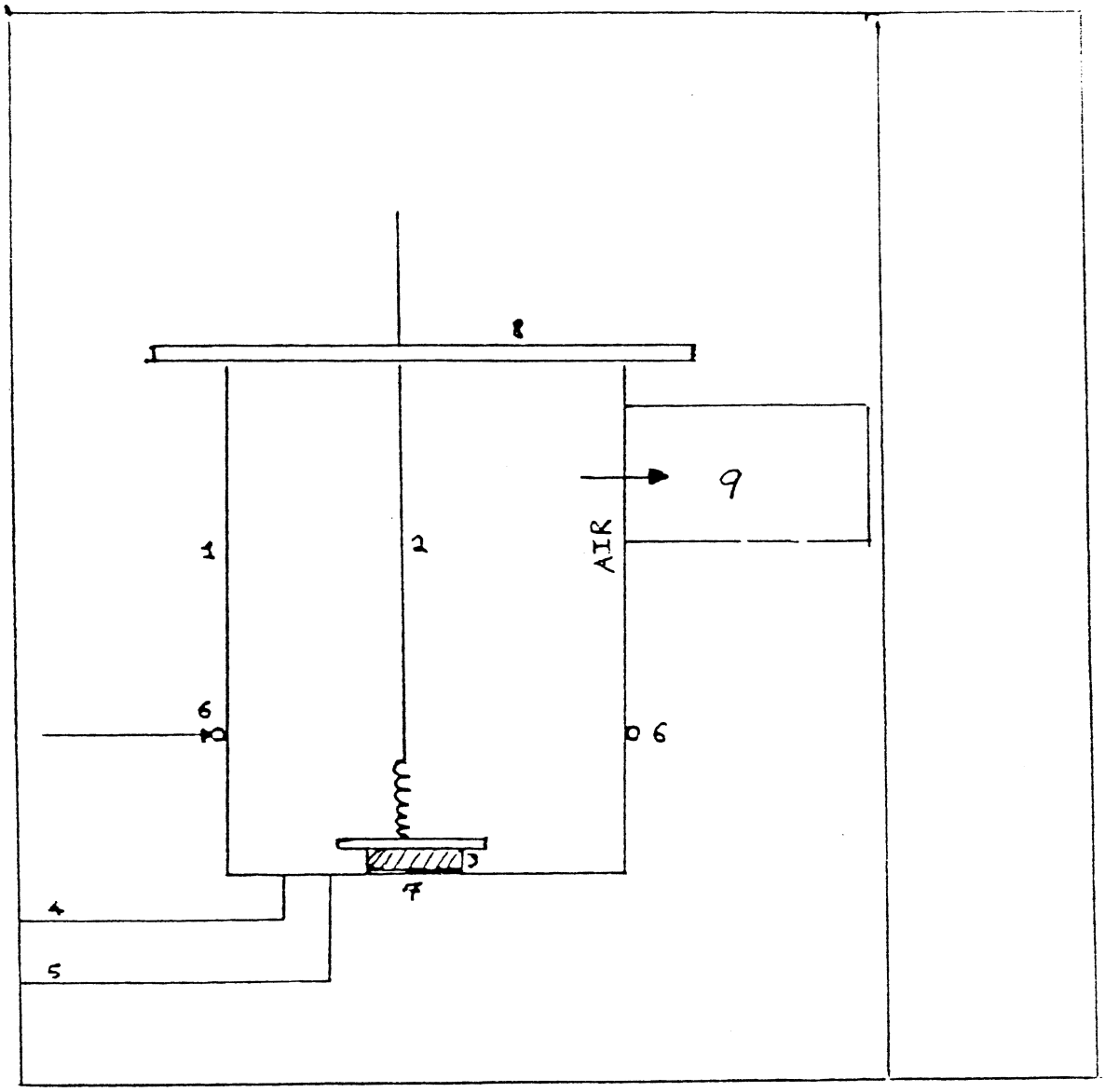

Figure 22. TSDC Cryostat

(1)	Cryostat Wall	(2)	Copper Probe
(3)	LiF Sample	(4)	Thermocouple
(5)	Thermocouple	(6)	Heat Input
(7)	Silver Paint	(8)	Insulation Cover
(9)	Vacuum System		

sample through a copper-constantan thermocouple. An electrometer is to measure the TSDC output. A chart recorder is to graphically record TSDC versus warm-up temperature. All the TSDC data is stored via a computer with which any processing of the data is available. The structure of the cryostat is very important for the measurement. There are several components of it. Copper wall and bottom making up the sample chamber are connected to the vacuum system. A copper probe is acting as a positive pole for the high voltage. The sample LiF:Mg.Ti has aluminum electrodes on the top and bottom surfaces. A thermocouple that goes to the DMM is to show the temperature of the sample. Another thermocouple that displays the temperature is also designed. The heat is provided from the temperature controller and a resistance heater. Silver paint is used to provide a good contact between the bottom of the sample and the chamber. An insulation cover is equipped to close the chamber.

Preparation of Samples for TSDC

A sample thickness of .4 mm is reported to be able to maintain 95% of the dipoles after a quench in liquid nitrogen following the standard annealing procedure [37]. The physical dimension is 5 x 5 x 0.4 mm^3, more or less. Experiences show that the selection of electrode material will directly affect the survival of the electrode during thermal quench procedures. After a sequence of trials, aluminum proved to be good for LiF:Mg.Ti TLD-700. For a

strong adhesive attraction between the aluminum and the LiF sample, delicate grinding of sample by use of fine carborundum paper is also necessary. Immediately before the TSDC measurement, the sample needs to be cleaned carefully with acetone or alcohol.

In general, the TSDC technique provides a straightforward method for a very accurate determination of the reorientation parameters E and τ_o. The dependence of relaxation time τ on temperature T for a particular material of interest can be easily determined. In addition, this technique is also highly sensitive. Very small dipole concentrations can be detected. In the case of LiF:Mg I-V dipoles as low as 5×10^{-2} ppm are still detectable.

Thermoluminescence

Generalized Thermoluminescence Process

An ideal insulator does not have energy states within its energy band gap. This is due to the fact that the potential in the crystal is perfectly periodic. However, if there are impurities within the lattice, or structural defects occur in a crystal, the periodicity of crystal will break down and additional energy levels will be introduced within the band gap. There energy levels may be discrete, or they may be distributed depending upon the exact nature of the defect and of the host lattice. A freed electron can wander through the crystal and become "trapped"; that

is, no longer able to take part in conduction. A direct consequence of being trapped is that the electron possesses energies within the band gap. The position of these localized energy levels within the gap is determined by the amount of energy required to free the electron from these levels.

An essential feature of the thermoluminescence process is the change in occupancy of the various localized energy states. These alterations in the population are implemented by electronic transitions from one energy state to another. Common electronic transitions are shown in Figure 23.

The localized energy levels can act either as traps or as recombination centers, depending on the relative probability of thermal release of trapped electrons and of recombination of holes and electrons at that energy level. If the former is greater than the latter, then this level is classed as a trap. Otherwise, it is a recombination center. Similarly, the same rule can apply to holes. Normally, for a given temperature those centers of small E are more likely to be traps than centers of large E. For this reason, recombination centers are located towards the middle of the forbidden gap and traps are located toward the edges. In addition, it is possible to see from this how a center which is a trap at one temperature may become a recombination center at a lower temperature, and vice-versa [39].

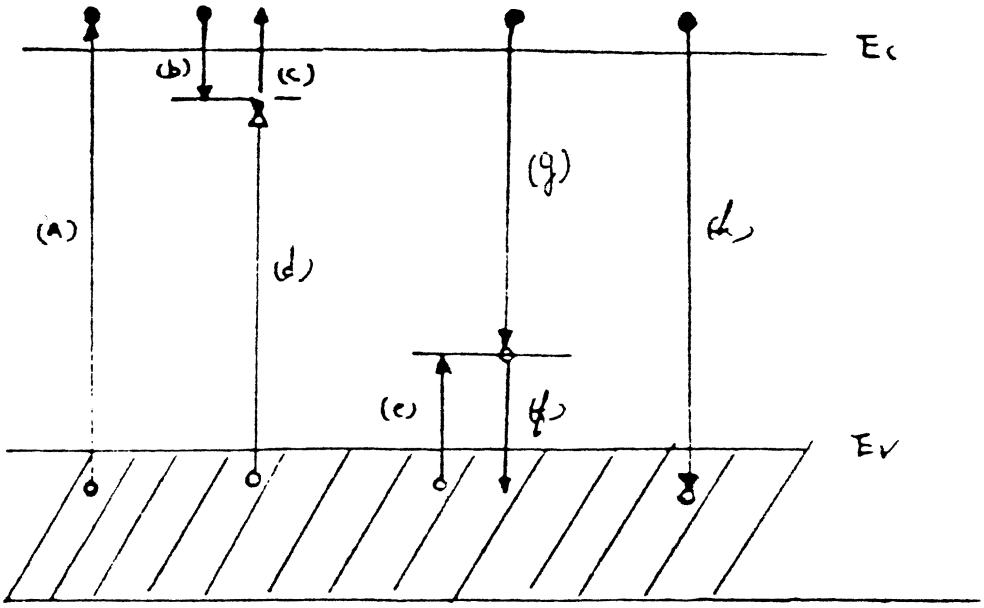

Figure 23. Common Electronic Transitions in an Insulator. (a) Ionization; (b) and (e) Electron and Hole Trapping, Respectively; (c) and (f) Electron and Hole Release; (d) and (g) Indirect Recombination; (h) Direct Recombination. Electron, Solid Circle; Electron Transition, Solid Arrows; Holes, Open Circles; Hole Transition, Open Arrows

Luminescence occurs when electron-hole recombination takes place. Band-to-center or center-to-center recombination are common recombination processes in impure insulators at normal temperatures [38].

Thermoluminescence Method

Exact procedures of performing TL vary from system to system. Basic steps are the following: The sample (LiF:Mg.Ti) is prepared in the form of either powder or small pieces. Different annealing treatments may be applied at this stage. Common treatments for LiF as used in this work: a) 400 ^{o}C./1/2 hour + liquid nitrogen quench. This may be followed by pulse annealing to a given temperature T. b) 400 ^{o}C./1.2 hour + liquid nitrogen quench +80 ^{o}C./24 hours + pulse annealing.

The sample is irradiated with β-rays, or γ-rays and is then heated inside the TL cryostat.

The heating is performed in a nitrogen atmosphere, achieved by first evacuating the cryostat until the pressure reads about 10^{-1} torr. Then fill slowly with nitrogen gas (the filling of N_2 gas or any other inert or inactive gases which have reasonably good conductivities ensure a uniform heating environment surrounding the sample and avoid the possible oxidation reactions from any element inside the cryostat which may also produce TL). The filling is stopped when the pressure reaches about 600 torr. During subsequent heating, the TL intensity versus

temperature, known as a "glow curve", can be obtained.

Major Models in TL

Various models have been proposed to explain the TL mechanism. Two of the most common models are electron-hole recombination model and F-center-H-center recombination model. In the first model, at least two energy levels have to be present as shown in Figure 24. The first step is ionization. The radiation source offers energy $h\nu$; if this energy is greater than the energy band gap of LiF (~14 ev), ionization will occur. Freed electrons are "pumped" to the conduction band and are free to migrate through the sample; holes are left in the valence band. Results of electrical conductivity measurements show that these electrons and holes are not likely to remain free. Instead, they will be "trapped" at defect energy levels. The trap capturing the electrons is called an electron trap. Similarly, the trap where holes are held is called a hole trap. In addition, if the band gap is wide, direct recombination of electrons and holes after crossing the gap is also not likely to happen. From these considerations, it can be seen that a large population of electrons and holes will be trapped and remain at their traps after the ionization radiation has ceased. In other words, ionization leads to filling of traps. Following this trap filling, confined electrons can be released thermally. This is called trap-emptying. The released electrons

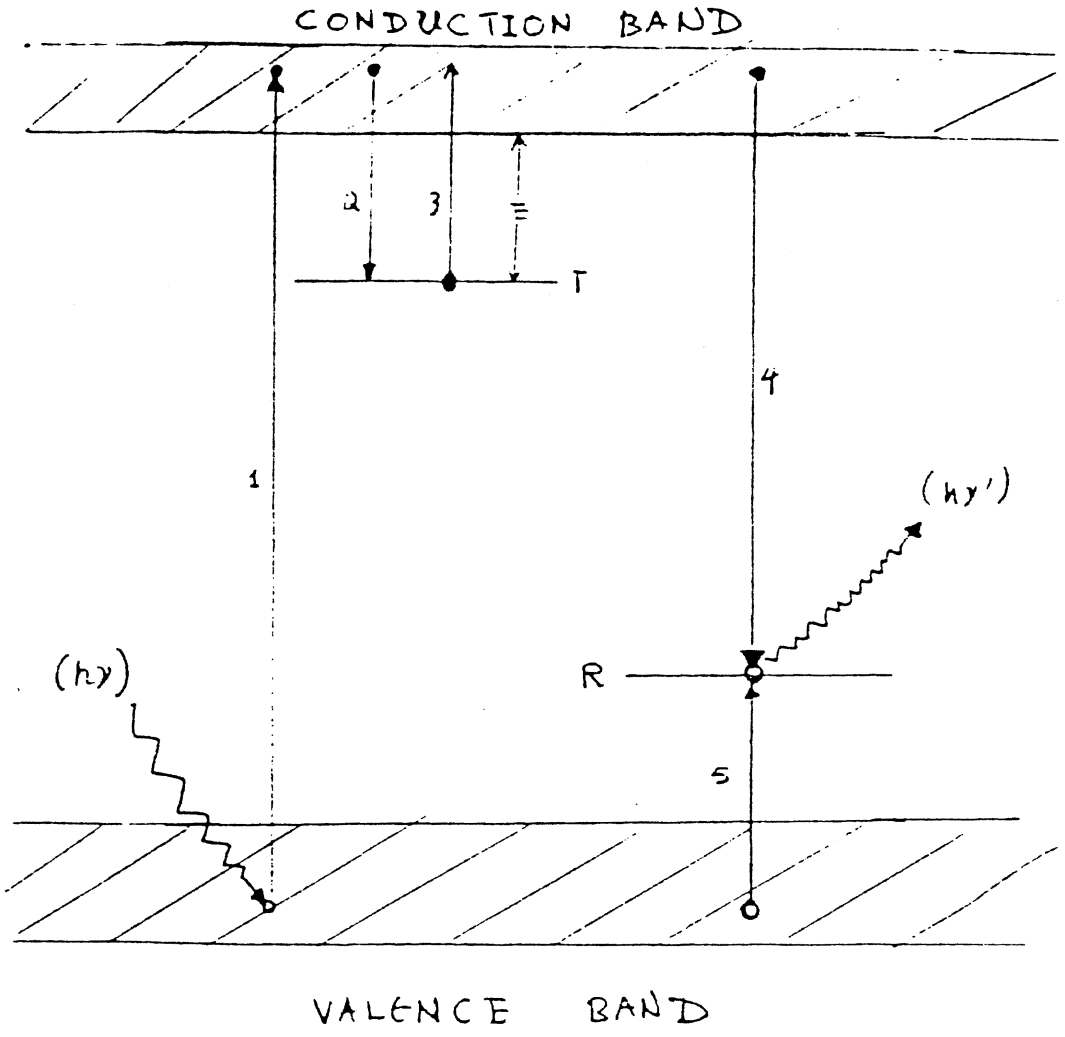

Figure 24. Simple Two-Level Model for TL (1) Ionization; (2) and (5) Traps Filling; (3) Trap Emptying; (4) Recombination of Electrons and Holes [39]

return to the conduction band and subsequently recombine with holes at hole traps. If the recombination is radiative, then emission of light will take place. In the second model, radiation creates a bound pair of an electron and a hole. This pair is called an exciton. The hole is left in a X_2^{-1} molecule and the electron is subjected to a coulombic attraction from the hole. Because of this, the exciton is unstable. The electron in the exciton always trys to recombine wih the hole. The result of recombination depends upon the temperature. At low temperature, if the recombination is radiative, then the luminescence will occur. At high temperature, the recombination is accomplished non-radiatively with the release of a significant amount of kinetic energy. After the recombination the electron becomes "trapped" in an available vacancy to form an F-center, and X_2^{-1} molecule which contains the hole, moves away along the <110> (Figure 25) direction and comes to stop finally at an interstial position to form a H-center. If the H-center is close to an impurity ion (e.g., Mg^{2+}), then it may be trapped at the defect. However, thermal stimulation may cause the H-center to gain mobility. When it moves and meets an F-center, the hole in the H-center will recombine with the electron in the F-center to give luminescence.

Basic Thermoluminescence Equations for a Simple Two-level Model in First-Order Kinetics

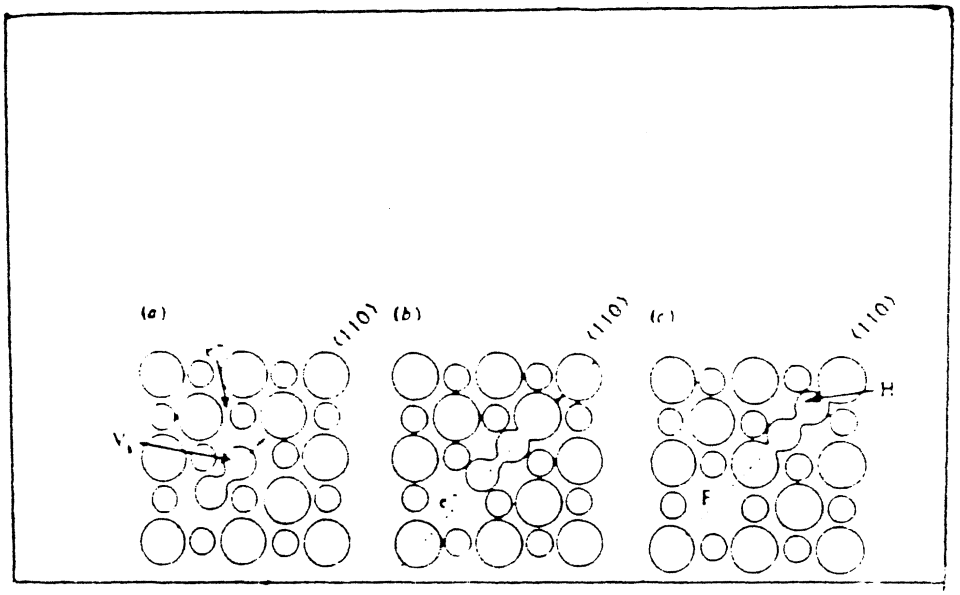

Figure 25. (a) Self-trapped hole (V_k-center) and free electron after irradiation.
(b) Dissociation of self-trapped exciton. X_2 molecule departs in a <110> direction following the non-radiative recombination of e^- and V_k.
(c) H-center forms some distance from the F center.

The TL intensity I is defined as:

$$I = -\frac{dn_h}{dt} \tag{3.11}$$

where n_h is the concentration of holes in recombination site; t is the time. A group of first-order differential equations describing the trap-emptying process are:

$$\frac{dn_c}{dt} = np - n_c(N - n)A - n_c n_h A_r \tag{3.12}$$

$$\frac{dn}{dt} = n_c(N - n)A - np \tag{3.13}$$

$$\frac{dn_h}{dt} = -n_c n_h A_r \tag{3.14}$$

where n_c is the concentration of electrons in the conduction band; n the concentration of electron in traps; n_h the concentration of holes in recombination sites; N the concentration of traps available to electrons; A_r the transition coefficient for trapping electrons to recombination sites; A the transition coefficient for trapping electrons from the conduction band, p the probability of trapped electron being thermally released from traps (Figure 26) and

$$P = K \exp\left(\frac{-F}{K_B T}\right) = s \exp\left(\frac{-E}{K_B T}\right) \tag{3.15}$$

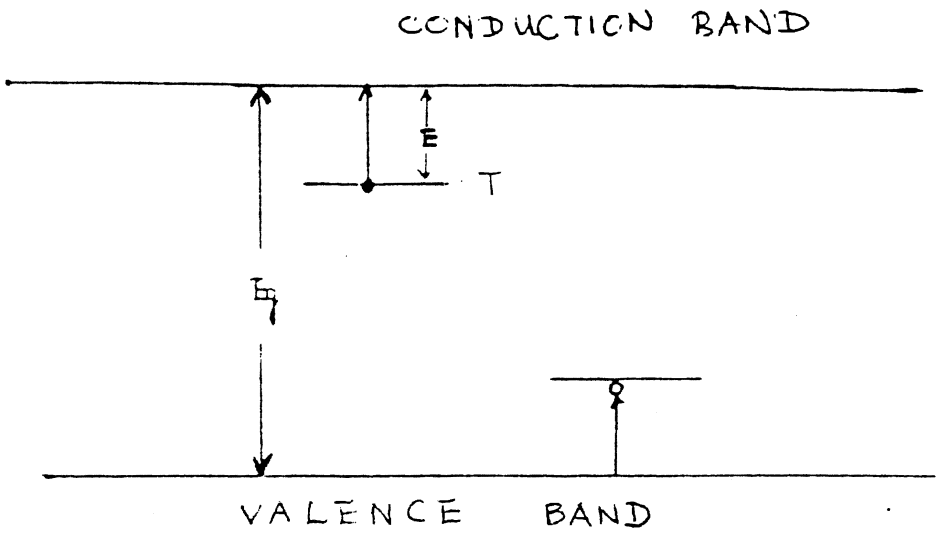

Figure 26. Life Time of Electron Trapped at Level T is $t = \tau_o \exp(E/K_B T)$, where E is the trap depth; τ_o^{-1} vibrational frequency of trapped electron in the trap potential well

where K = transition probability; ν = frequency of electron interaction with the lattice phonons; F = Helmholtz free energy F = E-TS, s = "attempt-to-escape frequency", S = entropy of the system. Thus

$$s = K \exp\left(-\frac{S}{K_B}\right) \tag{3.16}$$

From the law of detailed balance $s = N_c v \sigma$ where N_c is the density of states in the conduction band. Finally during the trap-emptying process, charge neutrality holds:

$$n_c + n = n_h \tag{3.17}$$

In addition, an assumption is that once a trap is empty, the free electron can no longer distinguish between it and other traps of the same type.

To solve the above 3 differential equations, further postulates have to be made. First, $n_c << n$, so most of electrons after ionization are trapped. Also, the rate of change of n_c is small compared with that of n, so $n_c \simeq$ constant. Besides

$$\frac{dn_c}{dt} << \frac{dn}{dt} \tag{3.18}$$

Combination of Equation (3.18) and $n_c << n$ means that lifetime of electron being free is much shorter than being

trapped. After these assumptions, the TL intensities can be expressed now as:

$$I = \frac{dn_h}{dt} = pnA_r n_h / (A_r n_h + A(N-n)); \quad (3.19)$$

also $n_h = n$ (because $n_h << n$) thus

$$I(t) = pn^2 / (n + R(N-n)) \quad (3.20)$$

where $R = A/A_r$. If we assume the probability of retrapping is negligible compared with the rate of recombination, then

$$n_h A_r >> A(N-n); \quad (3.21)$$

or $$R << n/(N-n); \quad (3.22)$$

$$\text{now} \quad I(t) = pn = ns \exp\left(\frac{-E}{K_B T}\right); \quad (3.23)$$

$$\text{and} \quad I(t) = \frac{dn_h}{dt} = \frac{dn}{dt}; \left(\frac{dn_c}{dt} << \frac{dn}{dt}\right) \quad (3.24)$$

$$\text{thus} \quad I(t) = -\frac{dn}{dt} = ns \exp\left(\frac{-E}{K_B T}\right); \quad (3.25)$$

or $$\frac{dn}{dt} = -pn; \quad (3.26)$$

$$\text{with} \quad p = s \exp\left(\frac{-E}{K_B T}\right). \quad (3.27)$$

Equation (3.26) is the first-order kinetics equation for TL. Solution of this equation is:

$$I(t) = I(T) = n_o s \exp\left(\frac{-E}{K_B T}\right) \exp\left[-\frac{s}{\beta}\int_{T_o}^{T} \exp\left(-\frac{E}{K_B T}\right) dt\right] \quad (3.28)$$

where $T = T_o + \beta t$; β = constant heating rate;

$$no = n(t)\Big|_{t = t_o}; \quad To = T(t)\Big|_{t = t_o}.$$

Thermoluminescence Apparatus

The schematic layout of the apparatus used to measure TL data is shown in Figure 27. The cryostat (Figure 28) contains the heater and it is connected to a vacuum pump and a N_2 gas tank. Operational pressure is ~600 Torr. Temperature controller is used to maintain a constant heating rate β (usually chosen about 2^{o} C./S). A photomultiplier tube, PMT (EMI 9635 QB) is operating in the integrated current mode. This device is to measure the intensity of the TL. High voltage DC power supply is for PMT. Digital multimeter is to measure and to display sample temperature through a Chromel-Alumel thermocouple. Picoammeter is to measure the current from PMT. The TL data is recorded in a chart recorder. Finally, the TL data is stored and processed in the computer.

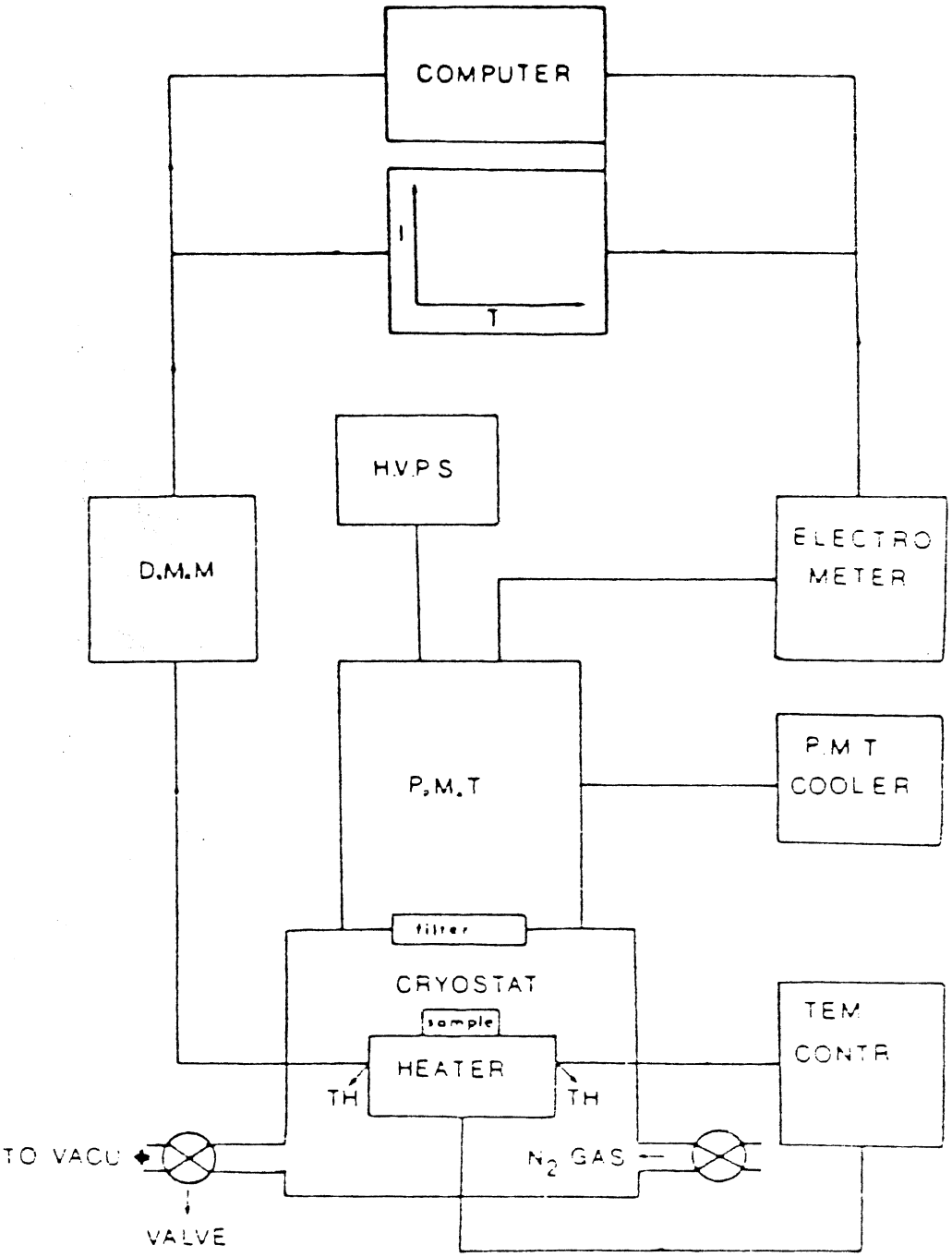

Figure 27. Schematic Layout of the TL Equipment as Described in Text

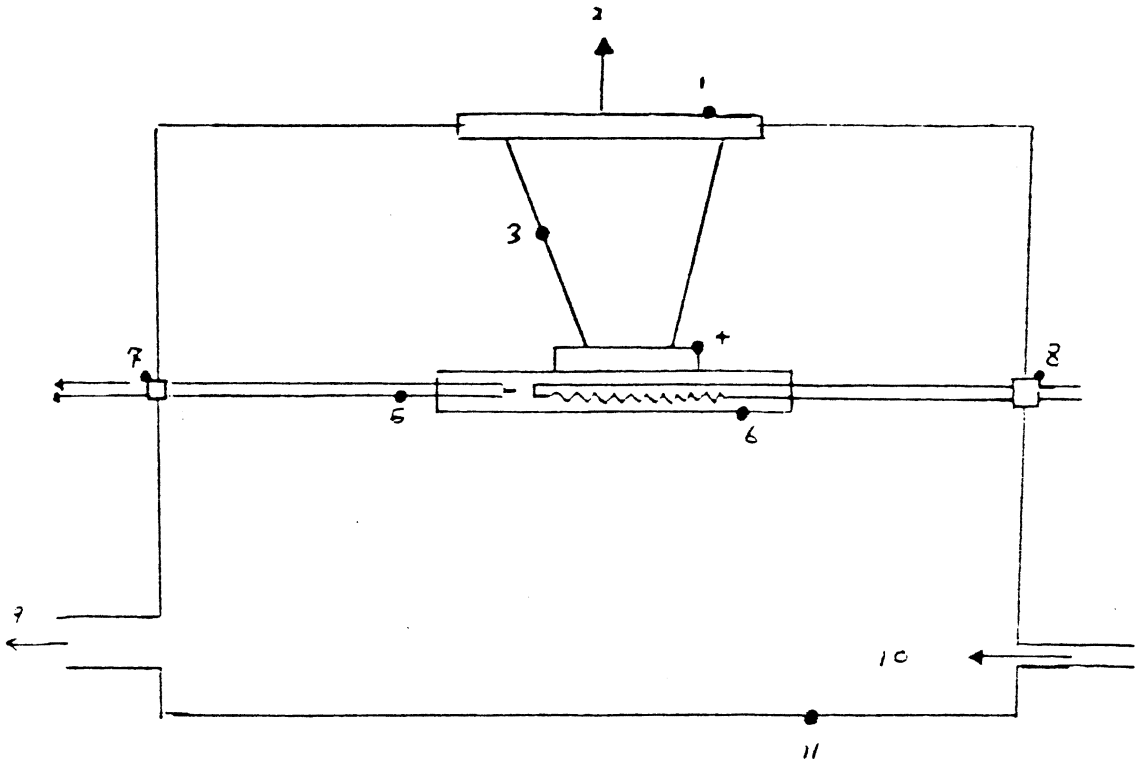

Figure 28. Schematic Layout of the TL Cryostat.

(1) Filter and/or windows
(2) PMT T
(3) Reflecting Cone
(4) Sample
(5) Thermocouple (Th/C)
(6) Heater
(7) Th/C Feedthrough
(8) Heater Power Feedthrough
(9) Vacuum
(10) Gas Inlet (N_2)
(11) Chamber

Optical Absorption

Basic Optical Absorption Theory

OA occurs in a material when a suitably spaced pair of energy levels exist which have an electron in the lower level. For the transition to be allowed, one also requires that the upper state is of the reverse parity [39]. Momentum conservation is possible, even if the levels are not vertically displaced on an E, k (energy, momentum) diagram, by addition or subtraction of lattice phonons.

The interaction of the phonons with the optical transitions determines the shape of the fundamental absorption edge and the width of absorption and emission bands.

In LiF:Mg.Ti, due to the interaction of impurities Mg and Ti, there exist a series of discrete energy levels within the band gap. Once photons possess enough energies (equal to the differences between the various energy levels) absorption of a photon may take place. In fact, OA of LiF:Mg.Ti at 380 nm is believed to be related to I-V dipoles and 310 nm absorption to trimers [28].

The theoretical shape of the OA band and the strength of the absorption can be computed moderately well, and estimates of the defect concentration from the measured absorption curves are generally made by comparison with the equations developed by Smakula. His equation is:

$$Nf = 8.21 \times 10^{16} \frac{n}{(n^2+2)^2} \int \mu(E)\, dE \qquad (3.29)$$

where N = number of defect centers; f = effective oscillator strength; n the refractive index n of the crystal; $\mu(E)$ = the absorption coefficient at the photon energy E; f is defined as:

$$f = \frac{4m}{3h} w_{ge} / r_{ge} /^2, \qquad (3.20)$$

where m = mass of an electron; h = Planck's constant; W_{ge} = $(E_g - E_e)/h$; r_{ge} = the position coordinate for this part of the configuration coordinate diagram; and f represents the number of oscillators at each of the allowed frequencies.

If $\mu(E)$ takes Gaussian form, then Equation (3.27) will have the following form:

$$Nf = 0.87 \times 10^{17} \frac{n}{(n^2+2)^2} \mu_{max} W \qquad (3.31)$$

where μ_{max} = maximum absorption band which is the height of OA band; W = width of OA band at half maximum.

From Equation (3.31), it can be seen that the effective number of defects is directly proportional to the height of an OA band. So by performing different annealing treatments, a change in the concentration of defects will be detected by observing the change in height of an OA band.

OA Apparatus

OA apparatus (Figure 29) consists of a UV-visible spectrophotometer. This device is to take OA measurements and perform simple manipulation of the stored data. The data of OA is stored and processed through the computer (IBM PC).

Photoluminescence

Basic Theory of Photoluminescence

The mechanism of the PL process can be described readily through the configurational coordinate diagram. Mott and Seitz [41] used the configurational coordinate to explain the electronic transitions between an excited state and a ground state within the same atom. The configurational coordinate is the displacements of the atoms in the neighborhood of the defect. In the ground state the electron is in the energy minimum at equilbrium (at point A) (Figure 30). After absorption from radiation, the electron is in a higher excited state B. If the absorption process happens much faster than the interaction process of the incident photon with the lattice phonon (Franck-Condon Principle), then B is vertically above A. In general, the minimum of the excited state occurs differently from that of the ground state. So once the electron is excited, it will return to the minimum of the excited state by losing thermal energy. Subsequently, photoluminescence takes

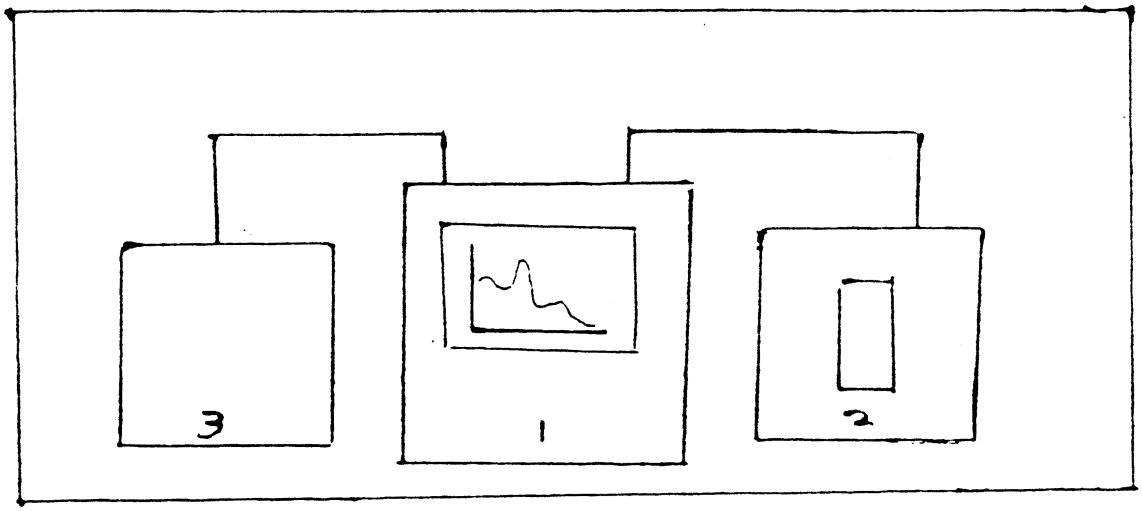

Figure 29. Layout of OA Apparatus
(1) and (2) UV-Visible Spectrophotometer, (3) Computer

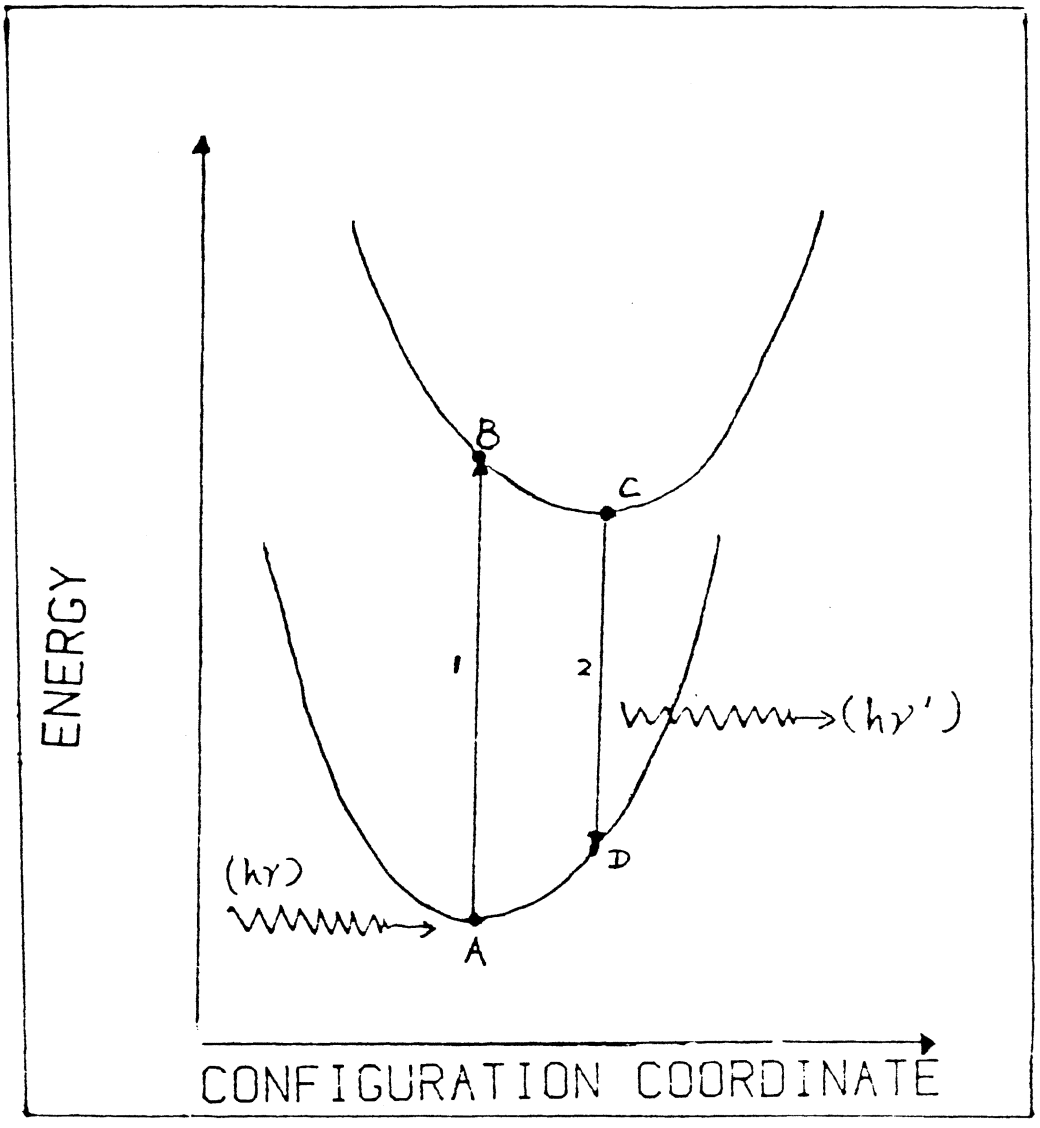

Figure 30. Schematic Layout of PL Process
(1) Photon Absorption
(2) PL

place when the electron goes back from C to D. After PL, the electron finally returns to A by rearrangement of the configurational coordinate and loss of heat. The whole process is illustrated in Figure 30.

In LiF:Mg.Ti, Ti^{*} (See Chapter II) is believed to be the luminesence site around which the configurational coordinate is referred to by the displacements of neighboring ions.

Photoluminescence Apparatus

A McPherson monochromator and Xenon light source are used for excitation. The monochromator was used to select the excitation wavelength from 105 um to 600 um from a 150w Xenon lamp. The slit width was 1-2 mm. The Grating is 1200 per mm. Dispersion is 2.6 nm/mm. A Spex monochrometer is used as the selector of the emission wavelength. The slit width was 1-5 mm. The Grating is 1200 per mm. Dispersion is 3.6 nm/mm. A photomultiplier tube (EMI 9635 QB) was used to detect the PL emission. A pair of CaF_2 lenses is used for focusing the excitation beam on the sample. An Omniscribe chart recorder is used for recording the emission spectrum or excitation spectrum. A high voltage DC power supply maintains DC voltage to the PMT. A Picoammeter is used for reading the current from PMT. The layout of the PL apparatus is illustrated in Figure 31.

Spectral Corrections

The intensity of the Xenon source has a dependence on wavelength. Besides the McPherson monochromator, Spex monochromater and PMT have their own quantum efficiency which also depend on the wavelength. These make the correction of excition spectra and emission spectra necessary. Assuming the Xenon source has the intensity $I_{IN}(\lambda)$; the McPherson monochromater has a quantum efficiency $E_M(\lambda)$; the PMT has a quantum efficiency $E_p(\lambda)$; the measured result of excitation spectrum from the sample is $I_{measure}(\lambda)$; the measured result from the Xenon lamp and McPherson monochromater by the PMT is $I'_{measure}(\lambda)$ (both $I_{measure}(\lambda)$ and $I'_{measure}(\lambda)$ are obtained in the form of experimental curves); then the actual intensity of excitation spectrum from the sample is $I_{act}(\lambda)$:

$$I_{act}(\lambda) = \frac{I_{measure}(\lambda)}{I'_{measure}(\lambda)/E_p(\lambda)} \qquad (3.32)$$

where $I'_{measure}(\lambda) = I_{IN}(\lambda)\, E_M(\lambda) E_p(\lambda)$.

For the emission correction, let the Spex monochromator have a quantum efficiency $E(\lambda)$; the intensity of beam before entering the Spex is $I_{IN}(\lambda)$; then $I_{IN}(\lambda)$ is:

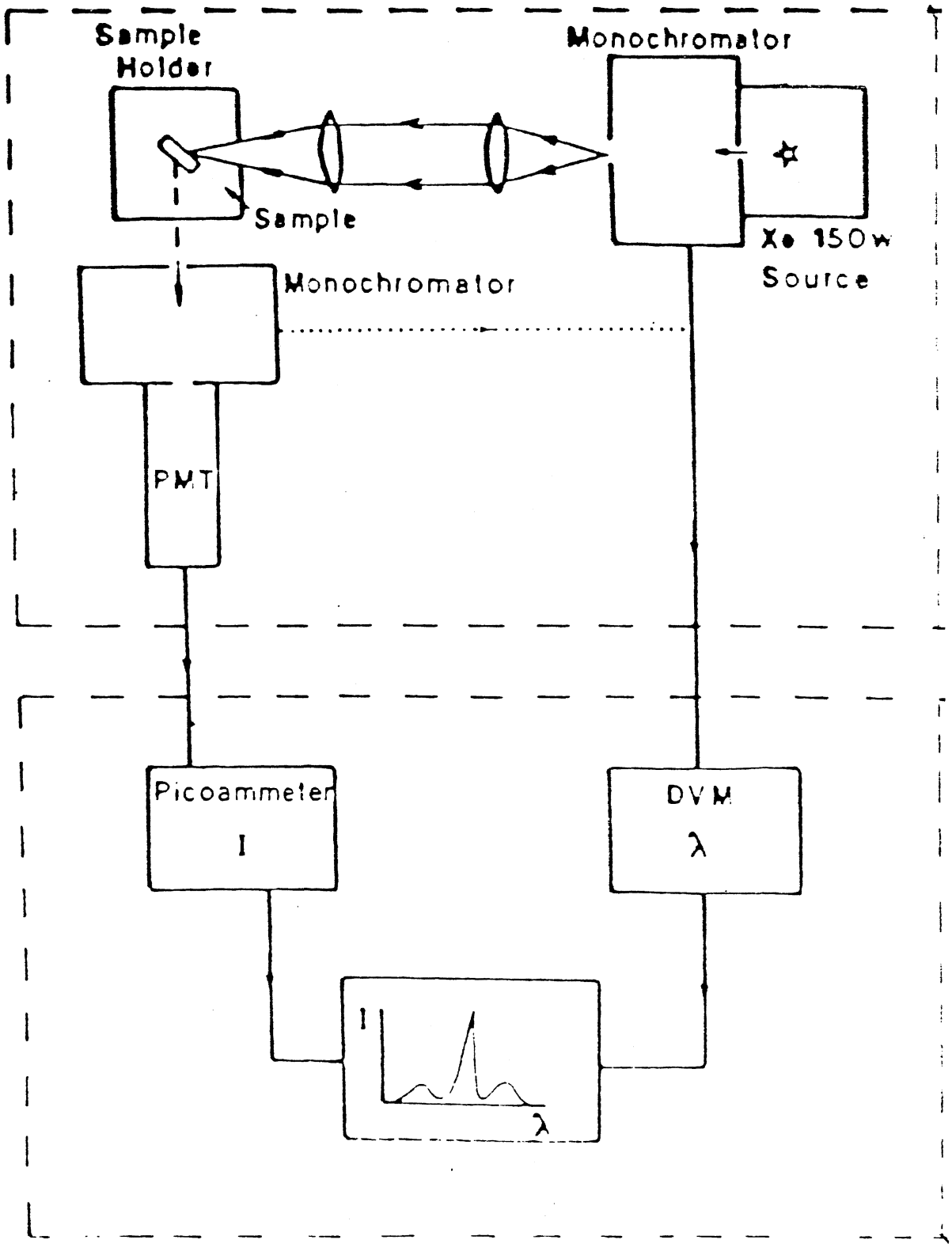

Figure 31. Schematic Layout of PL Apparatus

$$I_{IN}(\lambda) = \frac{I_{measure}(\lambda)}{E_p(\lambda)\, E_S(\lambda)} \qquad (3.32)$$

To obtain $E_p(\lambda)\, E_S(\lambda)$, we use a standard lamp, for the output is well-known; the measured emission from this lamp through the Spex and PMT is $I^{ST}_{measure}(\lambda)$, then

$$I^{ST}_{measure} = I^{ST}_{IN}(\lambda)\, E_P(\lambda)\, E_S(\lambda),$$

from this,

$$E_P(\lambda)\, E_S(\lambda) = \frac{I^{ST}_{measure}}{I^{ST}_{IN}(\lambda)} \qquad (3.33)$$

actual emission spectrum now is:

$$I_{act}(\lambda) = I_{IN}(\lambda) = \frac{I_{measure}(\lambda)}{I^{ST}_{measure} / I^{ST}_{IN}(\lambda)} \qquad (3.34)$$

In summary, all the excitation spectra and the emission spectra were corrected through Equation (3.32) and Equation (3.34), respectively.

CHAPTER IV

EXPERIMENTAL RESULTS AND DISCUSSION

Thermally Stimulated Depolarization-Currents

In Figure 32, TSDC peaks of LiF:Mg.Ti (TLD-700) are shown following the annealing treatment (1) which was previously described in Chapter III. The PAT is 65 ^{o}C. The TSDC peaked at about -56 ^{o}C. (~217K) is due to $[Mg^{2+} - V^{-}]$ dipoles. Occasionally, some other peaks, such as peak 2 (~180K) appeared irregularly and with variable heights when the TSDC measurements were repeated. With the sample inside the cryostat and with the identical application of voltage (~10^{3} v), a series of measurements indicated that the height of peak 2 changed randomly. Since we did not observe this peak when silver paint was not used, it is suspected that the silver paint may be the origin.

In Figure 33, the variation of the height of the TSDC signal is shown for three TSDC peaks. The PAT values are 105 ^{o}C. for the top curve in the figure; 125 ^{o}C. for the figure in the middle; 145 ^{o}C. for the lowest curve. A series of measurements was taken at regular intervals of temperature (~20 ^{o}C.). Overall, the PAT ranged from room temperature (~22 ^{o}C.) to 245 ^{o}C. The final and complete result of the changes of TSDC peaks versus PAT is

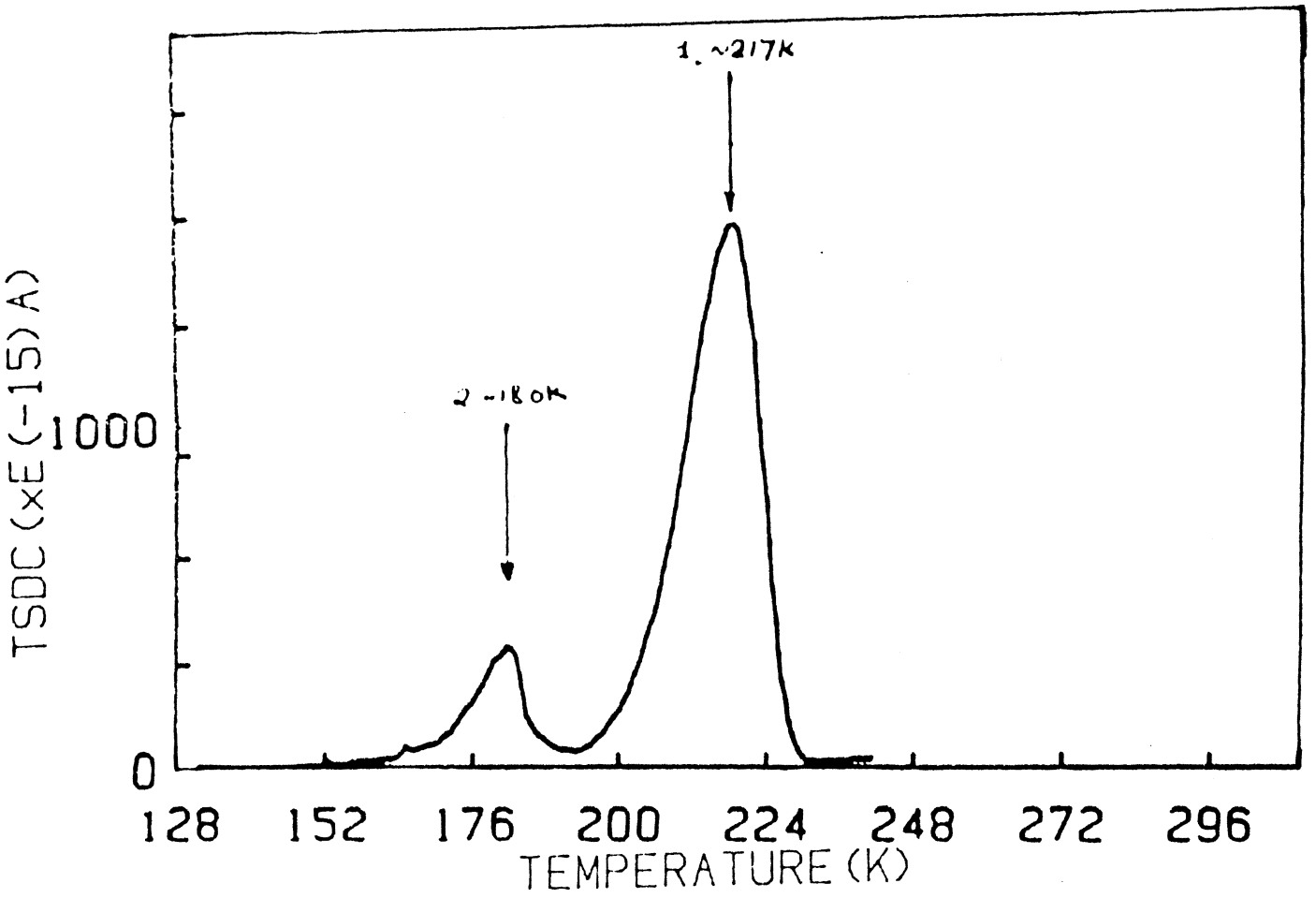

Figure 32. Normal TSDC Peak 1 of $Mg^{2+}V^{-}$ Dipole with Additional Peak 2 due to Another Species of Defect

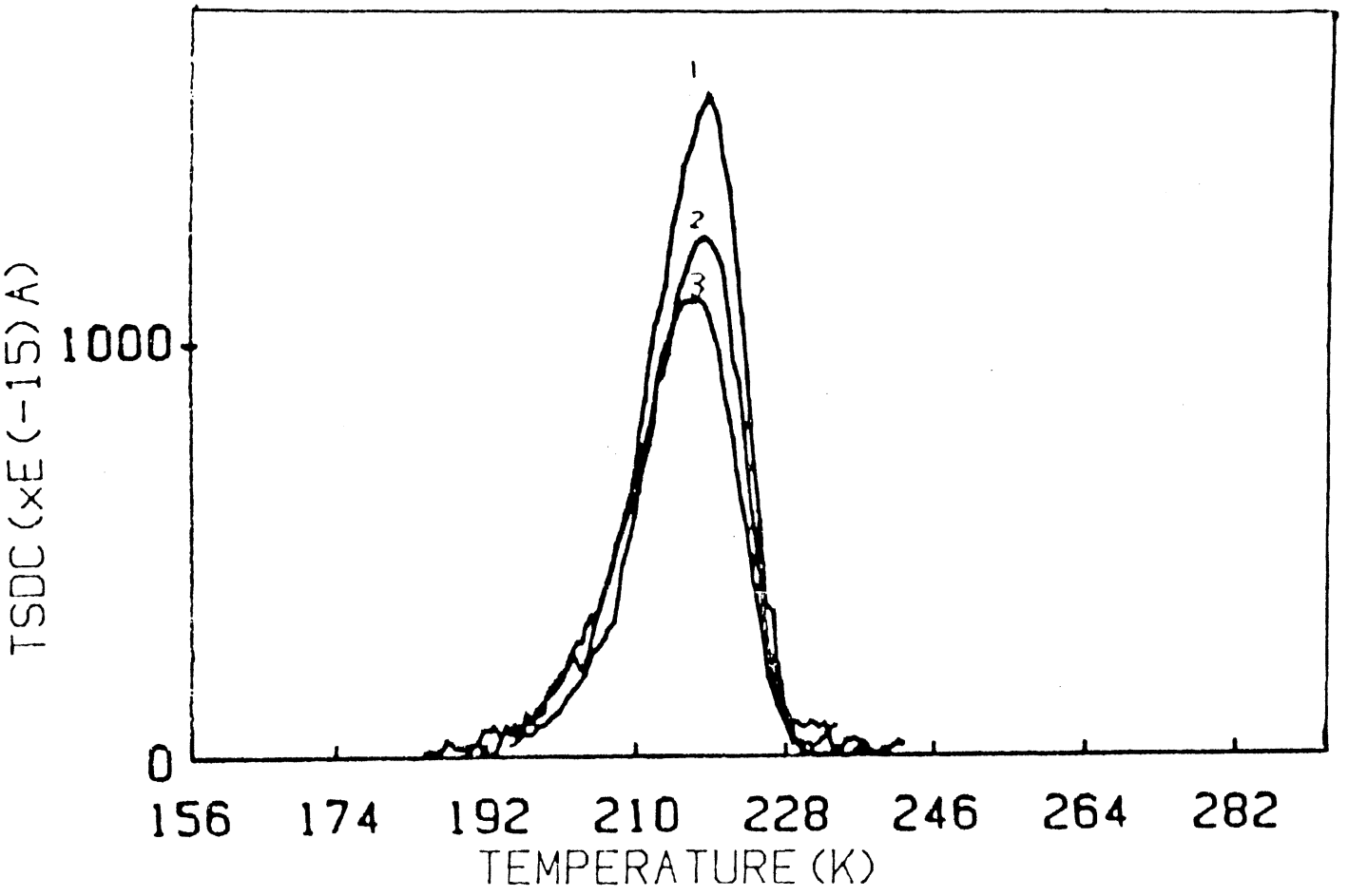

Figure 33. Variation of TSDC Peak with Change in PAI.
(1) 105 °C., (2) 125 °C., (3) 145 °C.,
after 400 °C./1/2 hour

illustrated in Figure 34, where the top curve (solid circles) is from the annealing treatments (1); and the bottom (empty circles) is from annealing treatment (2). The valley-like shape of the top curve shows that the decay of dipoles is very slow at the beginning (up to 100 ^{o}C.); becomes faster when the PAT is above 100 ^{o}C. and reaches a minimum at about 150 ^{o}C. During the range (100 ^{o}C. ~ 150 ^{o}C.), the forward reaction in the conversion dipoles into trimers (namely $3[Mg^{2+}V^{-}] == [Mg^{2+}V^{-}]_3$, see Equation (2.1)) predominates and the reverse reaction is very small. As the PAT increase above 150 ^{o}C., the concentration of dipoles starts increasing and the initial concentration is recovered finally at 250 ^{o}C. During this range (150 ^{o} ~ 250 ^{o}C.), the increase of the dipoles suggests that the reverse reaction (dissociation of trimers into dipoles) predominates. As a whole, about 35% of the initial dipoles decayed at the minimum.

The annealing treatment (2) (see Chapter III) initially maximizes the concentration of trimers. This directly implies that the dipole concentration is quite small after such treatments. As can be seen from the figure, the low-level flat plateau remains when the PAT goes from room temperature to about 100 ^{o}C. This is because the trimer is relatively more stable than the dipoles as discussed in Chapter I. However, further increasing the PAT brings in more and more thermal energy, and, as a result, trimers start to break up into dipoles.

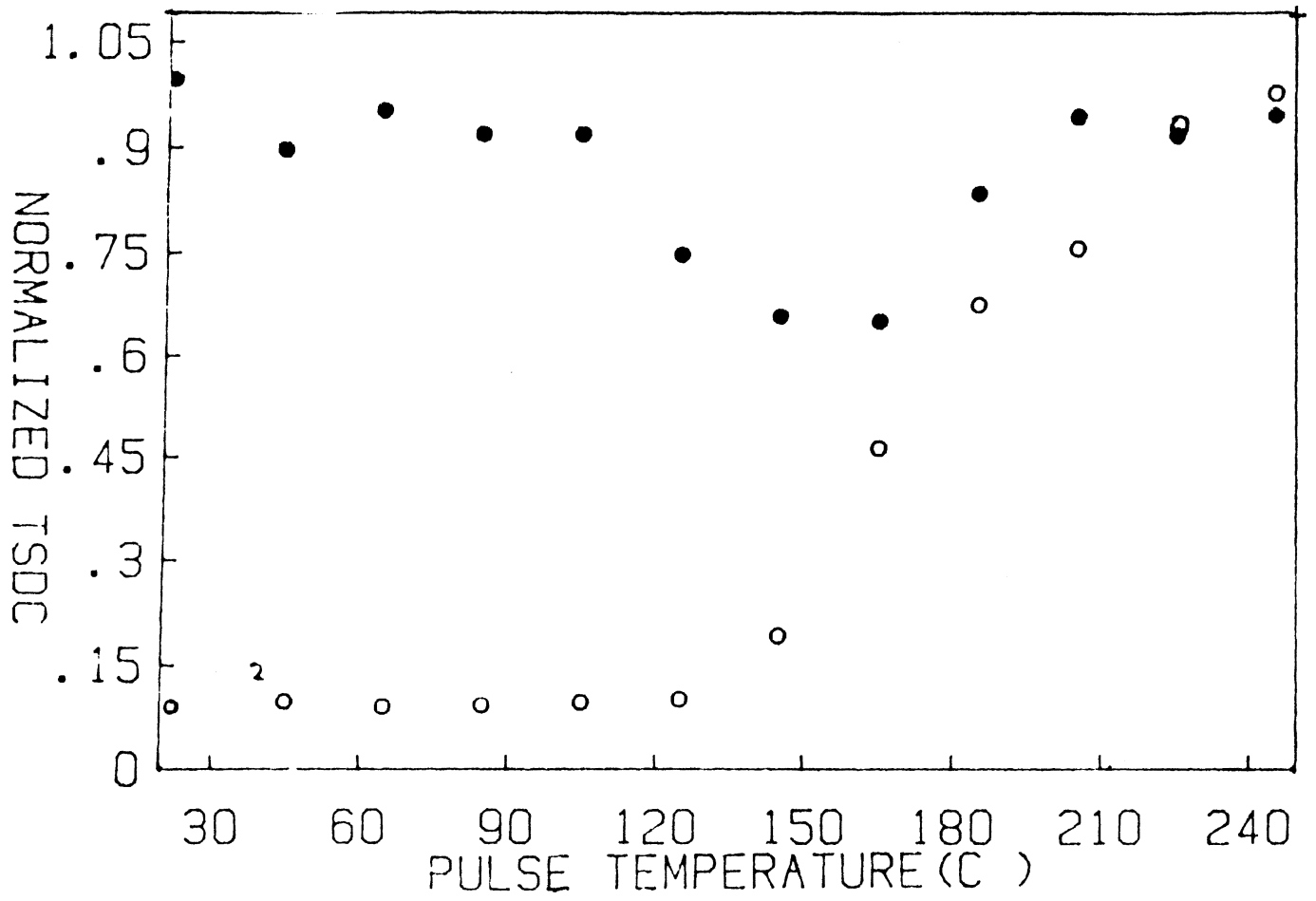

Figure 34. Change of TSDC versus PAT after Two Annealing Treatment (1) and (2)

thus, the dipole concentration goes up until its maximum is reached. After 100 °C., again, the reverse reaction predominates. At last, the two join together after a certain PAT (~170 °C. in this case).

Optical Absorption

In Figure 35, a typical OA spectrum is displayed. A beam of 1.7 Mev electrons obtained from a Van de Graaff accelerator was used to irradiate the sample. The incident beam current was 2μA and the irradiation period was 40 seconds. The distance between the sample and the beam outlet was approximately 50 cm.

The band at 200 nm is believed to be caused by Ti-OH complexes and this absorption is present before irradiation [28]. The absorption obtained after irradiation is shown by the curve 1 from which the 200 nm band was subtracted to give the curve 2. In this curve, the peak at about 250 nm is well-known and is due to F-centers [40]. A peak at ~445 nm is due to F_2-centers [41]. The peaks at 310 nm, 380 nm are believed to relate to Mg-type defects; especially we suspect that the 310 nm band is related to trimers and the 380 nm band to dipoles [28].

The OA spectrum of TLD-700 was resolved in Figure 36, into its individual components. Each component band was assumed to be in in the Gaussian form. However, sometimes the assumption works and sometimes it doesn't. In the latter case, no matter how much time one spends fitting the

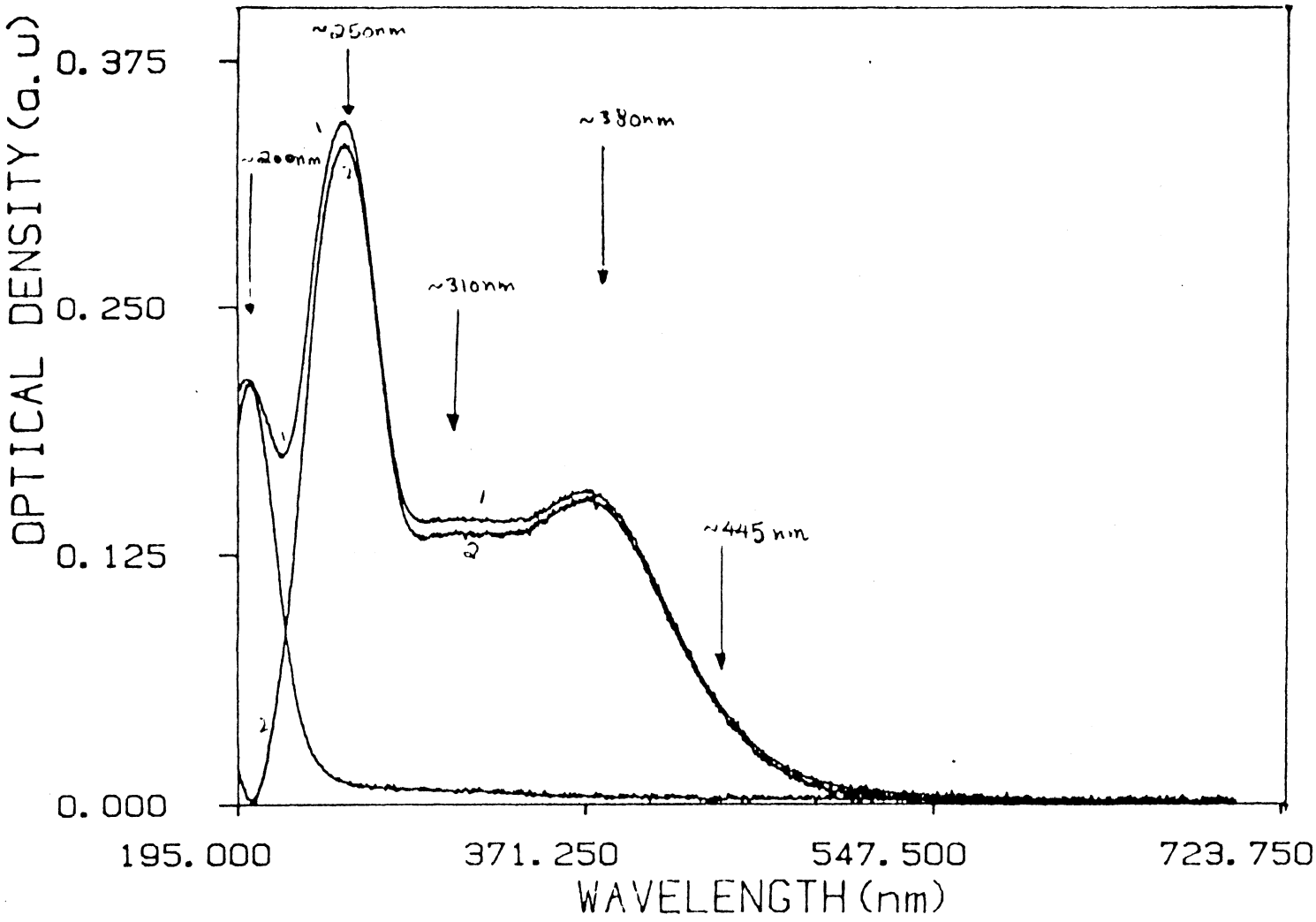

Figure 35. A Typical OA Spectrum Showing Five Bands Which are Related to Various Defects

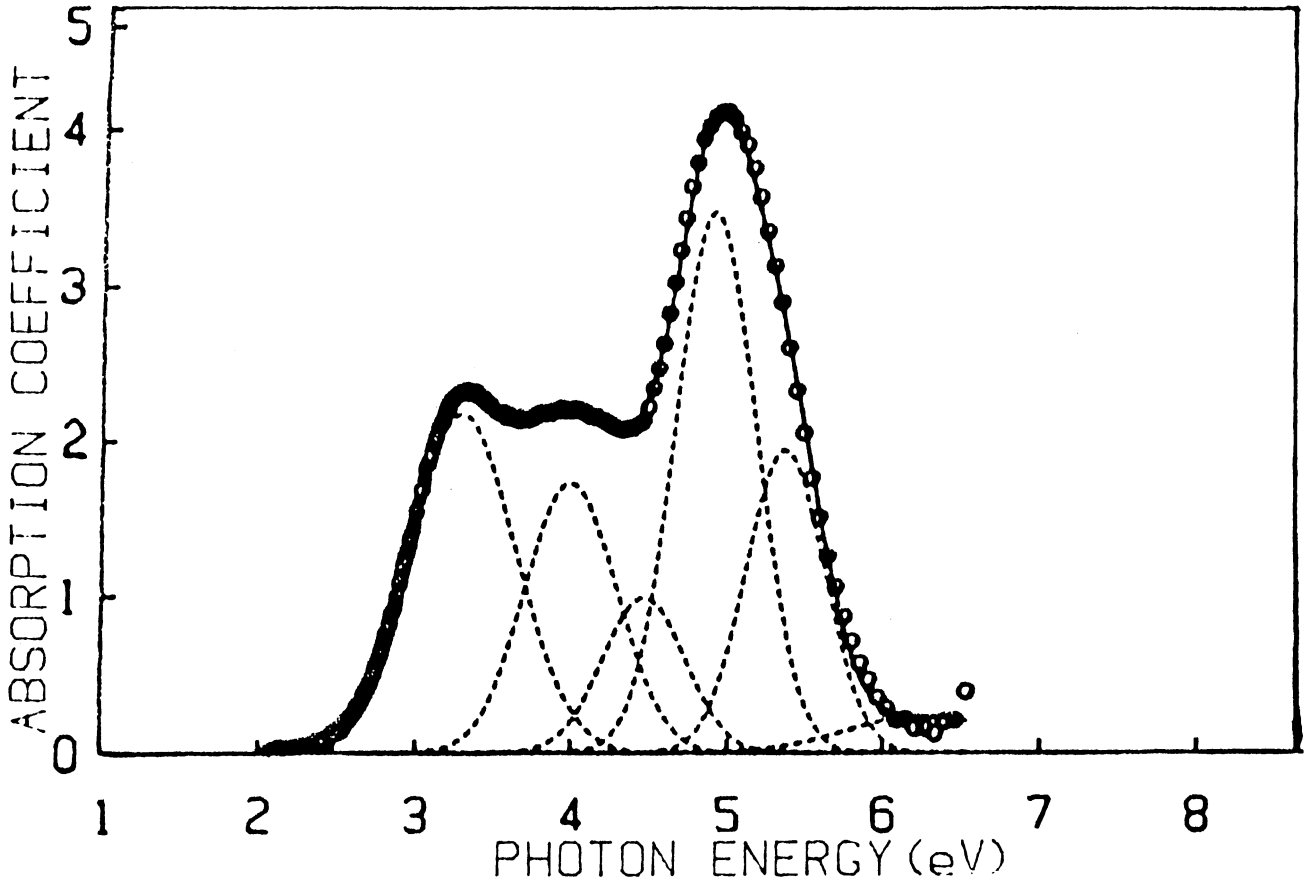

Figure 36. Resolution of an OA Spectrum into Component Gaussian Bands
Empty Circles = Experimental Data;
Solid Line = Sum of the All-Dashed Bands;
Dashed Line = Component Bands

experimental OA curve, no major improvement would result. The explanation involves the speculation that each component band is not a perfectly symmetric form such as a Gaussian, and in general is probably asymetric [40]. From Figure 36, the left-most component band corresponds to 380 nm (~2.38 ev); the next one to it corresponds to 310 nm (~4.019 ev). Ideally, every OA spectrum needs to be resolved to obtain the positions and heights of each peak, especially the 310 nm and 380 nm bands, for each PAT. Unfortunately, due to the slow efficiency of our computer-fitting routines and unavailability of a better fitting program, data presented here are the results of estimatations of the heights of the 380 nm and of the 310 nm from the spectra following each PAT. These factors will definitely introduce a certain amount of error. The 380 nm band overlaps only with the 310 nm peak and the 310 nm band overlaps not only with the 380 nm band, but also with the high-energy band next to it. Thus, changes in the height of the 380 nm band may "compensate" changes in the 310 nm band. We believe the estimations for the 380 nm band are more accurate and more reliable than those for the 310 nm band.

In Figure 37, three OA curves were provided to demonstrate the relative changes in heights of the 380 nm and 310 nm peaks. The Ti-related band at 200 nm was already subtracted for faster fitting. The Van de Graaff accelerator was used as the irradiation source, since it

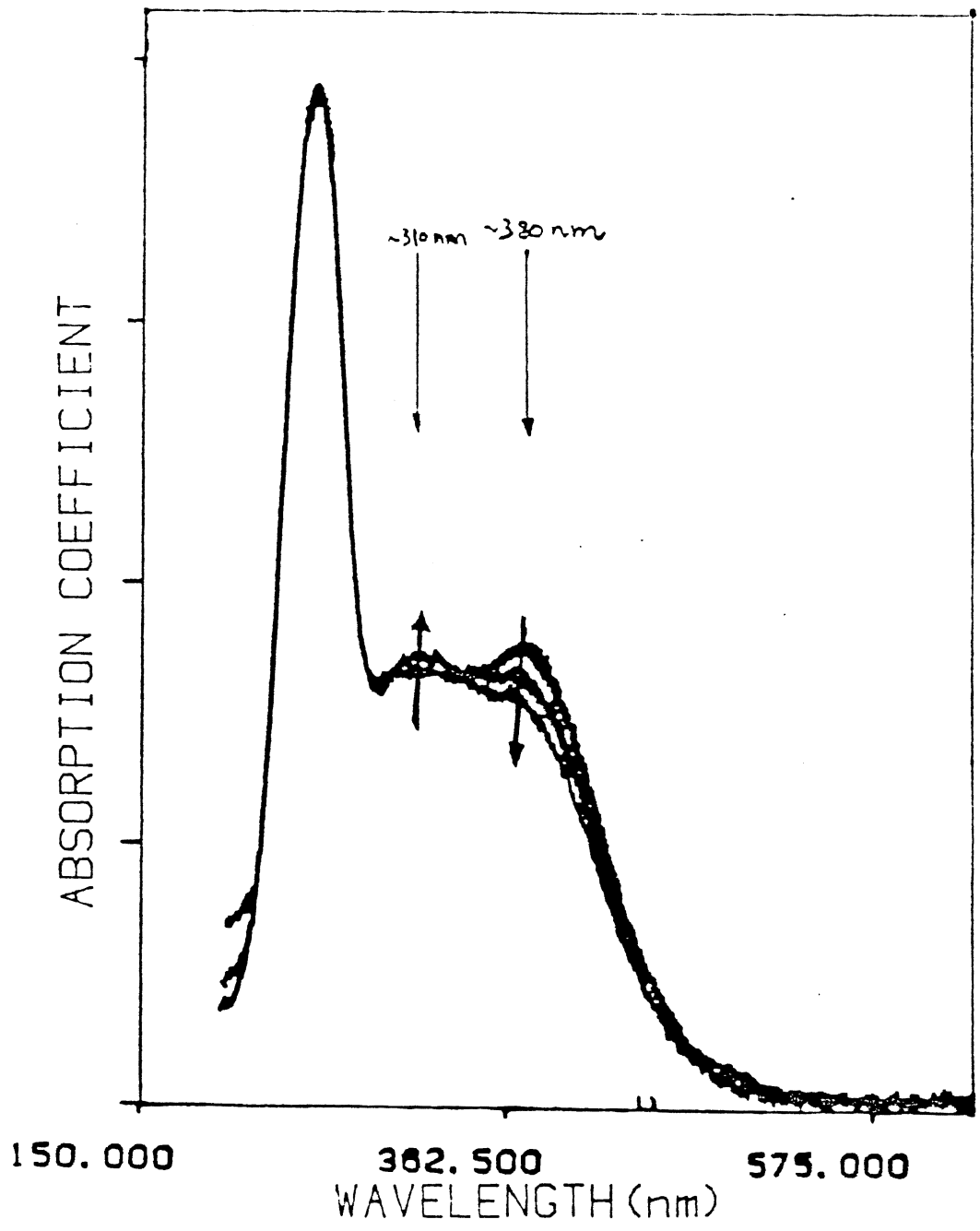

Figure 37.Demonstration of an OA Band Change after Different PAT

can provide a higher dose in a shorter period of time than the γ -ray source. This is important for this experiment. As argued in Chapter II, the shorter the irradiation time the fewer will be the amount of dipoles which have clustered into trimers during this period. Thus the condition of maximization of the dipole concentration will be maintained before each PAT following which OA measurements were performed.

The change in the 380 nm band height when the sample was subjected to the two annealing treatments are displayed in Figure 38. The general trends take similar forms to those seen from Figure 34 for the TSDC case. This clearly suggests that the 380 nm absorption band is closely associated with the presence of Mg-dipoles. The absorption intensity follows the dipole concentration.

However, the bottom curve shows a discrepancy from the Figure 34 in that it remains at a relatively higher plateau than is the case with the TSDC data. As discussed previously however, the overlapping of the 380 nm band with the 310 nm, and the estimation of the peak height from a direct measurement of the OA experimental curve (rather than a calculation from computer-fitting) probably causes this problem. The problem is even worse in the case of 310 nm band as seen in Figure 39. It is hard to see from it that the 310 nm band is caused by trimers, for if that was the case, the top curve (following annealing treatment (2)) should decrease as the PAT increases. Furthermore, the

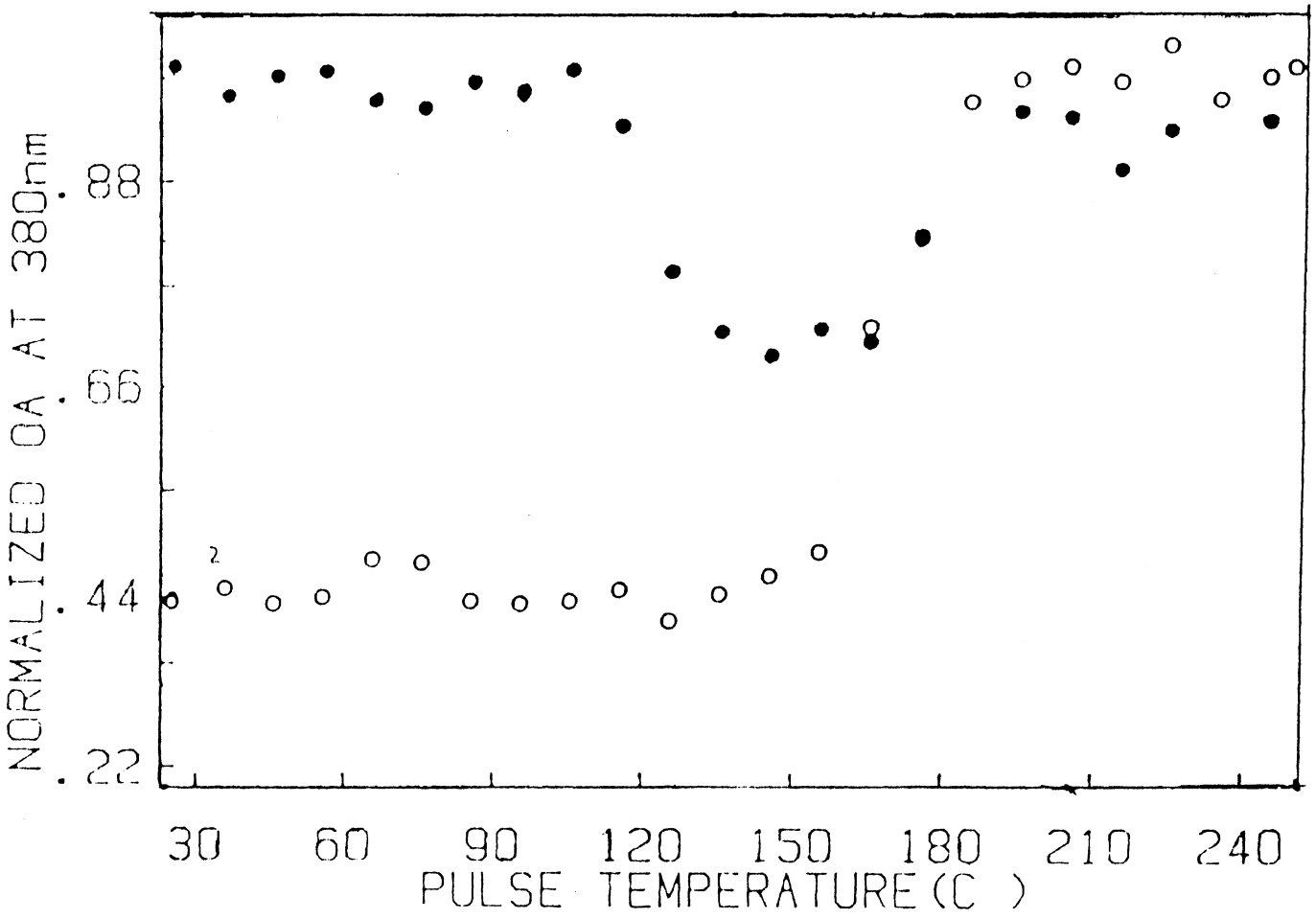

Figure 38. Variation of an OA Band at 380 nm after the Annealing Treatment (1) and (2)

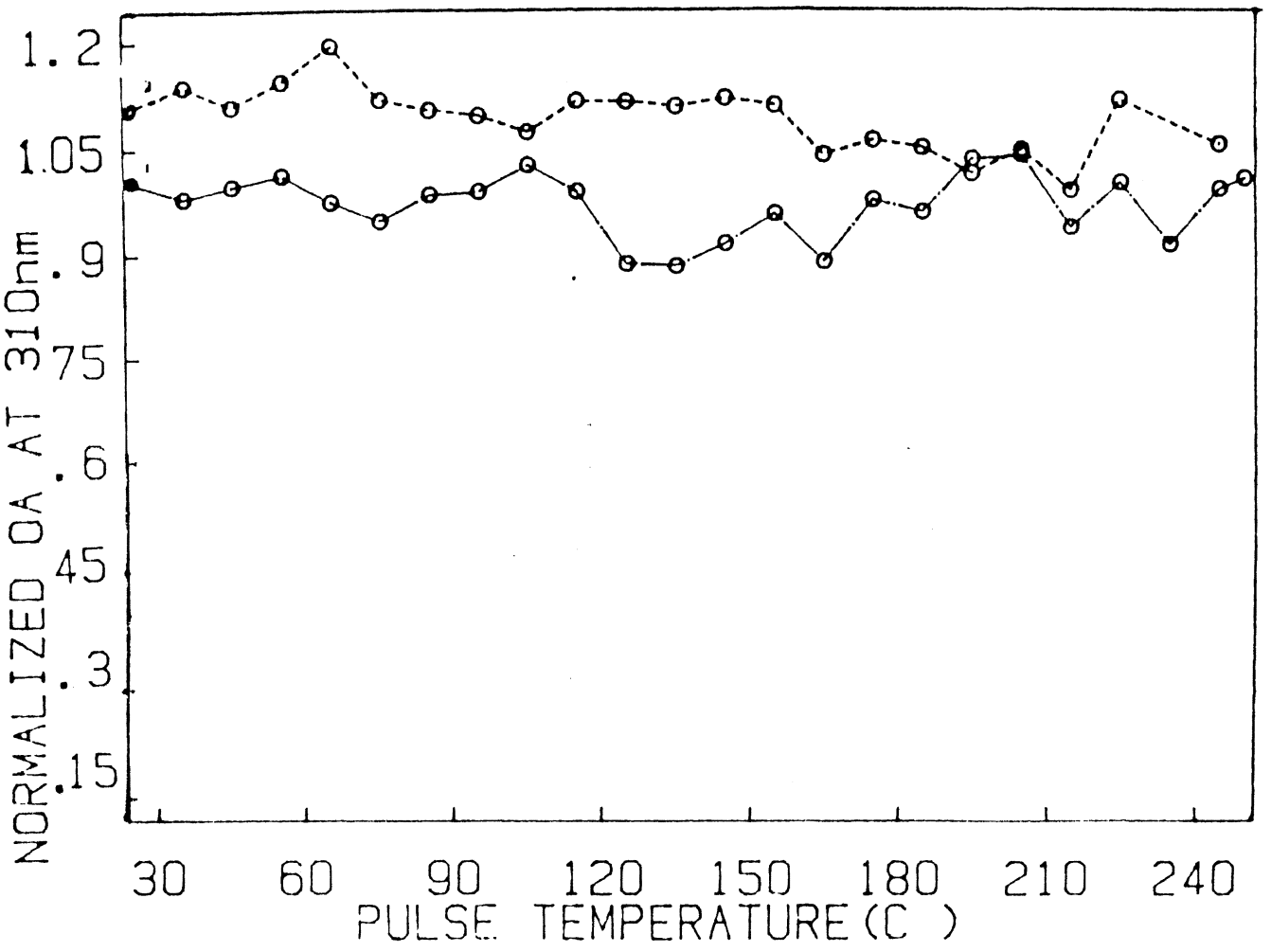

Figure 39. Variation of an OA Band at 310 nm after the Two Annealing Treatment, (1) and (2)

bottom curve should not be horizontal, because annealing treatment (1) should cause the trimer concentration to increase at a certain PAT, then decrease afterwards. Therefore, it is felt necessary to resolve the experimental curves if one wishes to get the "real" height of the 310 nm band such that the exact nature of the 310 nm band behavior can be revealed.

Thermoluminescence

A typical TL glow curve is shown in Figure 40 from TLD-700 following -ray irradiation (~330.5 rad). As seen from the figure, the peak 2 is at 123 °C; peak 3 at 157 °C.; peak 4 at 193 °C. and peak 5 at 220 °C. The positions of these peaks are in good agreement with the results from Harris and Jackson [41] except that the position for peak 5 differs by 10 °C.

In Figure 41, four TL glow curves are observed to display the change in height of peak 2 and peak 5. As it can be seen from the figure, peak 2 decreases as PAT goes from 85 °C. to 145 °C., and peak 5 increases except for curve 2.

The final results of the changes in the heights of TL peak 2 and peak 5 are illustrated in Figures 42 and 43. A comparison is made between Figure 34 and Figure 42. The general trends from two figures indicate strong similarities both between the top two curves and the bottom two curves. As in the case of TSDC, heights of peak 2 undergo

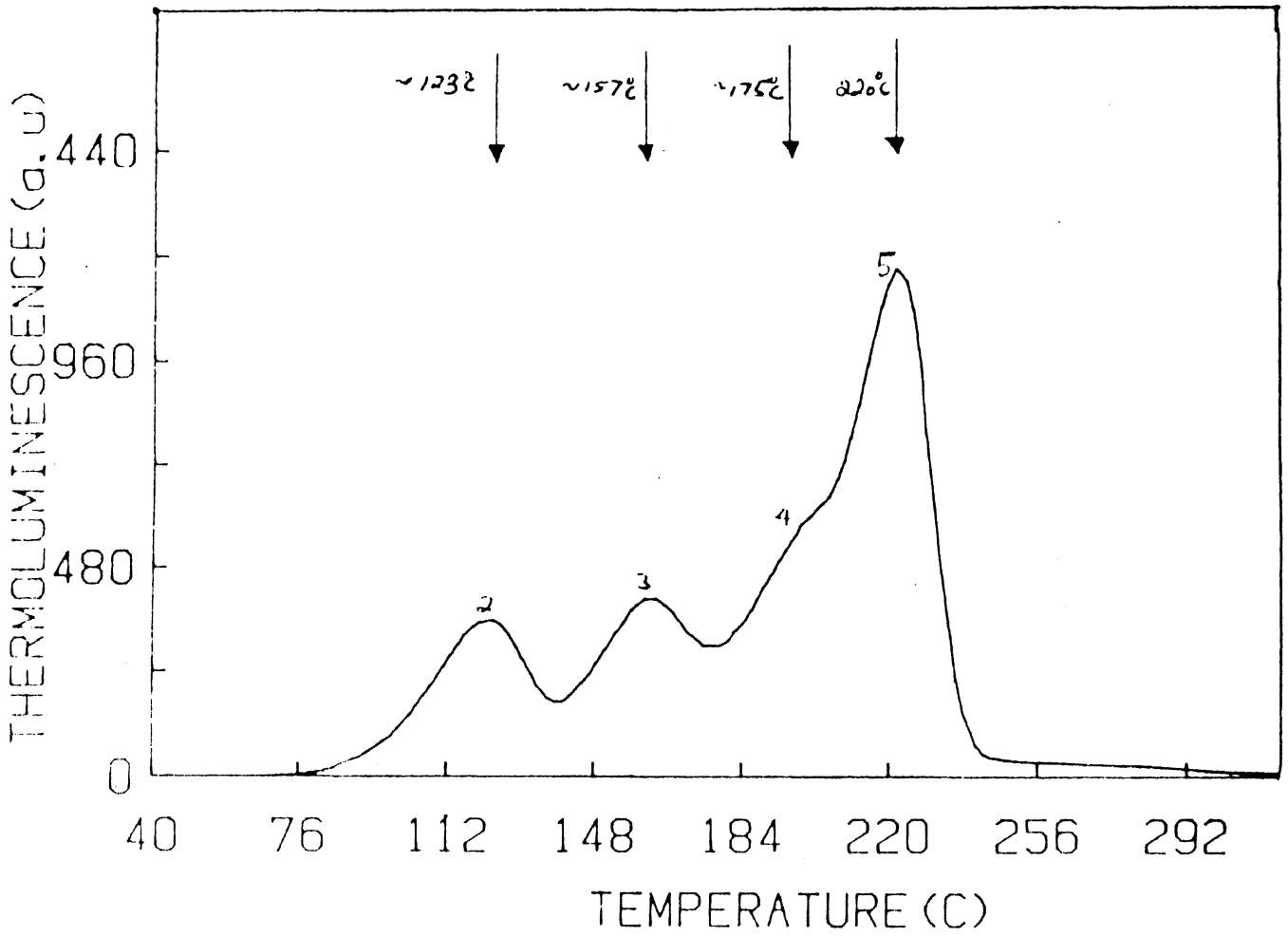

Figure 40. A Typical TL Glow-Curve from TLD-700 Showing the Positions of Each Peak

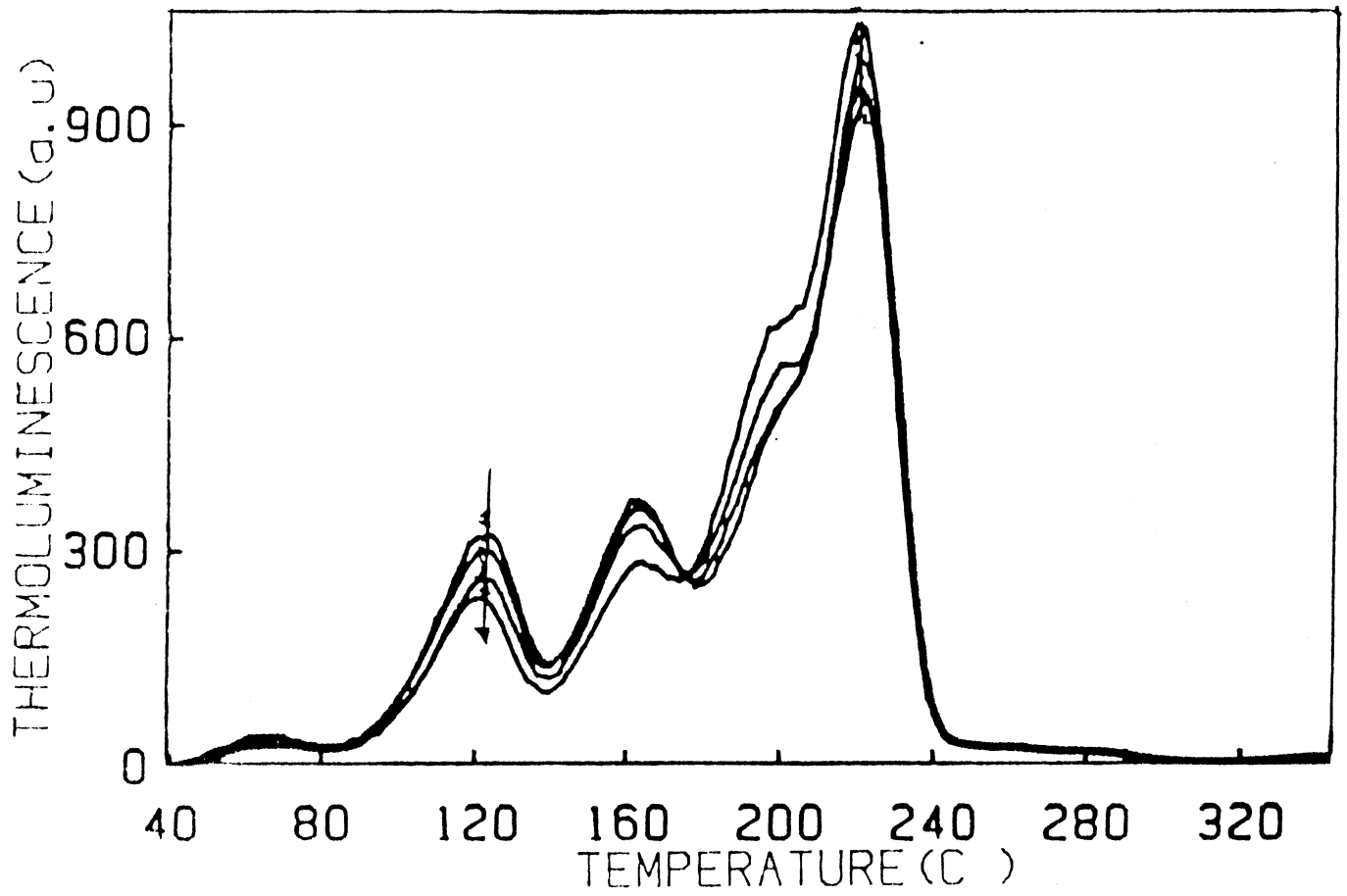

Figure 41. Demonstration of TL Peaks 2 and 5 Change after Different PAT. (1) 85 °C.; (2) 105 °C., (3) 125 °C.; (4) 145 °C.

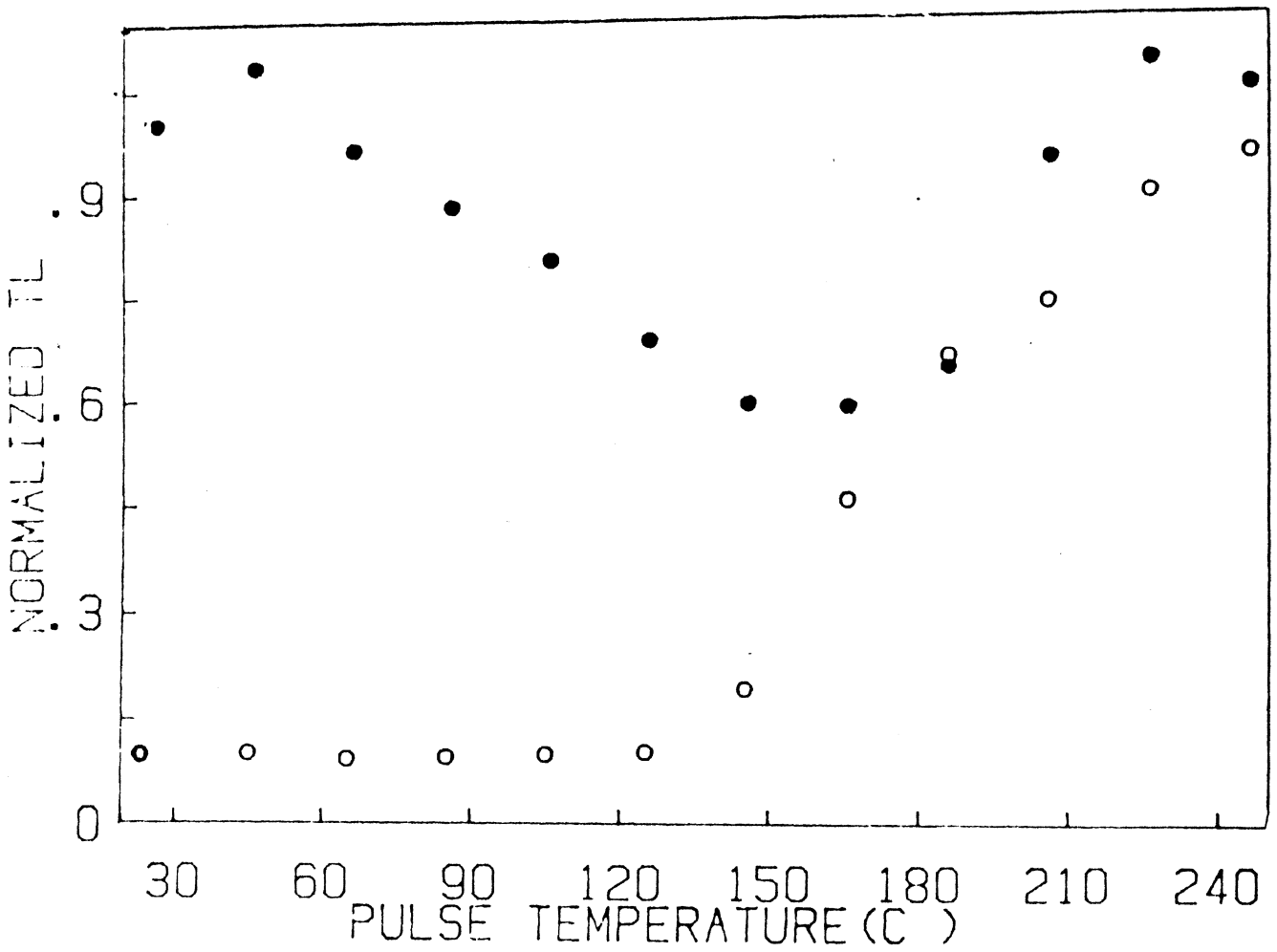

Figure 42. Variation of TL Peak 2 after the Two Annealing Treatments (1) and (2)

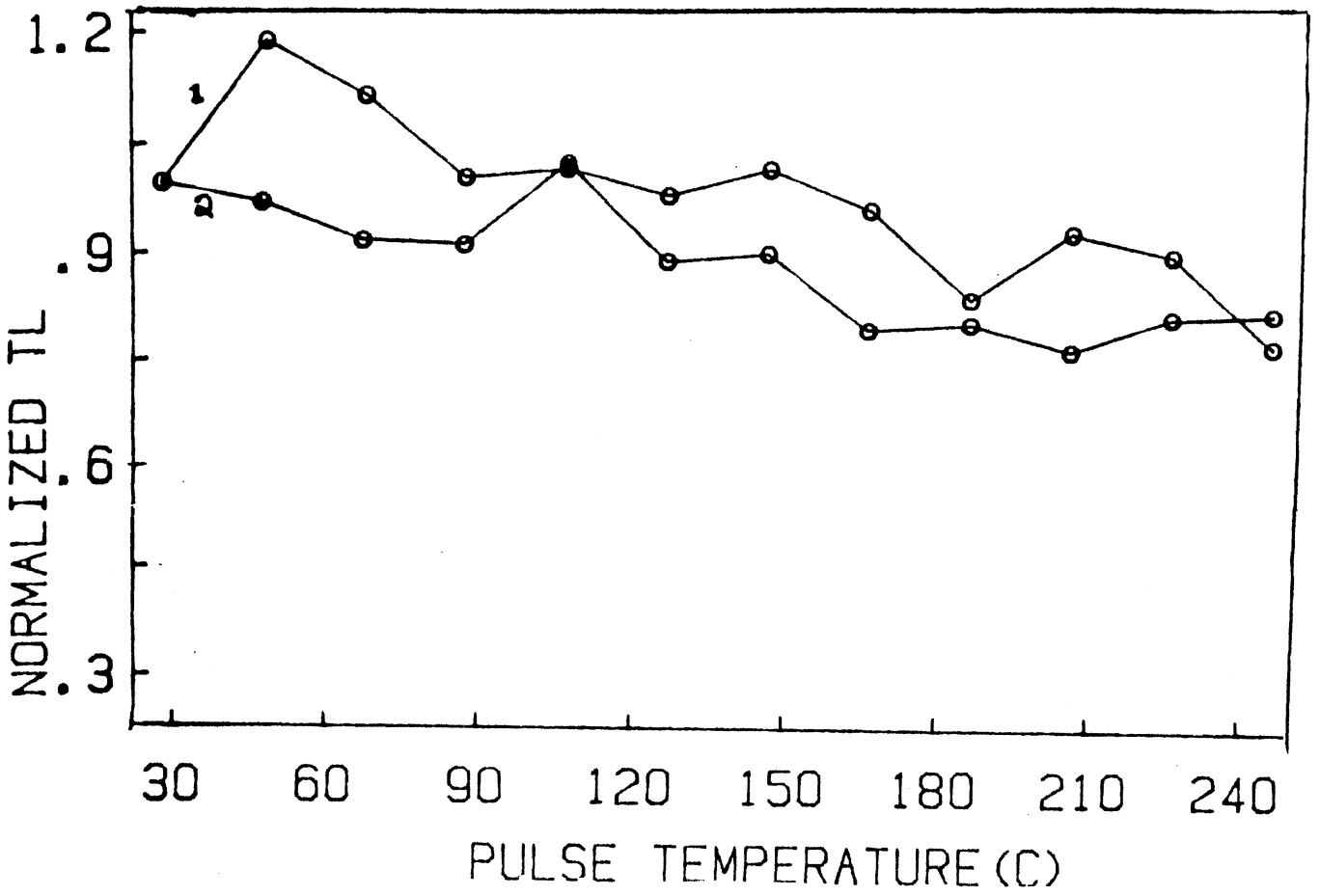

Figure 43. Variation of TL Peak 5 versus PAT

(1) 400°C./1/2 hour

(2) 400°C./1/2 hour + 80°C./24 hours

changes through basic three regions. The first region is initial decay and continues until a minimum is reached, again, at about 150 °C. This is the second region. The last region is the recovery region. After passing 150 °C., the height of peak 2 starts to rise and returns to its initial height at a PAT of ~250 °C.

The similarities are reinforced also from a consideration of the bottom curves. For TL peak 2, from room temperature up to 120 °C., it is as stable as the dipole concentration (in the case of TSDC) and starts rising when the PAT is above ~120 °C. eventually joining the top curve in a very similar way as dipoles do in Figure 34. Above all, the similarities affirmatively lead to the positive correlation between the $Mg^{2+}V^{-}$ dipole and TL peak 2.

A careful look at Figures 34 and 42, however, reveals that the decrease of TL peak 2 is more than that of TSDC at a particular PAT. This implies that not only $Mg^{2+}V^{-}$ dipoles but also some other defects give rise to the TL peak 2. Recall that in Chapter II, the complex $[Mg^{2+}V^{-}]/Ti$ was proposed to explain this peak. It seems now that is the case. Possibly, the association of a dipole with a dipole/Ti^{*} complex was taking place when the TL peak 2 was produced. We know that TSDC results from the presence of dipoles and TL peak 2, according to our result, from the complex dipole Ti^{+}. In addition, concentration of dipoles is much more than dipole/Ti^{+} (the former is around ~100 ppm, the latter

less than 10 ppm). There are probably two paths to cause the extra decay of TL peak 2. First, that three dipoles cluster together to form a trimer in TSDC is a third order reaction. However, the reaction of a dipole associated with dipole/Ti^{+} in TL is the second order, which is supposed to be faster than the third order. Consequently, this leads to that TL peak 2 decays more than TSDC. The second path will be readily explained by the following two reactions:

$$3[Mg^{2+}V^{-}] \underset{k_2}{\overset{k_1}{==}} [Mg^{2+}V^{-}]_3 \qquad (4.1)$$

where each notation remained as defined before except that k_1 is forward reaction constant and k_2 back reaction constant.

$$[Mg^{2+}V^{-}]^{*} + Ti \underset{k_2'}{\overset{k_1'}{==}} [Mg^{2+}V^{-}]^{*}/Ti \qquad (4.2)$$

where similarly k_1' is forward reaction constant and k_2' back reaction constant. From those two reactions, we can see that Equation (4.1) will proceed forward and Equation (4.2) will proceed backward. Therefore, when TSDC decays, so does TL peak 2. In addition, the reaction constant k_2' is different from k_1', causing the decay in TL peak 2 to be different from that in TSDC.

Figure 43 shows the data for TL peak 5. The bottom curve is for the annealing treatment (2) and broadly fits our expectations, assuming this curve is related to trimers. As we heat the crystal we expect that more and more trimers dissociate into dipoles. Thus the concentration of trimers should reduce gradually as the PAT increases. We could not get support for this notion from the top curve, however, since it also goes down gradually and we expected it goes up gradually, reaching maximum at certain PAT such as 150 ^{o}C. and then going down. Once again, the result of top curve is less reliable due to the overlapping with peak 4. As it can be seen from Figure 40, the degree of overlap between peak 4 and peak 5 (~27 ^{o}C. difference in peak positions) is much greater than between peaks 2 and 3 (~34 ^{o}C. difference in peak positions). Therefore, the exact behavior of the TL peak 5 can be obtained only if the TL glow curve is fully resolved into individual component bands as is the case for the OA band at 310 nm.

From these discussions based on Figures 34, 38, 42 and 43, the questions we asked before in Chapter II now have answers. First, the TL peak 2 is caused by $[Mg^{2+} V^{-}]/Ti^{*}$, i.e., the complex of the dipole and Ti^{*}. Thus, the model proposed by Grant and Cameron [26] is an incomplete model in which the $[Mg^{2+} V^{-}]$ dipole is believed to be solely responsible for the TL peak 2. It is wrong that only Ti^{*} (see Chapter II) is responsible for the peak as proposed by

Taylor and Lilley [27]. It is the combination of $[Mg^{2+} V^{-}]$ and Ti^{*}, or $[Mg^{2+} V^{-}]/Ti^{*}$ that is responsible for the TL peak 2 as proposed by McKeever [28]. Second, the suggestion that the TL peak 5 is caused by trimers cannot be fully confirmed unless the glow curve is resolved into individual bands, even though, we have a weak evidence that trimers were involved in the production of the peak. At last, it remains as a question that whether the combination of the trimer and Ti^{*}, or $[Mg^{2+} V^{-}]/Ti^{*}$, instead of $[Mg^{2+} V^{-}]_3$ only is related to the TL peak 5.

Photoluminescence

Figure 44 shows a PL emission spectrum (peaked at approximately 385 nm) obtained following excitation at 200 nm (empty circles). The spectrum was deconvoluted into three Gaussian component bands. The top component band is at 3.20 ev; the middle component band at 2.95 ev; the bottom band at 2.93 ev. The PL emission spectrum of Delgado's [32] has a complex emission peak at 420 nm. The positions of three component bands are 3.01 ev, 2.88 ev, and 2.70 ev, respectively [33]. The overall band in our data has shifted 0.27 ev compared with the peak from Delgado. There are probably two reasons to cause this difference. First, the annealing treatment of ours is different from his (including the cooling method). Second, the temperature at which the PL emission spectrum was performed is different. He did at 210 ^{o}C. We did at room

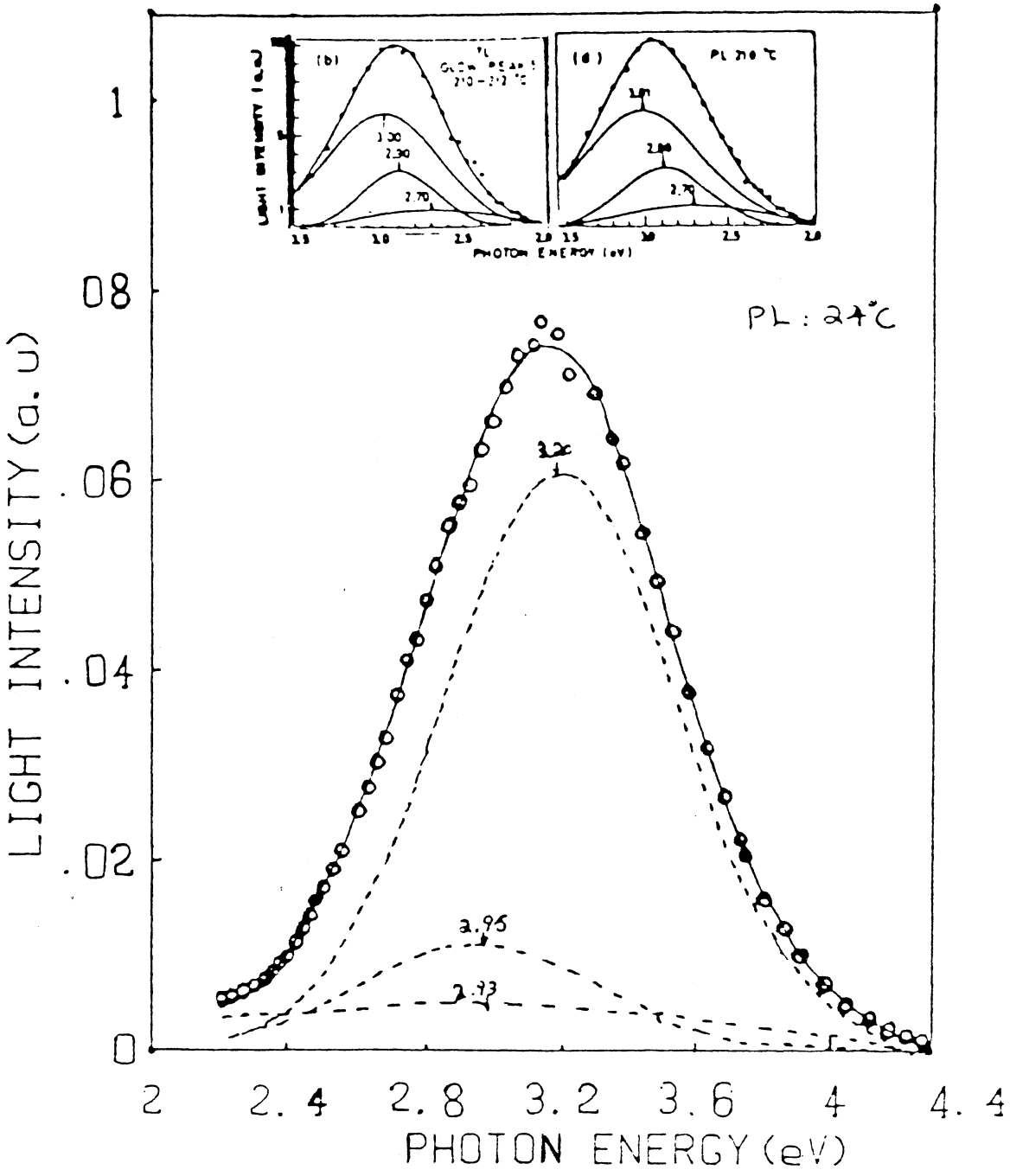

Figure 44. Resolution of PL Emission at 400 nm into Three Component Bands. The Figures on the Top are from Delgado [32]

temperature (~24 °C.). In addition, he used TLD-100. We used TLD-700. The difference in peak positions from TL data has already been observed in TLD-100 and TLD-700 in the previous section. Therefore, we may think the shift of the peak position in emission spectra is also due to the use of a different type of the LiF sample. Another striking difference of our spectrum from Delgado's is the top component band is much higher than the lower two component bands. The main reason we think is from the thermal quenching effect. This effect means that the relative heights of two or more than two PL emission bands depend upon the temperature at which the PL experiments were done and which of two bands were compared. In addition, for a known peak, the lower the temperature, the sharper (or higher) is the emission peak. These factors contribute to our difference from Delgado's.

In Figure 45, we see the PL emission spectrum obtained following excitation at 200 nm. The band width of the detection system is 3.6 nm/mm. The four curves represent four different annealing treatments as described in the figure caption. From the figure, we observed that curves 2 and 3 produce no change in the spectrum, curve 4 produces a slight increase relative to curves 2 and 3. Above all, curves 2, 3 and 4 are much higher than curve 1. Recall in our OA spectrum, 200 nm band is due to Ti-OH alone and is not related to Mg defects. When subjected to the different annealing treatments (1) and (2), OA band at 200 nm does

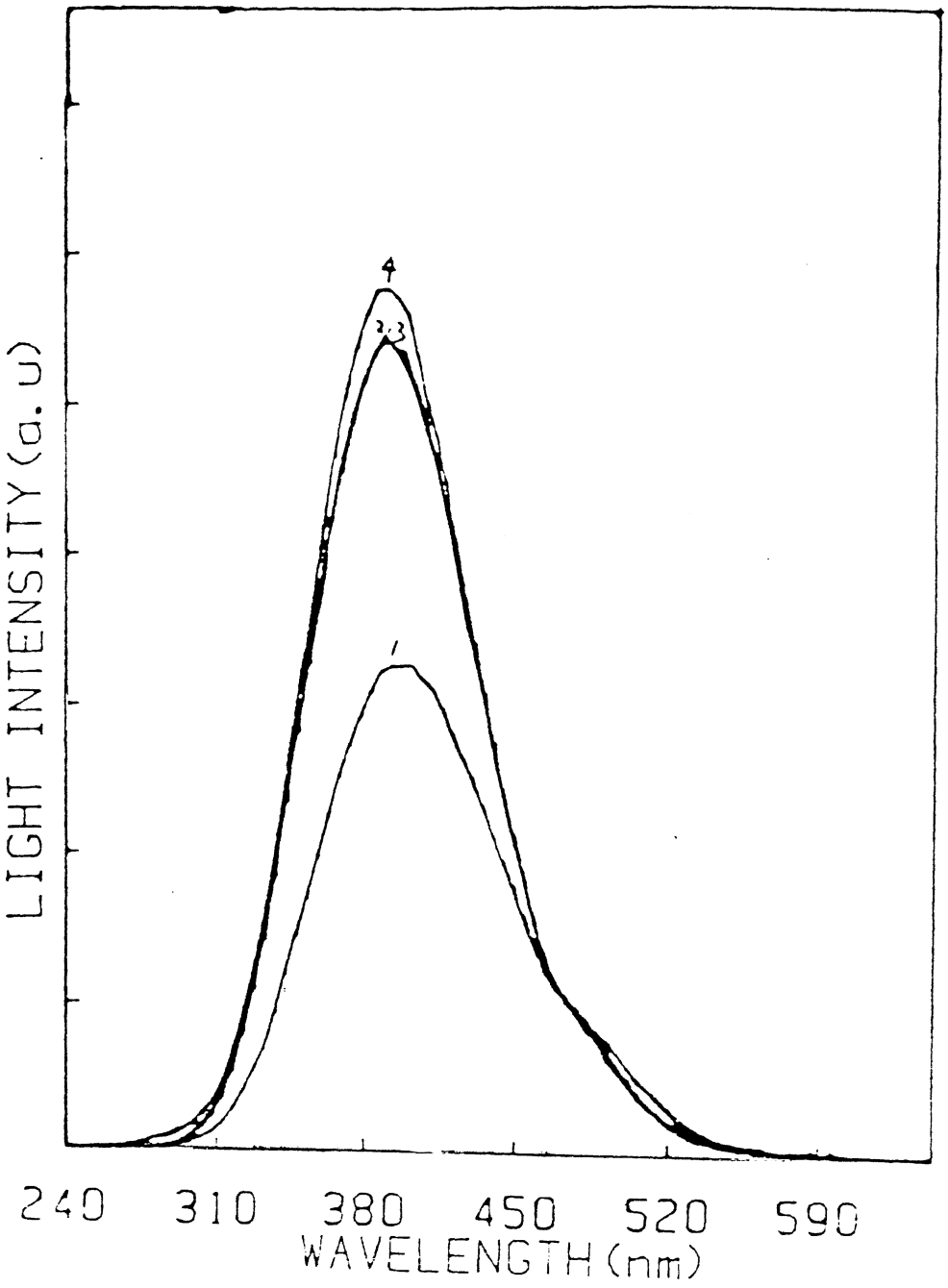

Figure 45. Emission Spectra from:
(1) As Received
(2) and (3) Annealing Treatments (1) and (2)
(4) Precipitate Treatment

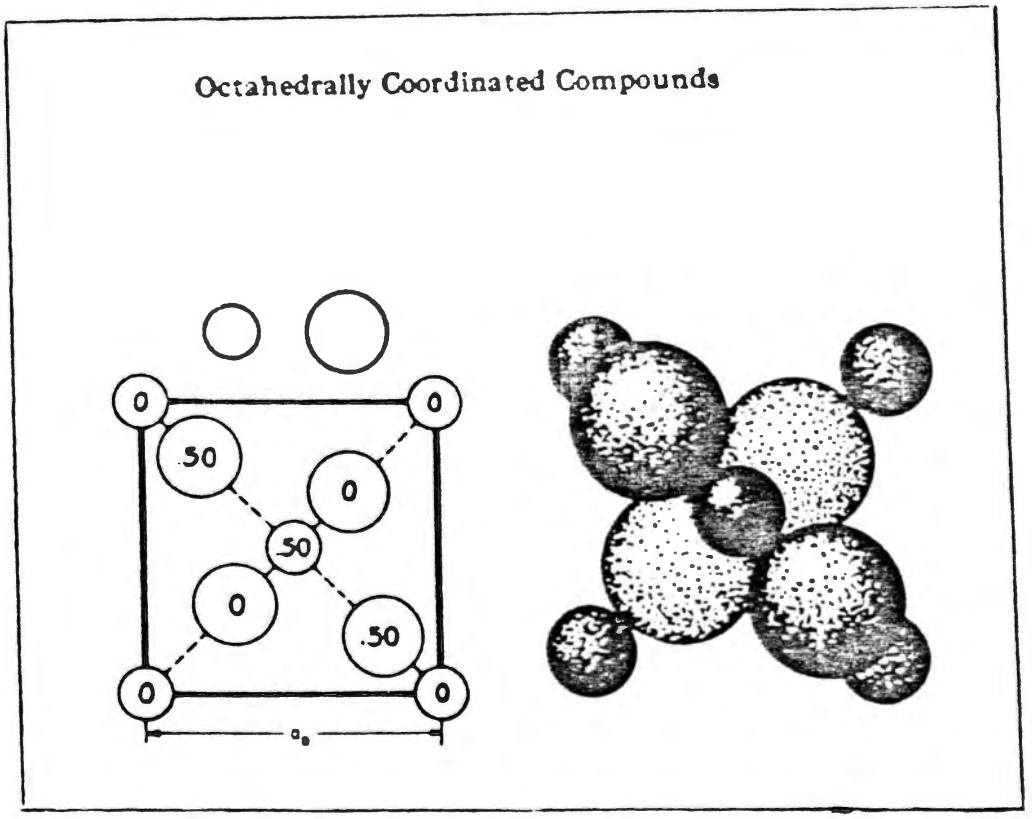

Figure 46. Structure of MgF_2

LEFT: The Atomic Arrangement in the Tetragonal Unit of MgF_2 Projected on the Basel, C, Face the Small Circle Represent Mg Atoms.
RIGHT: A Drawing to Show the Way the Atoms of MgF_2 Pack Together if They are Given Their Expected Ionic Sizes. The Large Spheres are the Fluorine Atoms [42]

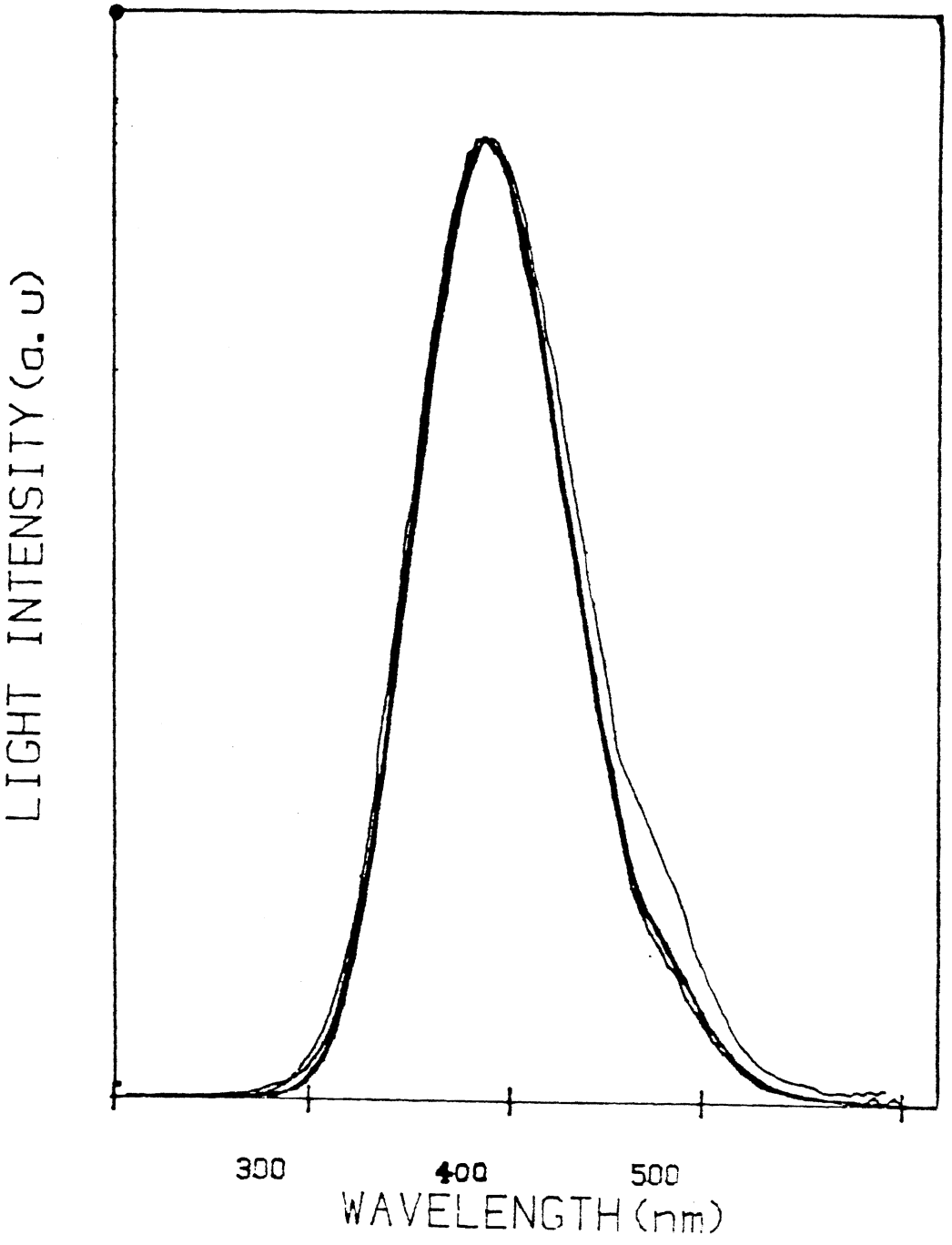

Figure 47. Normalized PL after 4 Different Treatments Mentioned in Figure 43.

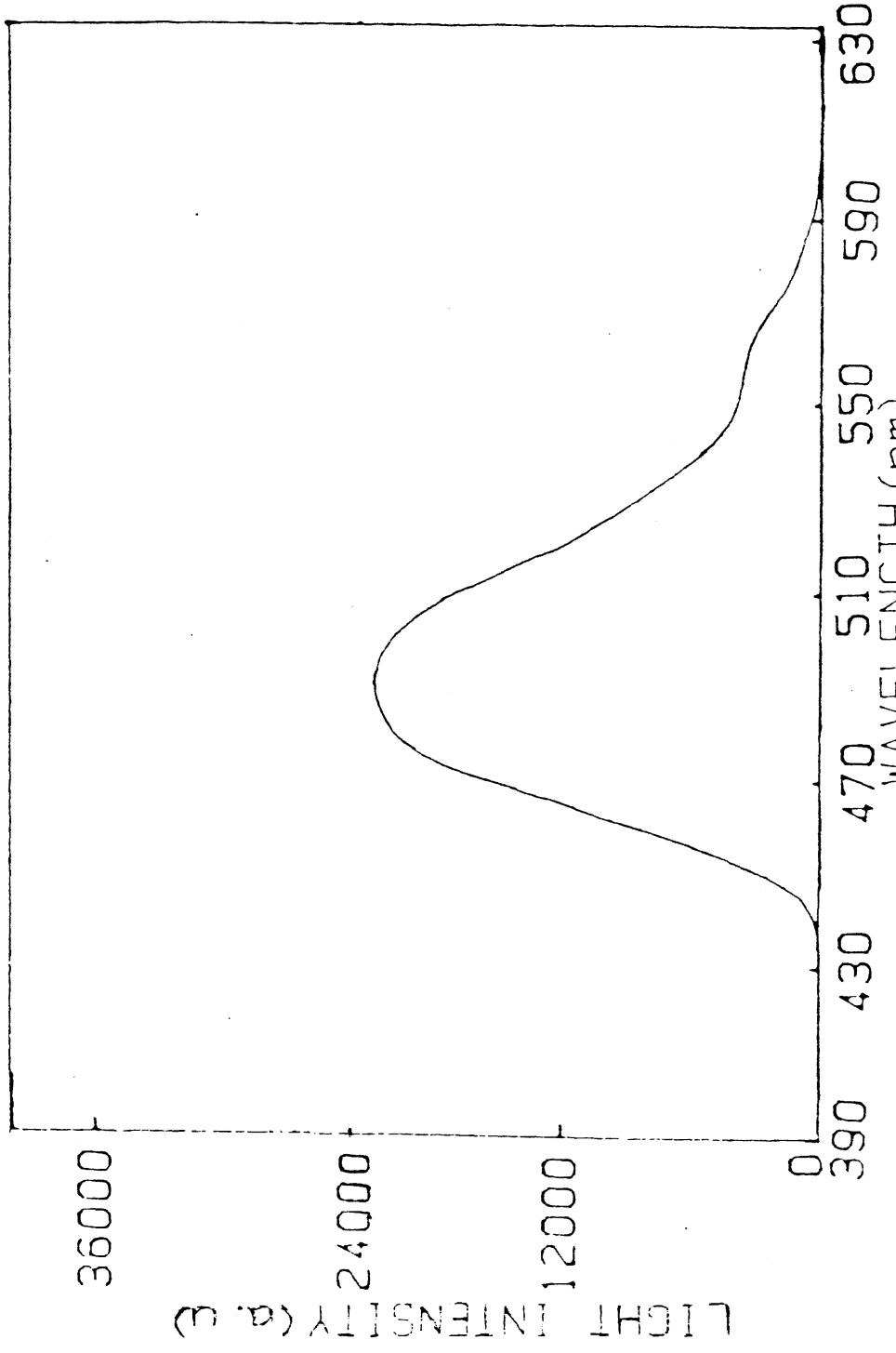

Figure 48. Emission Spectrum of TLD-700 When Excited at 440 nm.

not alter, therefore emission from this center does not alter either. This explains why there is no change from curves 2 and 3. When the sample underwent the precipitation treatment, the Suzuki phase 6 LiF.MgF_2 was formed. During the formation of this phase, Ti^* is insoluble in the precipitate which may nucleate on the Mg defect/Ti^* complexes. Thus, as the precipitates grow, Ti^* may be rejected from the nuclei [28] and produce slight increase in the emission spectrum. The curve 1 is from the sample which is "as received". It is unknown what kind of thermal history the sample has experienced. But during a long period of storage time, we can assume the formation of a more stable precipitate, i.e., MgF_2 (Figure 46). Ti existing in the crystal probably dissolves into this precipitate. As a result of the decrease of this amount of Ti, the curve 1 appears to be much lower than the other three curves 2, 3 and 4. From here, we have suspicion that 6 LiF.MgF_2 tends to reject Ti during its growth, but MgF_2 may attract Ti. The final figure (Figure 47) shows again four curves, but in normalized coordinate where no changes in shapes of these curves were observed.

The analysis so far is from the sample prior to irradiation. After irradiation, we observed no new PL signals following the excitation at 380 nm and 310 nm. This is consistent with the conclusion we had already reached before in OA selection that 380 nm absorption band is due to dipoles only, not $[Mg^{2+} V^-]/Ti^*$. The absence of

Ti^{*} thus leads to no emission if the crystal were excited at 380 nm and 310 nm. However, if the excitation was set at 445 nm, we did see emission (Figure 48) peaked at 500 nm. Absorption at 445 nm is due to F_2-centers which were formed after high dose or after heavy charge particle (HCP) irradiation. Horowitz [43] reported after high dose and/or HCP irradiation, one would get longer wavelength emission. We believe that re-absorption of ordinary emission at 445 nm will produce long λ emission, i.e., non-radiative energy transfer. Another finding is that excitation at 250 nm (LiF, F-center) does not cause any emission. This probably indicates that F-center is distant from Ti. The absorbed photon energy at 250 nm was simply released through phonon processes.

In summary, annealing treatments (1) and (2) don't make a difference in the PL spectra. Suzuki phase growth increases the emission slightly. The as-received sample probably has a stable precipitation MgF_2 formed to result in an apparent decrease in emission compared with the annealing treatment (1) and (2). The correlation that the OA band at 380 nm is directly related to $[Mg^{2+} V^{-}]$ dipoles has been supported. Non-radiative energy transfer resulting in long wavelength emission due to absorption by F_2-centers probably takes place. At last, absorption by F_2-centers (250 nm) does not give rise to new emission signals.

Dipole-Dipole Interactions and TSDC in TLD-700

In order to see the dipole-dipole interaction effect on the TSDC data obtained from TLD-700, two sets of measurements have been done. First, with one sample, the annealing treatment (2) was used before each PAT. Then, the relations of dipole concentrations and activitation energy versus PAT were obtained. Figure 49 shows the result of the activation energy versus dipole concentration. The energy values are from the Bucci-Fieschi fit. It can be seen from the figure that, if low concentration data are ignored, the general trend of activation energy versus dipole concentration for this "clustered" crystal is the same as that reported by Aceituno and Cusso [36], i.e., the activiation energy decreases as the dipole concentration increases up to 100 ppm. Recall this relation was obtained from the PAT method by means of which the dipoles cluster into trimers to different degrees. In order to see if there is a similar relation present in case of no clustering, a second set of measurements were done right after the annealing treatment (1) without PAT treatments from different content of LiF sample. The results were shown in Figure 50. It can be seen from it that there is no obvious trend, in other words, the data are scattered in such a way that one can hardly say if the activation energy decreases or increases as the dipole concentration increases. This figure was obtained from the Bucci-Fieschi

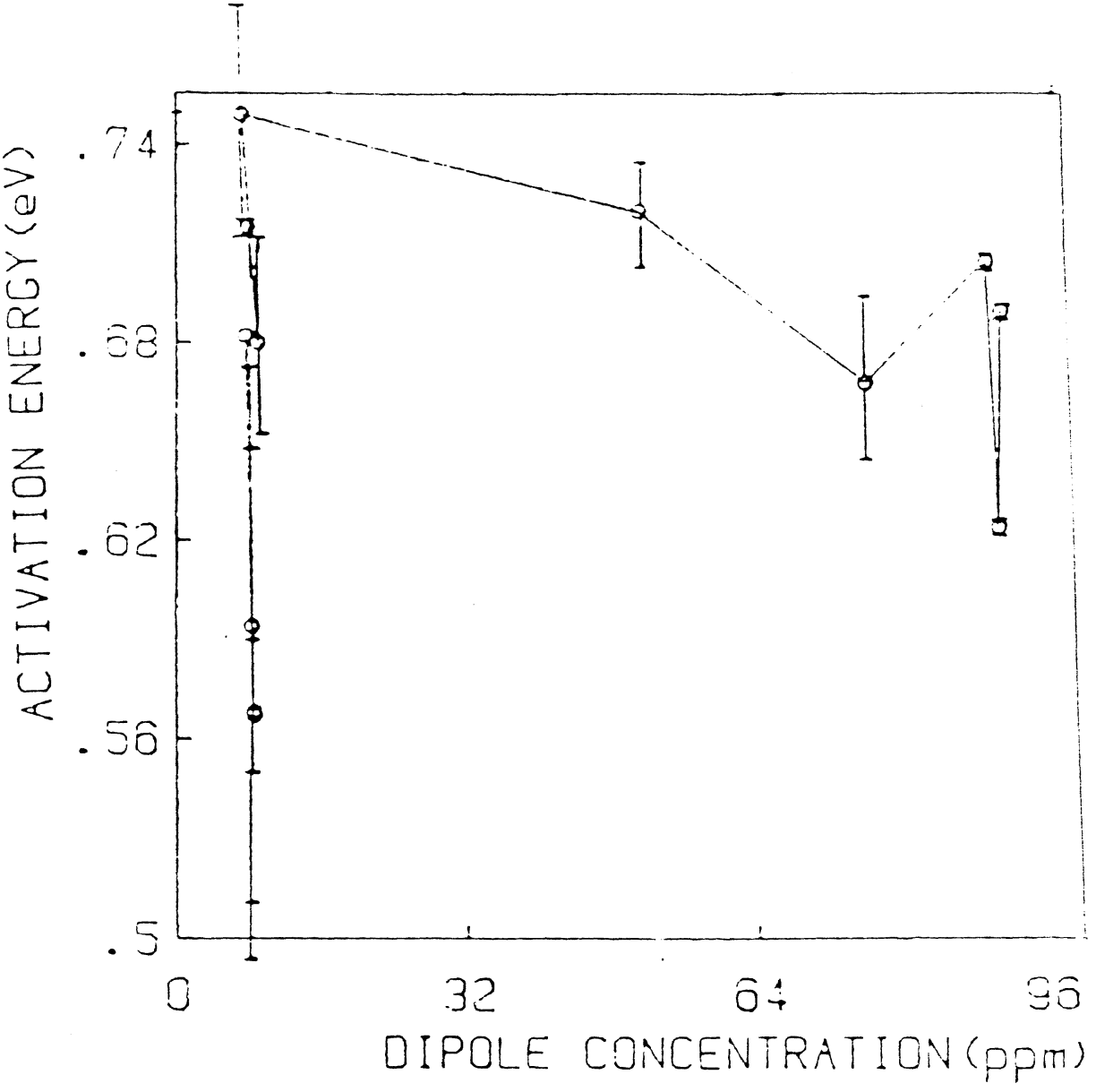

Figure 49. Variation of Activation Energy versus Dipole Concentration of Clustered Crystal from Bucci-Fieschi Fit

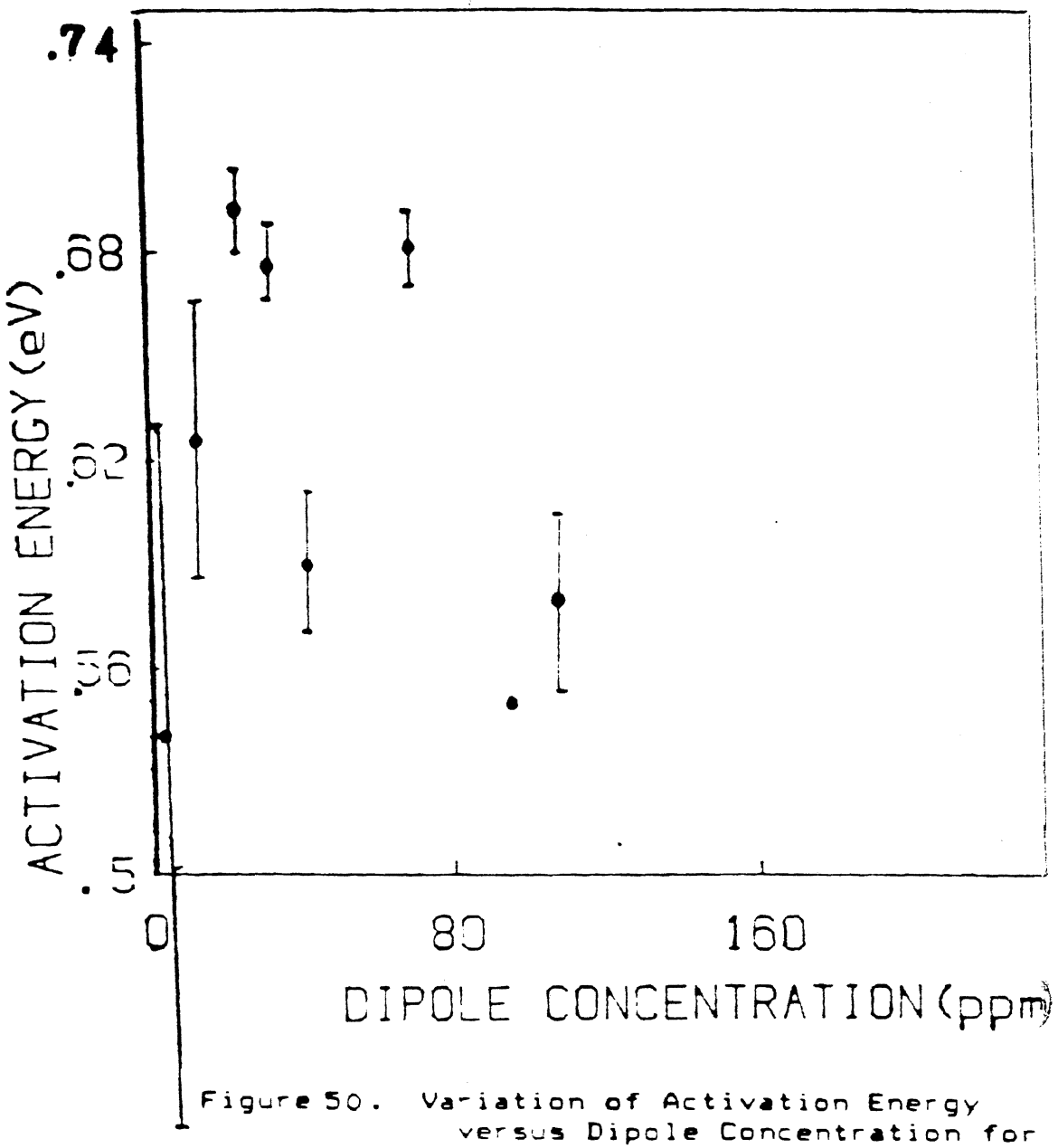

Figure 50. Variation of Activation Energy versus Dipole Concentration for Non-Clustered Crystal from Bucci-Fieschi Fit

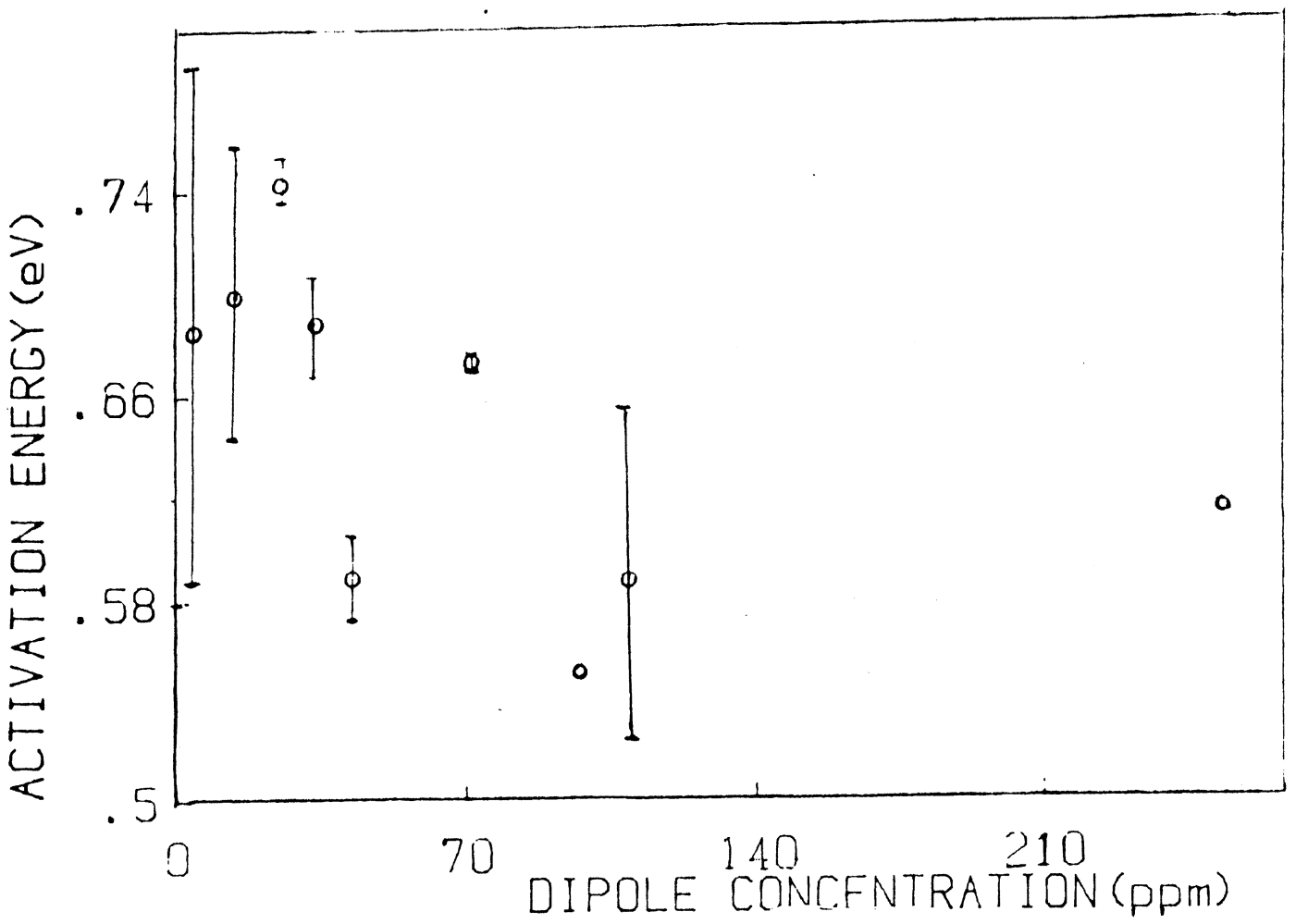

Figure 51. Activation Energy versus Dipole Concentration through Interaction Fit for Non-Clustered Crystal

fit. The corresponding results from dipole-dipole interaction fit are shown in Figure 51. From this figure, an apparent trend (activation energy versus the dipole concentration) appears. Roughly, it seems to be similar to that in Figure 50. Therefore, so far our results pretty much agree with Aceituno and Cusso [36].

Emphasis was also placed upon the effectiveness of different fitting routines. It has been reported that dipole-dipole interaction fit proves to be better than the monoenergetic fitting routine in alkali earth halides [35]. The width parameter p has been introduced (see Chapter III, Equation (3.7)) to solve the broading problem of the TSDC peak successfully. However, the situation in which the interaction fitting does not improve the fit was also reported in alkali halides [36]. In the process of obtaining Figures 50 and 51, two models were used - the interaction fit and the Bucci-Fieschi fit, to see which one is better. Results show that for low concentrations of dipoles, the TSDC is weak. Fitted activation energy E-values show large error and in this case, the interaction fit seems to fit better than Bucci-Fieschi fit. At high concentration, the interaction fit gives little improvement and is sometimes worse than the Bucci-Fieschi fit. In comparison, a fitting by use of two models is illustrated in Figure 52.

The relation of p-factor with dipole concentration is shown in Figure 53. Above 40 ppm, it can be seen from the

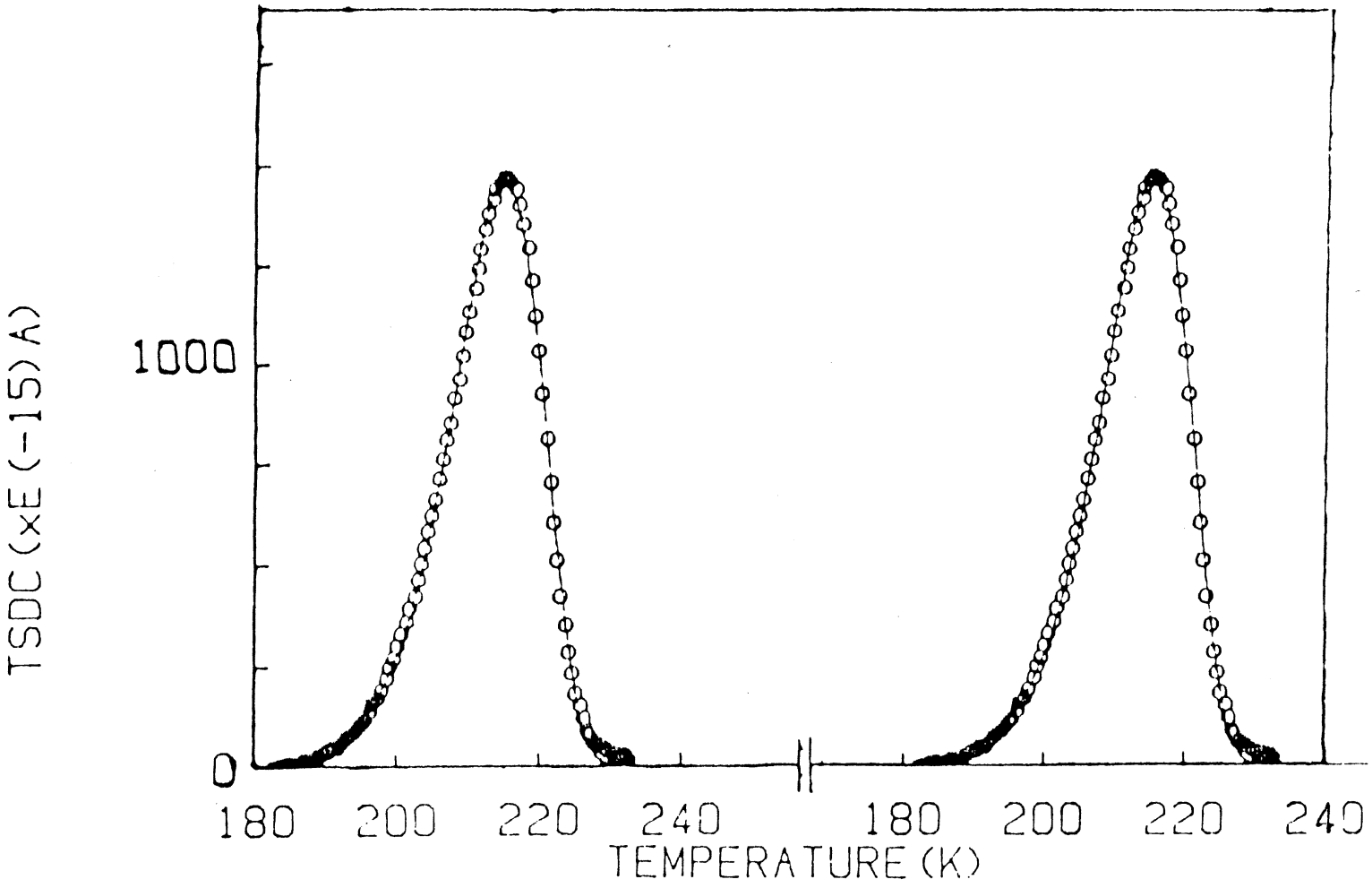

Figure 52. Comparison between Two Fittings. Left is the Interaction Fitting; Right is the Bucci-Fieschi Fitting

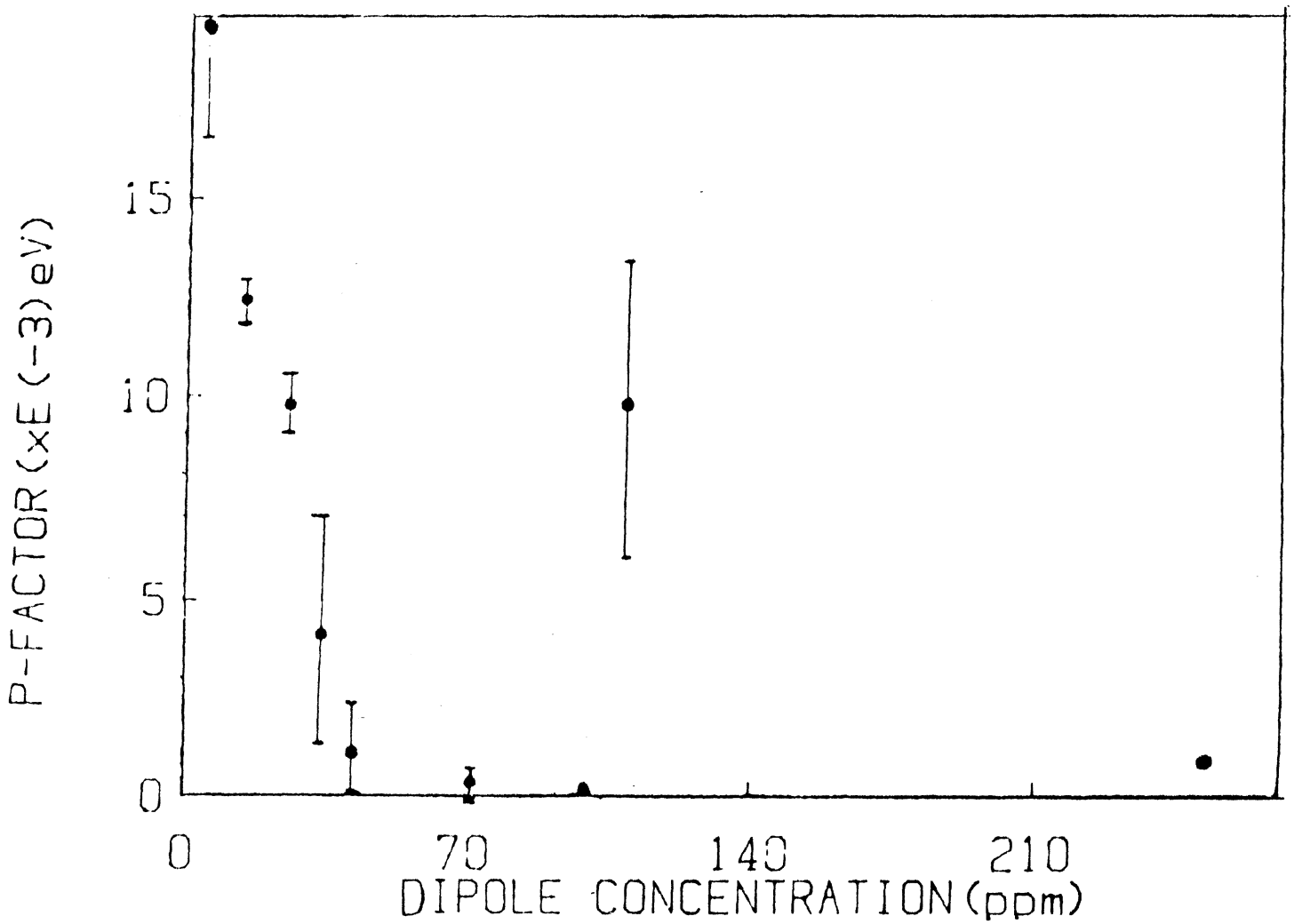

Figure 53. The Variation of p-Factor with Dipole Concentration for Non-Clustered Crystals

figure the p-factors are small and constant up to 250 ppm. This agrees with Aceituno and Cusso [36] where no improvement from interaction fit for alkalide halide system was observed, especially above 100 ppm. We did some extra measurements. We went to the concentration range below 40 ppm. It can be seen from the figure, the p-factors decreased monotonically with the increase in the dipole concentration. This result is just opposite to that from Weperan [35] where the p-factors increase directly proportional to the dipole concentration in alkali earth halide system. From this difference, we are led to the conclusion which we previously stated that there were no dipole-dipole interactions involved in our system for the concentration range we were working with. But, what causes the p-factor to behave in such a strange way remains a question now, which is expected to be solved in the future.

REFERENCES

1. McKeever, S. W. S., Ph.D. Thesis, University of Wales (U.K.) (1975).

2. Julius, H. and de Planque, Radiat. Prot. Dosim. 6, 253-256 (1984).

3. Cusso, F., Ph.D. Thesis, Madrid (1980).

4. Klein, B. J., Ph.D. Thesis, University of North Carolina (1970).

5. Unger, S. and Perlman, M. M., Phys. Rev. B10, 3692 (1974).

6. Dryden, J. S. and Heydon, R. G., J. Phys. C: Solid St. Phys. 10, 2333 (1981).

7. Cook, J. S. and Dryden, J. S., J. Phys. C: Solid St. Phys. 14, 1133 (1981).

8. Corish, J., Quigley, J. M., Jacobs, P. W. M. and Catlow, R. A., Phil. Mag. A, 44, B (1981).

9. Strutt, J. E., and Lilley, E. J., J. Phys. Chem. Solid, 42, 827 (1981).

10. Suzuki, K., J. Phys. Soc. Japan. 16, 67 (1961).

11. Lilley, E. and Newkirk, J. B., J. Mater. Sci., 2, 267 (1967).

12. Taylor, G. C., and Lilley, E., J. Phys. D: Appl. Phys., 15, 1254-1259 (1982).

13. Taylor, G. C., and Lilley, E., J. Phys. D: Appl. Phys., 15, 2057-2065 (1982).

14. Dryden, J. S., and Cook, J. S., J. Phys. B, 260 (1960), Proc. Phys. Soc. London 80, 479 1962).

15. Dryden, J. S., and Harvey, G. G., J. Phys. C2, 603 (1959).

16. Crawford, J. H., J. Phys. Chem. Solids, 31, 399 (1970).

17. McKeever, S. W.S., and Lilley, E., J. Phys. Chem. Solids, 43, 885 (1982).

18. Unger, S., and Perlman, M. M., Phys. Rev. B12, 809 (1975).

19. Hartmanova, M., Thurzo, I., and Besedicova, S., J. Phys. Chem. Solids, 38, 587 (1977).

20. A. Munoz F., E. Cabrera B., H. Riveros, R., Marco Patron, and J. Rubio O., Phys. Rev. B31, 12, (1985).

21. Barsis, E. H., Lilley, E., and Taylor, A., Prot. Br. Ceram. Soc., 9, 203 (1967).

22. Cook, J. S. and Dryden, J. S., J. Phys. C: Solid St. Phys., 14, 1133 (1981).

23. Lilley, E., Ph.D. Thesis, University of Cornell (1966).

24. McKeever, S. W. S., Nucl. Instrum. Methods, 175, 19 (1980).

25. Jackson, J. H., Harris, A. M., Phys. Letter, 29A, 423 (1969).

26. Grant, R. M. and Cameron, J. R., J. Appl. Phys. 37, 3791 (1966).

27. Taylor, G. C., and Lilley, E., J. Phys. D: Appl. Phys., 15, 1253-1259 (1982).

28. McKeever, S. W. S., J. Phys. 56 (10). (1984).

29. Taylor, G. C., Strutt, J. E., and Lilley, E., Phys. State, Solidi a at press (1981).

30. Townsend, P. D., Ahmed, K., Chandler, P. J., McKeever, S. W. S., and Witlow, H. J., Radiat. Eff. 72, 245 (1983).

31. Fairchild, R. G., Mattern, P. L., Lengweiler, K., and Levy, P. W., J. Phys. Appl. 49, 4512 (1978).

32. Delgado, L., and Delgado, A., J. Appl. Phys. 55 (2), (1984).

33. Bucci, C., and Feischi, R., Phys. Rev. Letters, 12, 16 (1964).

34. McKeever, S. W. S., and Lilley, E., J. Phys. C: Solid State Phys., 14 3547-3555 (1981).

35. Werperan, Van W., Lenting, B. P. M., and Bizuauk, E. J., and den Hartod, H. W., Phys. Rev. B18, 2857 (1978).

36. Aceituno, P., and Cusso, F., Phys. Rev. B25, 7577 (1982).

37. Taylor, G. C., Strutt, J. E., and Lilley, E., Phys. State Solidi (a) 67, 263 (1981).

38. McKeever, S. W. S., In Thermoluminescence of Solids (Cambridge University Press: Cambridge, 1985).

39. Townsend, P. D., and Kelley, J. C. In Color Centers and Imperfection and Semiconductors, Sussex University Press, U.K. (1973).

40. Dawson, R. K. and Poley, D., Phys. State Solidi. 35, 95 (1969).

41. Harris and Jackson, Appl. Phys. D: 3, 624-627 (1970).

42. Wackoff, R. W. G., In Crystal Structures, Interscience Publisher, 1, 250 (1963).

43. Horowitz, Y. S., In Thermoluminescence and Thermoluminescent Dosimetry, CRC Press, 2. 12 (1984).

VITA

Xiao-Lin Yuan

Candidate for the Degree

of Master of Science

Thesis: DEFECT CLUSTERING IN LiF TLD-700

Major Field: Physics

Biographical:

Personal Data: Born in Henan, China, November 20, 1962, the son of Ping Hu Yuan and Jin Fang Ou.

Education: Graduated from Xin Yang High School, Xin Yang, Henan, China, in September, 1979; received Bachelor of Science Degree in Physics from Zhengzhou University in 1983; completed the requirements for the Master of Science degree at Oklahoma State University in December, 1987.

Professional Experience: Graduate Teaching Assistant, Department of Physics, Oklahoma State University, 1985-1986; Graduate Research Assistant, Department of Physics, Oklahoma State University, 1986-1987.

Professional Organizations: Society of Physics Students, Department of Physics, Oklahoma State University.